Biomolecular Interactions with Synthetic Surfaces

by

Aftin Monique Ross

A dissertation submitted in partial fulfillment
of the requirements for the degree of
Doctor of Philosophy
(Biomedical Engineering)
in The University of Michigan
2012

Doctoral Committee:

Professor Joerg Lahann, Chair
Professor Paul Krebsbach
Professor Gary D. Smith
Professor Shuichi Takayama

DEDICATION

Lovingly dedicated to the memories of

Ms. Ruby Grace Jones

Mrs. Ida Dale Ross

Mr. LD Ross Sr.

Mr. LaMont Toliver

Ms. Imade Asemota

ACKNOWLEDGEMENTS

I would like to thank everyone who has played a role in my success thus far. First and foremost, I would like to thank God for giving me strength and this great opportunity. My parents LD Ross Jr. and Annetta Ross have provided unwavering love and support during this PhD process and I would like to thank them for going above and beyond for me. Astin, my identical twin sister, has been a pillar of support throughout proofreading my work and discussing various scientific approaches and ideas. My fiancé Justin has championed my efforts often attending major milestones and arranging his schedule around mine in order to put me in the best position for success. This has truly been a family affair and that has certainly enriched my graduate experience. I would also like to thank my siblings, grandparents, aunts, uncles, and cousins for all of their encouragement and for limiting the number of times that they asked me the dreaded question "When are you going to graduate?"

While God and my family have played significant roles in getting me to this point, I would be remiss if I did not acknowledge those who had a large role in my scientific development in graduate school. I am honored to have worked in the lab of Professor Joerg Lahann. Professor Lahann is an outstanding mentor who has encouraged collaboration, provided abundant tools and resources for tackling challenging scientific problems, and promoted my holistic development as a person and as an engineer. All mentors are not created equally and Professor Lahann has shown himself to be

exceptional by example. I would also like to recognize my dissertation committee Professor Paul Krebsbach, Professor Gary Smith, and Professor Shuichi Takayama for their insight and guidance over the course of my PhD. A spirit of excellence and collaboration is pervasive in the Lahann lab and I have had the pleasure to work with many good colleagues. Several senior grad students took an interst in me and my work, helping me to navigate the PhD process. In particular, I would like to acknowledge Dr. Himabindu Nandivada, Dr. Srijanani Bhaskar, and Xiaopei Deng for explaining various concepts and techniques as well as their friendship. I have also had the opportunity to work with several postdoctoral scholars internal and external to the Lahann group and would like to express my gratitude to Luis Villa-Diaz, Hakan Durmaz, Tae-Hong Park, Sampa Saha, Dong Woo Lim, Sangyeul Hwang, Kyungjin Lee, and Florence Bally for the wealth of knowledge they provided.

As the postdoctoral researchers aided in my scientific development, I have also sought to engage the next generation of scientists and engineers by mentoring undergraduate students. During my time at Michigan I have had the privilege to work with three undergraduate students: Di Zhang, Priya Moni, and Jonathan Oh. I really enjoyed working with them and each made significant contributions to the Lahann Lab. I would also like to thank the other graduate students in the lab, Yaseen Elkasabi, Jaewon Yoon, Thomas Eyster, Ekaterina Sokolovskaya, Domenic Kratzer, Sahar Rahmani, Ashish Misra, Kenneth Cheng, Gowthamy Venkidasubramonian, and Jacob Jordahl. It has been a pleasure to work with you. I also wish to acknowledge the various sources that have funded my graduate education including the GEM Consortium, Microfluidics in Biomedical Sciences (MBSTP) Training Grant, and the Rackham Predoctoral

Fellowship. Maintaining balance has been vital to my success as a graduate student and numerous organizations and individuals have enabled me to do so. The Society of Minority Engineers and Scientists Graduate Component (SMES-G), Movement for Underrepresented Sisters in Science and Engineering (MUSES), Alliance for Graduate Education and the Professoriate (AGEP), and the Biomedical Engineering Graduate Student Council have provided me with a sense of community and contributed to my development as a leader. Furthermore, I have experienced spiritual growth through my membership at Bethel AME Church Ann Arbor and through my association with Pastor Dr. Joseph Cousin and Reverend Yolanda Whiten. In addition to these wonderful organizations, I have a group of girlfriends that help me to have fun and keep things in perspective. Thanks Joy, Mia, Kyla, Angelique, Taeyjuana, Gamola, Jamie, and Sherleka. I also have several guy friends who have made this journey with me and whom I have commiserated with when I have had difficulty with experiments. Thanks Mustapha, Michael L., Gbenga, Memie, Korey, and Brian B. for lending me your ears.

My journey to a PhD actually began as an undergraduate at the University of Maryland Baltimore County (UMBC). There, I was part of the Meyerhoff Scholars program which groomed students for matriculation into PhD programs in science, technology, engineering, and math. I want to express my gratitude to the program staff for working with me on my graduate applications and for instilling in me the importance of community/collective success. I bonded with my Meyerhoff brothers and sisters during late night study sessions and their efforts inspired me to remain diligent even when I faced difficult challenges. In addition to the Meyerhoff Scholars program, participating in undergraduate research was also a vital part of my preparation for graduate school and I

had the opportunity to work in the biomaterials lab of Professor Dwayne Arola. Working in Professor Arola's lab was invaluable as I collaborated with graduate students, learned about the perseverance required in research, and presented my work at a national conference. I would like to thank him for mentoring me and stirring my intellectual curiosity.

TABLE OF CONTENTS

LIST OF FIGURES

LIST OF TABLES

ABSTRACT

Biomolecular Interactions with Synthetic Surfaces

by

Aftin M. Ross

Chair: Joerg Lahann

Augmenting the surface properties of synthetic materials can modulate biomolecular functions. In this dissertation research, the chemical vapor deposition (CVD) platform is used to generate reactive polymeric surfaces for various applications including sensing, "click" chemistry, and tissue engineering. For the first time, thin CVD films are used as novel sensors for imaging surface plasmon resonance enhanced ellipsometry (SPREE), a tool used in biosensing/diagnostics. CVD coatings are advantageous because they have better long-term stability and do not require special storage conditions. CVD-coated sensors are capable of detecting many biomolecules which may be tuned by altering film reactivity.

Another area of this dissertation research is the use of a reactive CVD coating as a binding partner in thiol-based "click" chemistry reactions and a Diels Alder "click" reaction, types of immobilization strategies used to modify surfaces. Successful surface modification with thiols and maleimides is demonstrated and further exploited to create

multifunctional surfaces, which may serve as building blocks for complex surface architectures. CVD coatings are beneficial as they extend the utility of thiol-based “click” chemistry reactions by increasing the number of binding substrates.

In the final portion of the dissertation research, a polymeric brush was generated that undergoes a change in wettability (how water interacts with a surface) as a function of brush thickness. At low thicknesses, this brush is known to maintain human stem cells in a form that allows them to become any cell type. The use of a synthetic substrate to maintain this state is advantageous because material parameters can be tightly controlled. By altering wettability and other material characteristics, properties important for maintaining these cells are evaluated and may be utilized for future biomaterials designs. This dissertation research has made numerous contributions to the field of biomaterials science through the generation of a range of surface modification platforms that could ultimately aid in elucidating cellular and biomolecular behaviors, which have applications in diagnostics, molecular self-assembly, and tissue engineering/regenerative medicine.

CHAPTER 1

INTRODUCTION

The materials in this chapter have been adapted with minor modifications from the following published articles:
Ross, A.M., Nandivada, H., Lahann, J. Switchable Surface Approaches. In Handbook of Stimuli-Responsive Polymers; M. Urban, Ed.; Wiley NY, 2010.

Nandivada, H., Ross, A.M., Lahann, J., "Stimuli-responsive Monolayers for Biotechnology", *Progress in Polymer Science* 2010, 35(1-2), 141-154.

1.1 MOTIVATION AND BACKGROUND

The treatment and diagnosis of disease may be improved by innovations in materials science and in the methods utilized in the surface modification of these novel biomaterials.[1-5] Synthetic materials are utilized in a host of biomedical applications from the use of nanowire sensing arrays in point of care diagnostics[6] to the use of polymer scaffolds for bone regeneration.[7] As a result, there has been an increased interest in the design and surface modification of synthetic biomaterials. Ideally biomaterials are biocompatible, generated from repeatable processes, and should maintain their form and function for the desired time period.[8] However, an important factor that influences the success of these materials in a given application is their interaction with various biomolecules, which is the focus of this dissertation research.

1.2 SURFACE MODIFICATION: SWITCHABLE SURFACE APPROACHES

In this chapter, general methods for surface modification using synthetic materials and biomolecules are detailed with a specific emphasis on switchable surfaces. Switchable surfaces can reversibly alter material properties in response to changes in the environment or an external stimulus. Currently, a myriad of stimuli are utilized to control surface properties including electrical potential, light, pH, temperature, and mechanical forces. Exposure to stimuli results in changes in surface conformation, wettability, optical properties, and biocompatibility. Switchable materials exist in nature and their synthetic analogues may find wide ranging applications. Because the behavior of stimuli-responsive materials can be controlled, potential benefits of their utilization abound, particularly in the biotechnology industry. Exploiting macroscopic changes in these "smart" materials is useful for a variety of applications including tissue engineering, microfluidics, biosensors, molecular electronics, and colorimetric displays. Diverse material platforms that function as switchable surfaces are highlighted and **Table 1.1**. provides a listing of the materials discussed herein and their respective stimuli.

1.2.1 Electro-active Materials

1.2.1.1 High density and low density self-assembled monolayers

The behavior of electro-active materials is controlled by the application of an electrical stimulus. Changes in surface properties as a result of electrical exposure include alterations in wettability, conformation, and protein adsorption. A self-assembled monolayer (SAM) is a single layer of amphiphilic molecules that spontaneously organizes onto a substrate as a result of an affinity between the amphiphile and the substrate and is an example of

an electro-active material. [9] A gold-alkanethiolate system is commonly utilized due to the ease of SAM formation and the use of gold as an electrode. Traditional SAMs result in densely packed structures called high-density self-assembled monolayers (HDSAMs). Because HDSAMs have limited steric freedom due to their dense packing, the structure is unable to undergo conformational changes. Thus low-density self-assembled monolayers (LDSAMs) were created to decrease molecular steric hinderance, allowing for greater conformational freedom of the molecules and the creation of reversibly switchable surfaces. SAMs are created via physioabsorption onto a substrate. Typically a substrate is immersed in a SAM solution for a sufficient period of time (generally 12 to 24 hours) to form a homogenous layer. Modifications can be made to the SAM both before and after assembly to augment SAM responsiveness to various stimuli.

HDSAMs are characteristically made electro-active by changing the electric potential of the gold substrate acting as the electrode. Modulating the electrical potential can result in desorption of thiols from the substrate leading to changes in surface properties, such as the wettability, or hydrophilicity and hydrophobicity, of the material. [10-12] Several methods exist for creating LDSAMs that are modulated by electric potentials. [13-15] In one method, SAMs with bulky end groups are assembled onto a surface. This SAM is densely packed with respect to the end groups which are then cleaved resulting in a monolayer that is loosely packed with respect to the alkyl chains. Loosely packed chains are capable of undergoing reversible conformational transitions in response to an external electrical stimulus.[16-18] Lahann et al. utilized this concept to reversibly modulate the wettability of LDSAMs. [19] Upon the application of an electric potential, the top of the molecule, which is negatively charged, bends into a loop shape as it is attracted to the positively charged surface as seen in **Figure 1.1**. Thus the surface changes

from hydrophilic in the "straight" conformation to hydrophobic in the "bent" conformation due to the exposure of the hydrophobic alkyl chains. This conformational alteration also results in a change in impedance, or resistance to current flow.[17] Potential applications for this technology abound and include diagnostics, cell adhesion/motility studies, and tissue engineering.

An alternative method for creating an LDSAM is the assembly of pre-formed inclusion complexes (ICs) comprised of cyclodextrin and alkanethiol.[15] The space-filling cyclodextrin is subsequently unwrapped via dissociation in an appropriate solvent, generating an LDSAM. Liu et al. found that tuning the applied electrical potential resulted in reversible changes in surface wettability as well as protein adsorption. This system was extended when low-density acid and amino terminated SAMs were used to coat microfluidic devices in order to reversibly and selectively adsorb proteins of varying isoelectric points in a mixture. When a negative potential was applied, acid-terminated LDSAMs were able to adsorb the positively charged protein and released the protein upon the application of a positive potential. Thus this method could play a role in protein separation studies for applications in proteomics and sensing technologies.

1.2.1.2 Self-assembled monolayers with hydroquinone incorporation

The incorporation of electro-active hydroquinone moieties into SAMs has also been utilized to generate electro-active monolayers. Hydroquinone moieties can be reduced by electrochemical oxidation to generate benzoquinone and this has been used to release ligands attached to a substrate surface.[20] For example, Yeo et al. detached RGD peptides which function as a cell adhesive from the substrate surface which triggered the

release of cells adhered to the peptides.[21] Furthermore, benzoquinone units resulting from this reduction were then utilized (by means of a Diels-Alder reaction) to selectively immobilize diene-functionalized peptides. This reaction resulted in cellular reattachment and migration.

1.2.2 Photo-responsive Materials

In addition to electric potential, light can also be used to trigger switching properties of surfaces and polymers. Application of ultraviolet light to these materials may result in reversible changes in characteristics such as hydrophilicity/hydrophobicity, structural arrangement, and shape. Commonly utilized photo-responsive materials include azobenzene molecules, spiropyran molecules, and shape memory polymers.

1.2.2.1 Molecules containing azobenzene units

Upon the application of a certain wavelength of light, azobenzene units switch their structure from the trans (straight) to the cis (bent) isomerization. This conformational change corresponds to different dipole moments, with the cis-isomer having a higher dipole moment. Alterations in molecular spatial arrangement can then be translated into macroscopic changes in surface wettability.[22, 23] For example, azobenzene treated surfaces have demonstrated the ability to control liquid droplet and liquid crystal (LCs) alignment.[24, 25] Ichimura et al. formed azobenzene monolayers on quartz substrates and established that exposure of ultraviolet light resulted in a reversible conformational change that led to the parallel alignment of LCs in contact with the monoloayer. Changes in the molecular shape of azobenzene molecules also result in mechanical acutuation. Ji

et al. demonstrated the efficacy of azobenzenes in actuation by coating a micro-cantilever with a thiol-terminated azobenzene derivative.[26] Application of UV light caused the downward deflection of the coated cantilever because alterations in azobenzene arrangement from the trans-to-cis conformation resulted in the repulsion of molecules within the monolayer.

The photoresponsiveness of azobenzenes have been exploited in biology via the incorporation of azobenzene units into peptides. Hyashi et al. synthesized a peptide with an azobenzene backbone and then utilized this peptide and its corresponding RNA binding aptamer as an in vitro selection tool for RNA-ligand pairing.[27] The peptide exhibited reversible photoresponsive binding to target RNA that was turned "on" in the presence of visible light and turned "off" upon application of UV light. Auenheimer et al. utilized Arginine-Glycine-Aspartic acid (RGD) peptides in conjunction with azobenzene to influence cellular adhesion.[28] Adding an azobenzene derivative to the peptide sequence enabled spatial control as the trans-conformation of azobenzene is 3 Å longer than the cis-conformation. After coating a substrate with the photoresponsive peptide, a reduction in spacing between peptides and substrates in the cis-conformation resulted in lower cell adhesion while the converse was true for molecules in the trans-conformation.

1.2.2.2 Molecules containing spiropyran units

Spiropyrans are another class of photoresponsive materials with reversible switching capabilities. In this instance, switching is modulated by the photochemical cleavage of a C-O in the presence of UV light which changes it from a closed non-polar form to an open polar form.[29-34] Because the closed form of the molecule is hydrophobic

and the merocyanine form is hydrophilic, exposure to UV light alters wettability. Thus incorporating spiropyrans into a substrate or using them as a surface coating, allows for the control of substrate wettability.[35]Athanassiou et al. exploited the ability of spiropyrans to modulate wettability in conjunction with nanopatterning to control volumetric changes.[36, 37] In this work, a nanopatterned poly(ethyl methacrylate)-*co*-poly(methyl acrylate), P(EMA)-*co*-P(MA) was doped with spiropyran and then exposed to UV illumination. The contact angle of the doped P(EMA)-*co*-P(MA) was reduced as compared to the material without the incorporation of spiropyran indicating increased hydrophilicity. Upon exposure of green laser pulses, the doped material returned to a hydrophobic state and the contact angle increased. Alterations in wettability are ascribed to dimensional changes in the nanopatterning due to light irradiation.

Control of wettability is also imperative in modulating cell behavior, particularly cell attachment. Higuchi et al. utilized a copolymer of nitrobenszospiropyran and methyl methacralate, poly (NSP-co-MMA) to control platelet and mesenchymal stem cell adhesion to substrates.[38] After exposure to UV irradiation, cells or platelets that were previously attached to the copolymer coated substrate were detached. As protein adsorption, specifically fibrinogen adsorption, is known to play a significant role in platelet adhesion, the impact of UV exposure on fibrinogen adhesion was measured. Because no substantial differences in fibrinogen adhesion were observed in the presence of UV light, it was concluded that cell and platelet detachment resulted from a change in surface energy and/or an alteration in the surface conformation derived from the switch of spiropyran from the closed non-polar state to the polar merocyanine state upon UV light exposure. Edahiro et al. exploited the wettability control afforded by spiropyrans to

create a photo-responsive cell culture surface.[39] In this instance, spiropyrans were incorporated as side chains for a poly (N-isopropylacrylamide) polymer. Conformational transitions of spiropyran from the non-polar to polar states after UV exposure modulated the adhesion of living CHO-K1 cells.

A unique application of spiropyrans can be found in molecular gating. Aznar et al. utilized spiropyrans to control nanoarchitecture through the creation of a gating system consisting of mesoporous MCM-41 incorporated with spiropyran moieties (which functioned as a 3-D support) and 1.5 poly(amidoamine) dendrimers which served as naonmechanical stoppers.[40] UV light exposure resulted in the attraction of the negatively charged dendrimers to the positively charged spiropyrans in the polar conformation. This led to the entrapment of the dye molecule, $Ru(bipy)_3Cl_2$ as seen in **Figure 1.2**. However, the dendrimers and therefore the dye molecules were released to the bulk solution upon the application of visible light as spiropyran reverted to its neutrally charged non-polar conformation.

1.2.2.3 Photo-responsive Shape-memory Polymers

Shape-memory polymers can undergo reversible structural transitions in response to UV light.[41-45] These polymers are typically comprised of elastic polymeric networks and molecular switches. The polymeric network provides the support structure and determines the permanent shape while the molecular switch undergoes reversible cross-linking in the presence of a photostimulus.[46] Shape-memory polymers modulated by temperature, thermally induced shape-memory polymers, also exist. However polymers that are light actuated are advantageous in that structural changes in these materials occur

at room temperature, thereby diversifying the application scope. For example, external heating effects may damage tissue if the material was utilized in an implant. Applications for shape memory polymers include optical sensors and actuators, microrobots, optical microtweezers, and photoresponsive medical technologies.[44, 47]

Lendlein and co-workers created two types of photoresponsive shape-memory polymers. The first is a grafted polymer containing hydroxyethyl ethylene-glycol-1-acrylate-2-cinnamic acid (HEA-CA) molecules and the second is a doped star-poly (ethylene glycol) polymer network containing cinnamylidene acetic acid (CAA) molecules. Both of these materials are modulated by the application of an external force and UV light greater than 260 nm.[41] Materials were stretched from some original length and then exposed to UV irradiation. After irradiation, the polymers were fixed in an elongated state because of the [2+2] cycloaddition reaction that occurred in response to the UV exposure. This elongated state was maintained upon removal of the external force but could be reversed upon the application of UV light less than 260 nm due to crosslink cleavage. In addition, the authors found that if UV irradiation greater than 260 nm was only applied to a single side of the stretched polymer, the resulting temporary shape was that of a corkscrew spiral. The corkscrew shape occurred because two layers were formed, a top layer with a fixed elongation and a bottom layer that retained its elasticity and thus could contract upon the release of the external stress. The reversible polymer conformations are displayed in **Figure 1.3**.

1.2.3 pH-responsive Materials

Unlike several of the other stimuli considered in this chapter, pH is an internal stimulus and thus requires alteration of the chemical environment. As a result, the use of pH triggers are limited, particularly for basic cell studies which are confined to a narrow pH range. The complexity of reversibility is another drawback that arises with the use of pH responsive materials because the solution must be removed or extracted before reuse which may also alter the physical environment. Nonetheless, pH responsive materials have shown promise in fields such as drug delivery and micro-processing.[48]

1.2.3.1 pH Switchable Surfaces Based on Self-assembled Monolayers (SAMs)

As manufactured products become miniaturized, there is a need to enhance assembly processes. One of the primary issues is the interaction of the assembly tools with the surfaces forces of the object (e.s., van der Waals forces) that result in adhesion of the object to the assembly tool(s) thereby preventing object release.[49] Recently this problem has been addressed through the use of pH-modulated SAMs.[50] In this work, the micro-object (a glass microsphere) and the silica gripper tool (microcantilever) were chemically modified with SAMs consisting of aminosilane-grafted 3-(ethoxydimethylsilyl) propylamine (APDMES) and (3-aminopropyl)triethoxysilane (APTES). Both SAMs are amine-functionalized and thus can be protonated at acidic pH. The authors found that as the solution environment pH was modulated so were the attractive and repulsive forces between the tool and the micro-object. In particular, as the liquid pH was increased from acidic to basic conditions, the repulsive forces increased enabling object release. This concept could be utilized to create a submerged

microhandling tool that could grasp and release microbjects based on the solution environment.

1.2.3.2. pH Switchable Surfaces Based on Polymer Brushes

Polymer brushes are comprised of polymer chains that are tethered on one end to a solid substrate.[51, 52] Two methods are commonly employed in the synthesis of polymer brushes, grafting to and grafting from. In the grafting from approach, brushes are created via surface initiated polymerization (SIP) of the polymer chains.[53] Brushes generated in the grafting to method involve adhering pre-synthesized polymers to the substrate surface.[54] Polyelectrolyte brushes are pH-responsive materials that undergo structural changes at interfaces when their chains are charged and/or discharged because of the protonation/dissociation of acid/base groups. As a result, upon an alteration in pH, polyelectrolyte brushes transform from the swollen state to a shrunken state in which the polymer chains are collapsed.[55, 56] Tam et al., exploited this property of polyelectrolyte brushes to create a responsive interface with tunable/switchable redox properties.[57]In this system, indium tin oxide (ITO) served as the substrate and a modified poly(4-vinyl pyridine) modified with an Os-complex redox unit was grafted to the surface. At an acidic pH (pH = 4), the polymer brush was swollen and thus the redox units were in direct contact with the conducting ITO surface resulting in an active electrode. However, at a neutral pH (pH > 6), the brush was in the shrunken state which restricted the mobility of the polymer chains and therefore access of the redox units to the conducting surface yielding a non-active electrode state as indicated in **Figure 1.4**.

The pH-responsiveness of polymer brushes has also been exploited as a molecular gate. Motornov et al. created a mixed polyelectrolyte brush consisting of poly(2-vinylpyridine) (P2VP) and poly(acrylic acid) (PAA) that had switchable permeability for anions and cations.[58] In this work, ITO was used as the electrode substrate and the mixed brush was assessed via two soluble redox probes $[Fe(CN)6]^{4-}$ and $[Ru(NH3)6]^{3+}$. When the environment pH was acidic (pH < 3), the P2VP chains (which were positively charged) were permeable to the anionic probe. However the redox process for the cationic probe was prohibited resulting in a lack of transport for positively charged ions. The converse was true when the solvent environment was more neutral or basic (pH > 6). This switchable and selective gating technique has applications in drug delivery and could be utilized in biosensors.

1.2.4 Thermo-responsive Materials

Temperature variations may result in reversible changes in properties such as structural arrangement, size, solubility, and shape. Many materials designed for biomedical or biotenchnology applications are confined to a narrow temperature spectrum in order to be effective in a physiological environment. The following thermo-responsive materials will be discussed in the section that follows: poly(N-iso-propylacrylamide (PNIPAAm), polymer brushes, and shape memory polymers.

1.2.4.1. Temperature-dependent Switching Based on Poly(N-iso-propylacrylamide (PNIPAAm)

Poly(N-isopropylacrylamide) (PNIPAAm) is a widely studied thermoresponsive polymer that exhibits a lower critical solution temperature (LCST).[59, 60] Below the LCST the polymer is expanded and hydrophilic and is soluble in water. Above this critical temperature, there is an abrupt phase transition leading to a collapsed and hydrophobic polymeric structure which renders the polymer insoluble in water.[61-63] The LCST of PNIPAAm is approximately 32 °C in a solution environment and therefore operates in a physiologically relevant design space.[64, 65] In addition, fine adjustments of the LCST of this material are possible by augmenting the polymer structure. For example, the LCST can be increased by adding ionic co-monomers or formulating the polymer with salts or surfactants as pH changes may alter the repulsive forces between the co-monomers and thereby influence swelling.[66, 67] Because the LCST of the polymer can be augmented, a wealth of potential applications abound in selective protein adsorption,[68] control of cellular adhesion,[69] and drug delivery.[70-73]

Thermoresponsive polymers have been utilized in basic cell studies. For example, a PNIPAAm thiol (PNIPAAm-PEG-thiol) was synthesized and used to regulate the adhesion of cells in a microfluidic channel.[74] Fibroblasts were initially cultured at 37 °C to induce cell spreading and adhesion to the microfluidic surface. Then the temperature of the microfluidic environment was reduced to 25 °C for a period of time. After 20 minutes, cell monolayers became detached and the morphology of individual

cells was transformed to a spherical shape. Cell attachment and detachment as a function of the surface response to changing temperature is provided in **Figure 1.5**.

The thermoresponsive switching of PNIPAAm is also advantageous for the therapy of cancerous tumors. Chilkolti et al. designed a PNIPAAm polymer with an LCST of ~40 °C to be used in combination with the thermal heating of tumors.[66] The LCST was increased by incorporating increased amounts of the acrylamide (AAm) copolymer as it is hydrophilic. This enabled a polymer loaded with a small fluorescently labeled hydrophobic molecules (used to simulat a chemotherapeutic drug) to remain soluble when injected into a mouse body. However, as tumor permeability was increased by targeted heating to ~42 °C, the polymer underwent a transition to the hydrophobic state and thus aggregated in the tumor. The performance, degree of polymer localization within the heated tumor, was compared for the thermo-sensitive polymer and a thermo-insensitive control. Preferential localization of the thermoresponsive polymer was demonstrated while localization was not apparent in the control.

1.2.4.2. Temperature-dependent Switching in Polymer Brushes

In addition to pH-responsiveness, the behavior of polymer brushes may also be altered by temperature. For instance, electrochemistry induced radical polymerization was utilized to fabricate a PNIPAAm brush.[75] The authors used this PNIPAAm brush in conjunction with indium titanium oxide (ITO) to create an electrically heated electrodes (HE). Altered HEs exhibited rapid temperature increases upon heating and this temperature enhancement was reversible. The control and release properties of the HE system were then assessed by means of the model protein hemoglobin. Hemoglobin

diluted in phosphate buffered saline was exposed to the brush at 20 °C when it was in the expanding state. Upon a temperature change above the brush LCST, the brush transitioned to the shrunken state, capturing the hemoglobin molecules. The hemoglobin was released when the temperature was reduced to 20 °C. UV-Vis absorbance indicated that the hemoglobin maintained its native fold as evidenced by a characteristic absorption ban at 408 nm as seen in **Figure 1.6**.

Zhang et al. controlled the size of nanoparticles by exploiting the pH and temperature responsiveness of a poly(2-(dimethylamino)ethyl methacrylate) (PDMAEMA) brush.[76] Briefly, a PDMAEMA brush was synthesized onto a polystyrene latex nanoparticle via atom transfer radical polymerization (ATRP). Dynamic light scattering events indicated that pH changes led to temperature changes in solution which resulted in an alteration in particle size. This approach could be useful in enzyme immobilization or protein separation.

1.2.4.3. Thermo-responsive Shape Memory Polymers

Thermally induced shape memory effects occur in numerous materials including polymers, metallic alloys, and ceramics.[77-79] Lendlein and Langer synthesized degradable thermoplastics that undergo conformational changes in response to a temperature increase.[80] Polymers were comprised of oligo(ε-caprolactone) diol (OCL) which served as the switching segment and a crystallizable oligo(p-dioxanone diol) (ODX) which provided the physical cross-links. The material conformational transition from the temporary to the permanent shape was induced by heating the polymers above their transition temperature (T_{trans}) which was 41°C in this instance. Shape-memory properties

were assessed via a range of cyclic thermomechanical tests and then the polymer was utilized *in vivo*. Sutures were created from the degradable thermoplastics and used to loosely close the wound on a rat. At 41°C, the shape memory-effect was induced which resulted in a tightening of the wound sutures.

Further use of thermo-responsive shape memory polymers in the biomedical arena is found through the use of main chain liquid crystalline elastomers (MC-LCEs). The mesophase structure of MC-LCEs may be varied and Rousseau and Mather designed thermosensitive main chain smectic-LCEs.[81] These new materials incorporated two benzoate-based mesogenic groups combined with hydride-terminated poly(dimethylsiloxane) spacers. Dynamic and mechanical analysis was utilized to investigate the shape-memory effects. It was found that heating the material above the polydomain smectic-C transition temp lead to a loss of smectic ordering which caused a large increase in deformability. At this point a secondary shape can be obtained via mechanical manipulation and this shape may be maintained by cooling below the transition temperature.

1.2.5 Switchable Surfaces Based on Supramolecular Shuttles

Supramolecular machines contain a discrete number of molecular components capable of converting energy into mechanical work.[82] Like macroscopic machines, users of molecular machines are concerned with energy input, processing time, and output quality. Designers of supramolecular machines need only to look to mother nature for inspiration as several examples of these systems exist. The most significant of these natural motors include adenosine triphosphate (ATP) synthase, myosin, and kinesin.[83]

Myosin and kinesin are linear motor proteins that traverse microtubules and actin filaments respectively, converting energy from ATP hydrolysis to molecular motion.[84] Promising synthetic supramolecular assemblies for nanotechnology applications include rotaxanes and catenanes.

1.2.5.1. Rotaxane Shuttles

Like other materials included in this chapter, rotaxanes can be utilized to control the hydrophilicity and hydrophobicity on surfaces. Rotaxanes are supramolecular systems comprised of an axis molecule shaped like a dumbbell and a ring molecule identified as a macrocycle.[85] Molecular switching is ideal for rotaxane and pseudorotaxe monolayers because of the interlocking cavities contained within the monolayers.[86-90] Structures that incorporate these supramolecular machines allow programmable surfaces that can be reversibly switched to be created. One example of the use of rotaxanes in control of wettability is based on rotaxanes incorporated into SAMs.[91] The SAMs were comprised of rotaxane combined with mercaptoundecanoic acid on gold. This system was utilized to move liquid droplets in response to light-induced changes which is seen in **Figure 1.7**.

In addition to light, pH may also modulate the behavior of rotaxanes. Jun et al. created a fluorescent rotaxane in which the fluorescent intensity of the molecule was pH responsive.[92] The rotaxane was comprised of a fluorenyltriamine axle and a cucurbituril macrocyle. Nitrogen atoms in the fluorenyltriamine axle could be protonated at a low pH such as pH = 1 and this resulted in the placement of the macrocyle at the protonated diaminohexane site. Once deprotonation occurred at a high pH such as pH = 8, the

macrocycle was transported to the diprotonated diaminobutane site causing a change in color and fluorescence intensity.

Bio-electronics is another application area in which rotaxanes, particularly redox-active rotaxanes, could make a significant impact. Enzyme electrodes are altered in these applications by direct electron transfer between the electrode surface and the redox enzyme. Electronic communication between the surface and the redox enzyme centers is hindered because a separation exists. This impediment can be circumvented by aligning the enzyme with the electrode and utilizing the redox relay units as go-betweens. The aforementioned concept has been exploited to associate an apoprotein, apo-glucose oxidase (apo-GOx)), onto relay functionalized materials including (flavin adenine dinucleotide (FAD)) monolayers, nanoparticles, and carbon nanotubes with electrodes. [93-96] Katz et al. used reversible redox-active rotaxane shuttles in the bioelectrocatalyzed oxidation of glucose.[88]

1.2.5.2. Switches Based on Catenanes

Like rotaxanes, catenanes are mechanically interlocked molecules. However, instead of interlocking a one ring shaped macrocycle and a dumbbell shape, catenanes consist of interlocked macrocycles. The number of macrocycles contained in a catenane is indicated by the numeral that precedes it. Catenanes have bistable and multistable forms and a switchable, bistable [2]catenane is commonly exploited in nanotechnology and molecular electronics because its behavior can be controlled by electrochemical processes.[97] Collier et al. was the first to demonstrate the electro-activity of interlocked catenanes.[98] The authors affixed phospholipid counterions to a monolayer of [2]catenanes

and then sandwiched this system between two electrodes. This work resulted in a molecular switching device that opened at a positive potential of 2 volts and closed at a negative potential of 2 volts.

Recently, Spruell et al. synthesized and characterized a single-station [2]catenane that exhibited fundamental differences from the bi- and multi-station catenane switches that currently exist.[99] Tetrathiafulvalene (TTF) is a electrochemically switchable unit that is often incorporated into catenanes to yield architectures that can be controlled electrically. Normally, electrochemically switchable catenanes are comprised of a primary binding station consisting of tetracationic cyclophane cyclobis(paraquate-p-phenylene) ($CBQT^{4+}$) which releases oxidized TTF^{2+} via electrostatic repulsion, and a secondary binding station that provides reversibility following the release of TTF2. However, in this work a single-station [2]catenane that functions as a reversible switch between two translational states was created eliminating the need for the secondary station and thus reducing system complexity. Applications for this technology may include solid-state electronic devices.

1.2.6 Switchable Surfaces Comprised of DNA and Peptide Monolayers

The specificity of DNA base pairs is advantageous in biosensing applications such as genetic screening because it results in highly specific binding between targets of interest and probe moieties.[100-102] In addition, DNA can be analyzed with a myriad of surface analysis techniques including those that are label-free, or methods that do not require fluorescent tagging of the DNA. Some of these techniques include atomic force microscopy,[103]electrochemical methods,[104, 105] and surface plasmon resonance

spectroscopy.[106, 107] Mass, conductivity, and electric field measurements may also be utilized to characterize DNA biosensing.[108] Though DNA monolayers have attracted significant attention, peptide monolayers are beginning to gain momentum in biotechnology areas.[109] In particular, researchers are interested in utilizing these building blocks to create materials from a bottoms-up approach.

1.2.6.1 DNA based surface switches

DNA molecules can be directed by electrical potentials when tethered to electrode surfaces and this interaction is commonly exploited with gold as the substrate.[110-112] Kelley et al. was able to modulate the conformation of a thiol-modified oglionucleotide by altering electric potential exposure.[113] Originally the monolayer was 50 angstroms in length and tilted at a 45° in open-circuit voltage. Application of a negative potential resulted in an increase in monolayer thickness to 55 angstroms and a distinct orientation change. When a positive potential was applied, the thickness was decreased to 20 angstroms. Electrical modulation has been combined with fluorescence to facilitate real-time optical monitoring of switchable DNA monolayers.[114] Single-stranded oligonucleotides were labeled with a fluorophore and DNA hybridization was initialized by the addition of unlabeled complimentary strands. As a result of the phosphates in the sugar-phosphate backbone of the negatively charged oligonucleotides, the DNA monolayers can be switched from a tilted or flat conformation to a vertical conformation. This orientation difference was indicated by changes in fluorescence intensity because the tilted conformation partially quenched the fluorescence signal. The system set-up is described in **Figure 1.8**.

Electric field changes have been used in conjunction with pH changes to alter the conformation of DNA monolayers.[115-118] For example, DNA comprised of two distinct domains, one domain consisted of a single strand linked to the gold substrate and the other domain contained four strands designated as an i-motif.[115] The i-motif could be modulated by modifications to the system pH. As these DNA molecules formed a self-assembled monolayer, the i-motif functioned as a bulky headgroup, resulting in a monolayer that was densely packed with respect to the i-motif but loosely packed with respect to the single-stranded DNA. As a result of this configuration, small molecules could not penetrate the monolayer. However, upon an increase in pH the i-motif transitioned to a single-stranded conformation which increased the permeability of the system to small molecules.

1.2.6.2 Switches Based on Aptamers

An aptamer is a short, single stranded DNA and RNA sequence. These molecules typically demonstrate a high affinity to a multitude of molecules from proteins to cells.[119] The sensitivity and selectively with which aptamers bind make them promising options in diagnostic and therapeutic applications. [119, 120] Because aptamers experience reversible denaturation and regeneration, their use is particularly attractive in reusable sensing technologies.[121] Many of the potential uses for aptamers require that these molecules are immobilized to the surface. This requirement complicates their use because the retaining method employed must sustain the high binding affinity aptamers demonstrate in solution. Another challenge concerns the need to acquire a flexible, ordered receptor molecule while maintaining the appropriate aptamer folding that induces binding.

Numerous techniques are employed to study the reversible binding of aptamers and various biomolecules including cantilever-based sensors, surface plasmon resonance (SPR), and electrochemical impedance.[122] An aptamer that binds thrombin was assembled on a gold nanowire by Huang and Chen.[123] In this work, the aptamer probe was controlled by changes in electric potential and was utilized in a fluorescent protein test. The probe was affixed to the nanowire and specifically interacted with a biotinylated, fluorescently labeled thrombin. Upon the application of an electric potential, this complex was either attracted or repelled depending on the sign of the applied potential. Because the complex was negatively charge, a positive potential resulted in a reduction in the fluorescence intensity due to increased distance between the fluorescent label and the nanowire.

1.2.6.3. Switches Based on Helical Peptides

Helical peptides address a limitation of alkanethiol monolayers; that a size mismatch between the functional head group and the alkyl chain exists. With these molecules, a disulfide group acts as an anchor on one side and the functional group is present on the other side. Another unique feature of α-helical peptides is the speed of electron transfer because this speed is faster along the dipole moment of the peptides than against it. SAMs comprised of two peptide sequences, with dipole moments in opposing directions were generated by Yasutomi et al.[124] The sensitizer head groups on the helical peptides could be actuated at a precise excitation wavelength and each head group could be augmented independently. An aniodic or cathodic current was produced depending on the excitation wavelength leading to a directional change in the overall photocurrent.

Yasutomi deviated from the two peptide monolayer system and generated a single component SAM that was pH responsive.[125] The 16-mer helical peptide was composed of a pH responsive carboxyl group and a L-3-(3-N-ethylcarbazolyl)alanine at the C-terminus. For this system, changing the solution pH reversed the orientation of the photocurrent.

1.2.6.4 Switchable Surfaces of Elastin-like Polypeptides (ELP)

Elastin-like polypeptides (ELPs) are thermoresponsive biopolymers with a broad range of biotechnological applications including tissue engineering, drug delivery, biosensing, and protein purification.[126, 127] Like PNIPAAm, ELPs also experience reversible hydrophilic-hydrophobic phase transitions at a LCST. At temperatures below this LCST the peptides are soluble in aqueous environments but above this temperature the peptides become dehydrated and aggregate resulting in insolubility. Sequence $(VPGXG)_m$ serves as the common structural motif for ELPs with X being any amino acid but proline and m indicating the number of repeats. It is this structural motif that provides the polypeptides with thermosensitivity. ELP structure can be controlled via genetic engineering and thus augmentations to the peptide sequence and/or molecular weight can alter the LCST of the polypeptide.[128]

Dip pen-lithography (DPN) has been utilized to anchor ELPs to patterned monolayer on a gold surface.[129] The surface was used to investigate reversible release and binding of biomolecules of interest upon changes in temperature and ionic strength. Gao et al. synthesized ELP fusion proteins that were complexed with antibodies and then immobilized said complexes onto a hydrophobic surface to create an antibody array.[130]

Complex immobilization stemmed from hydrophobic interactions that were triggered by temperature changes. Furthermore, this method was extended to fabricate a tumor detection system by immobilizing a capture antibody for the tumor marker of interest utilizing the ELP-antibody complex as depicted in **Figure 1.9** .[130] Recently, the thermo-reversible phase properties of ELPs were utilized to generate a stimuli-responsive cell-adhesion system.[131] $[(VPGVG)_4(VPGKG)]_8[(VPGVG)]_{40,}$ a polypeptide sequence, was synthesized and then immobilized onto aldehyde-derivatized surfaces. These surfaces could then selectively control the attachment and release of fibroblasts to a substrate.

1.3 CONCLUSIONS

In this chapter, the use and means of actuation of various stimuli-responsive materials have been described in the context of creating programmable surfaces. With the ability to modulate a wide range of surface properties from hydrophobicity and hydrophilicity to structural arrangement, dynamic surfaces can be fine-tuned to address needs that span the biotechnology industry. As opportunities for innovation continue to be explored, materials and stimuli will emerge to generate more complex surface architectures with defined responses. This bodes well for the future of reactive materials.

1.4 FIGURES AND TABLES

Table 1.1. Switchable surface materials and their stimuli.

	Electrical potential	**Light**	**pH**	**Temperature**
Self-assembled monolayers (SAMs)	X		X	
Azobenzene molecules		X		
Spiropyran molecules		X		
Shape memory polymers		X		X
Brushes			X	X
Poly(N-iso-propylacrylamide) (PNIPAAm)				X
Rotaxane	X	X	X	
Catenane	X			
DNA monolayers	X		X	
Peptide monolayers	X		X	X

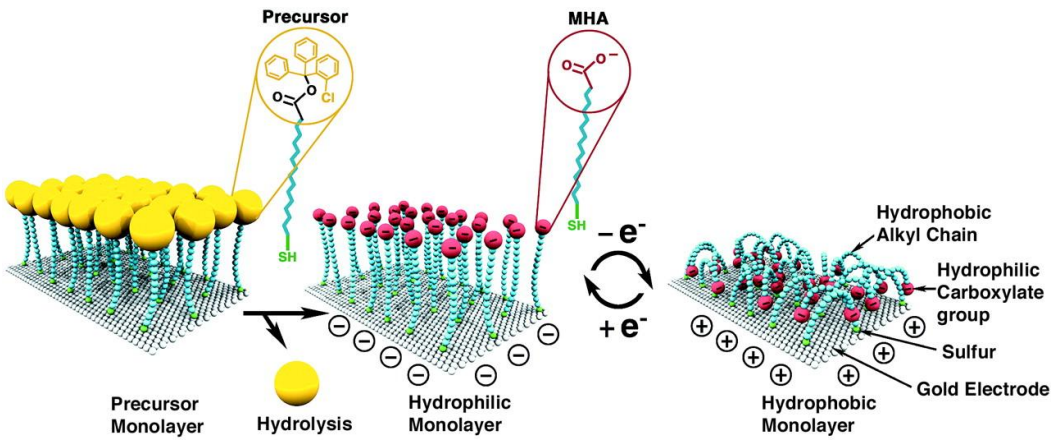

Figure 1.1.Low density self-assembled monolayer on gold response to an external electric potential. [Lahann et al. Science. 2003]

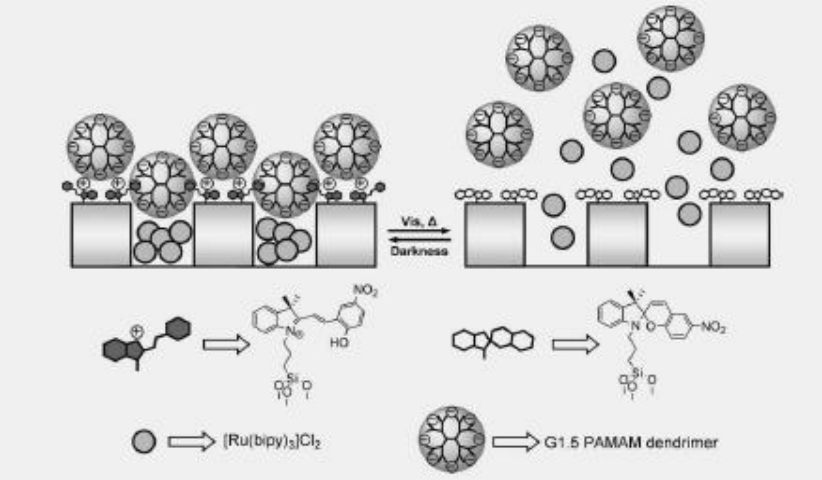

Figure 1.2. Schematic of a gating system which consisted of a mesoporous framework containing a photo-switchable anchored spiropyran, a dye entrapped in the inner pores, and carboxylate-terminated dendrimers as molecular caps. [Aznar et al. Adv. Mat. 2007]

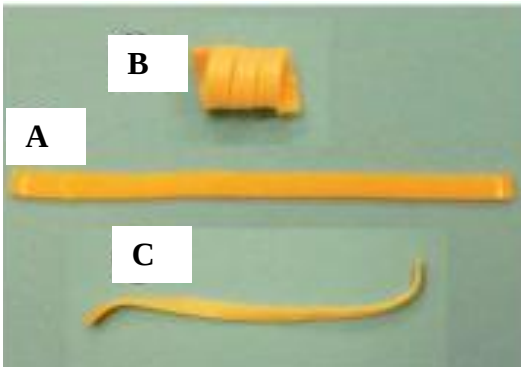

Figure 1.3. Polymer film doped with CAA molecules where (A) is the permanent shape, (B) is the temporary shape and (C) is the recovered shape. [Yu and Ikeda. Macromol.Chem. Phys. 2007]

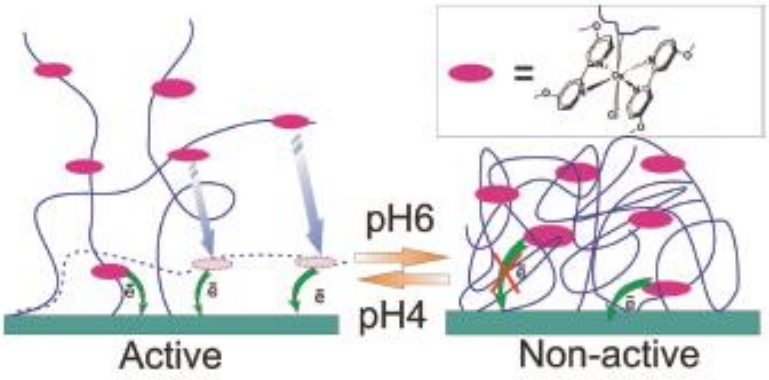

Figure 1.4. Reversible pH control of the redox-poly polymer brush between electrochemically active and inactive states. [Tam et al. J. Phys. Chem. C. 2008]

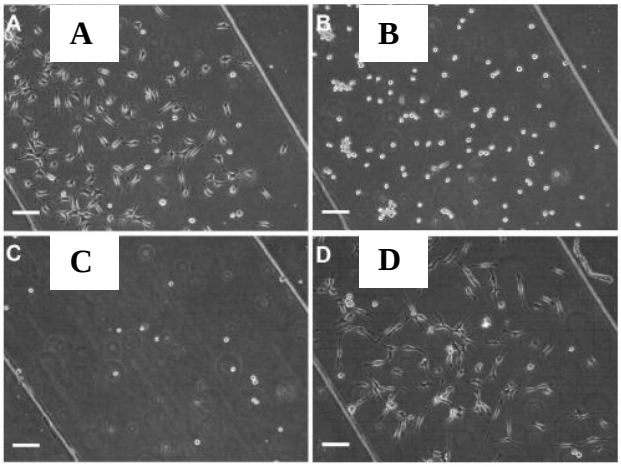

Figure 1.5. Exposure of fibroblasts on PNIPAAm-PEG coated gold surface to laminar flows in a PDMS fabricated microfluidic channel (A) fibroblasts well adhered to polymer surface at 37°C (B) cell rounding upon temperature decrease from 37°C to 25°C (C) cell detachment of rounded cells upon the application of laminar flow at 560 µm s^{-1} (D) spread cells remain attached to polymer surface in presence of 700 µm s^{-1} flow [Ernst et al. Lab Chip. 2007]

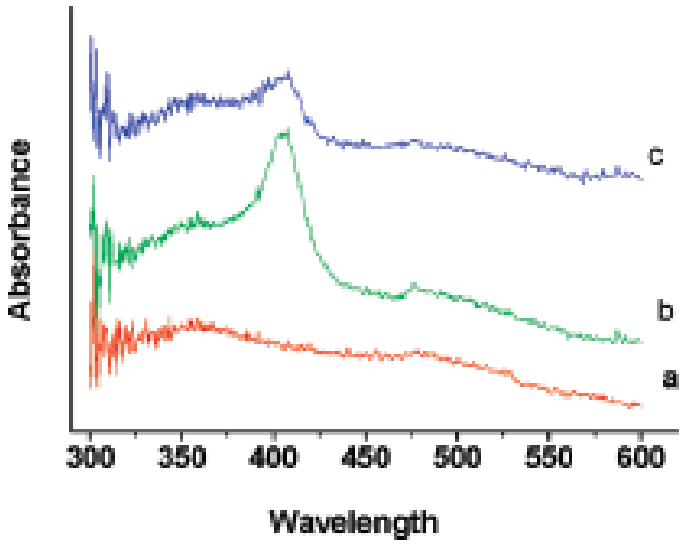

Figure 1.6. UV-Vis spectra of hemoglobin incorporated into the PNIPAAm brush (A) without hemoglobin (B) with hemoglobin at 40°C and (c) upon release of hemoglobin at 20°C [Yin et al. J. Phys. Chem. C. 2009]

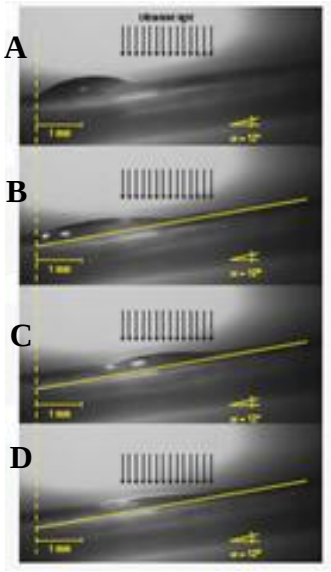

Figure 1.7. Lateral photographs of light-driven transport of a 1.25 µl diiodomethane drop on a E-1.11-MUA Au(111) substrate on mica up a 12° incline. The yellow line indicates the substrate surface. (A) before irradiation (B) after 160s of irradiation (just before transport) (C) after 245s of irradiation (just after transport) (D) after 640s irradiation (at photostationary state) [Berna et al. Nat. Mater. 2005]

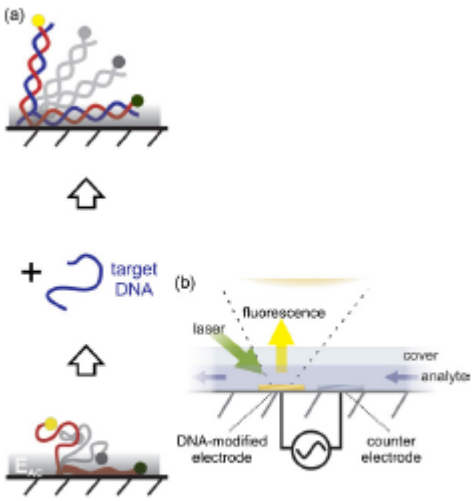

Figure 1.8. (A) Electrically controllable DNA films; (B) schematic describing the measurement setup consisting of gold electrodes modified by ss-DNA molecules and a fluidic channel containing the analyte sequences. [Rant et al. PNAS. 2007]

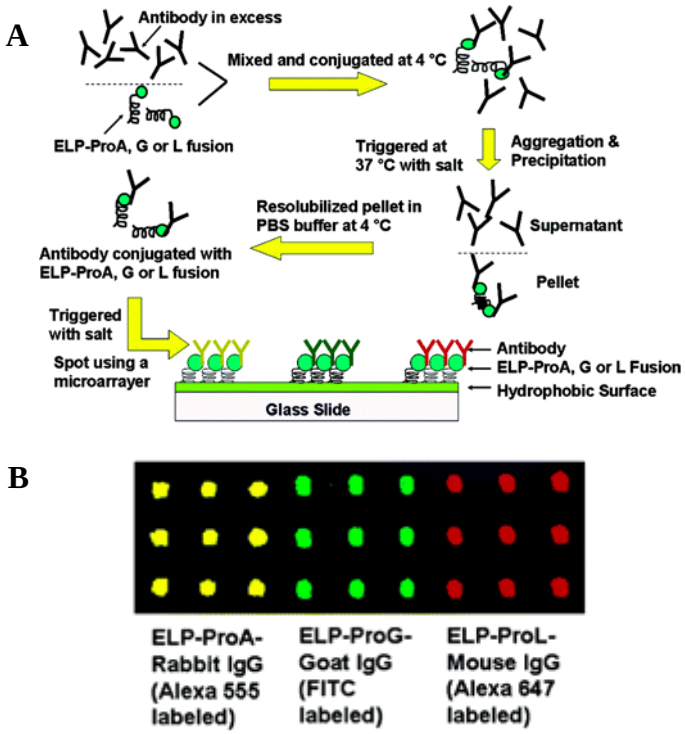

Figure 1.9. (A) Schematic illustrating the formation and purification of ELP−protein fusion−antibody complexes that are spotted onto the glass slide to fabricate antibody microarrays. (B) Fluorescence image of microarrays fabricated by immobilizing antibodies from rabbit, goat, and mouse, in complexes formed with ELP−ProA, ELP−ProG, and ELP−ProL fusions, respectively. Antibodies from rabbit, goat, and mouse are labeled with fluorophores Alexa 555, fluorescein isothiocyanate (FITC), and Alexa 647, respectively. [Gao et al. JACS. 2006]

1.5 REFERENCES

1. Cuenca, A. G.; Jiang, H. B.; Hochwald, S. N.; Delano, M.; Cance, W. G.; Grobmyer, S. R., Emerging implications of nanotechnology on cancer diagnostics and therapeutics. *Cancer* **2006,** 107, (3), 459-466.
2. Yezhelyev, M. V.; Gao, X.; Xing, Y.; Al-Hajj, A.; Nie, S. M.; O'Regan, R. M., Emerging use of nanoparticles in diagnosis and treatment of breast cancer. *Lancet Oncology* **2006,** 7, (8), 657-667.
3. Gilmore, J. L.; Yi, X.; Quan, L.; Kabanov, A. V., Novel nanomaterials for clinical neuroscience. *Journal of Neuroimmune Pharmacology* **2008,** 3, (2), 83-94.
4. Mathuria, J. P., Nanoparticles in Tuberculosis Diagnosis, Treatment and Prevention: A Hope for Future. *Digest Journal of Nanomaterials and Biostructures* **2009,** 4, (2), 309-312.
5. Xu, H.; Nguyen, K. T.; Brilakis, E. S.; Yang, J.; Fuh, E.; Banerjee, S., Enhanced Endothelialization of a New Stent Polymer Through Surface Enhancement and Incorporation of Growth Factor-Delivering Microparticles. *Journal of Cardiovascular Translational Research* **2012,** 5, (4), 519-527.
6. Chua, J. H.; Chee, R. E.; Agarwal, A.; Wong, S. M.; Zhang, G. J., Label-Free Electrical Detection of Cardiac Biomarker with Complementary Metal-Oxide Semiconductor-Compatible Silicon Nanowire Sensor Arrays. *Analytical Chemistry* **2009,** 81, (15), 6266-6271.
7. You, Z. W.; Bi, X. P.; Fan, X. Q.; Wang, Y. D., A functional polymer designed for bone tissue engineering. *Acta Biomaterialia* **2012,** 8, (2), 502-510.
8. Piskin, E., Biodegradable Polymers as Biomaterials. *Journal of Biomaterials Science-Polymer Edition* **1995,** 6, (9), 775-795.
9. Smith, R. K.; Lewis, P. A.; Weiss, P. S., Patterning self-assembled monolayers. *Progress in Surface Science* **2004,** 75, (1-2), 1-68.
10. Abbott, N. L.; Gorman, C. B.; Whitesides, G. M., Active Control of Wetting using Applied Electrical Potentials and Self-assembled Monolayers. *Langmuir* **1995,** 11, (1), 16-18.
11. Gorman, C. B.; Biebuyck, H. A.; Whitesides, G. M., Control of the Shape of Liquid Lenses on a Modified Gold Surface Using an Applied Electrical Potential Across a Self-assembled Monolayer. *Langmuir* **1995,** 11, (6), 2242-2246.
12. Abbott, N. L.; Whitesides, G. M., Potential-Dependent Wetting of Aqueous-Solutions on Self-assembled Monolayers formed from 15-(ferrocenylcarbonyl)pentadecanethiol on Gold. *Langmuir* **1994,** 10, (5), 1493-1497.
13. Berron, B.; Jennings, G. K., Loosely packed hydroxyl-terminated SAMs on gold. *Langmuir* **2006,** 22, (17), 7235-7240.
14. Wang, X. M.; Kharitonov, A. B.; Katz, E.; Willner, I., Potential-controlled molecular machinery of bipyridinium monolayer-functionalized surfaces: an electrochemical and contact angle analysis. *Chemical Communications* **2003**, (13), 1542-1543.
15. Liu, Y.; Mu, L.; Liu, B. H.; Zhang, S.; Yang, P. Y.; Kong, J. L., Controlled protein assembly on a switchable surface. *Chemical Communications* **2004**, (10), 1194-1195.

16. Peng, D. K.; Lahann, J., Chemical, electrochemical, and structural stability of low-density self-assembled monolayers. *Langmuir* **2007,** 23, (20), 10184-10189.
17. Peng, D. K.; Yu, S. T.; Alberts, D. J.; Lahann, J., Switching the Electrochemical Impedance of Low-Density Self-Assembled Monolayers&#x2020. *Langmuir* **2007,** 23, (1), 297-304.
18. Peng, D. K.; Ahmadi, A. A.; Lahann, J., A Synthetic Surface that Undergoes Spatiotemporal Remodeling. *Nano Letters* **2008,** 8, (10), 3336-3340.
19. Lahann, J.; Mitragotri, S.; Tran, T. N.; Kaido, H.; Sundaram, J.; Choi, I. S.; Hoffer, S.; Somorjai, G. A.; Langer, R., A reversibly switching surface. *Science* **2003,** 299, (5605), 371-374.
20. Yeo, W. S.; Mrksich, M., Electroactive self-assembled monolayers that permit orthogonal control over the adhesion of cells to patterned substrates. *Langmuir* **2006,** 22, (25), 10816-10820.
21. Yeo, W. S.; Yousaf, M. N.; Mrksich, M., Dynamic interfaces between cells and surfaces: Electroactive substrates that sequentially release and attach cells. *Journal of the American Chemical Society* **2003,** 125, (49), 14994-14995.
22. Barrett, C. J.; Mamiya, J. I.; Yager, K. G.; Ikeda, T., Photo-mechanical effects in azobenzene-containing soft materials. *Soft Matter* **2007,** 3, (10), 1249-1261.
23. Wan, P. B.; Jiang, Y. G.; Wang, Y. P.; Wang, Z. Q.; Zhang, X., Tuning surface wettability through photocontrolled reversible molecular shuttle. *Chemical Communications* **2008**, (44), 5710-5712.
24. Ichimura, K.; Suzuki, Y.; Seki, T.; Hosoki, A.; Aoki, K., Reversible change in alignment mode of nematic liquid crystals regulated photochemically by command surfaces modified with an azobenzene monolayer. *Langmuir* **1988,** 4, (5), 1214-1216.
25. Ichimura, K.; Oh, S. K.; Nakagawa, M., Light-driven motion of liquids on a photoresponsive surface. *Science* **2000,** 288, (5471), 1624-1626.
26. Ji, H. F.; Feng, Y.; Xu, X. H.; Purushotham, V.; Thundat, T.; Brown, G. M., Photon-driven nanomechanical cyclic motion. *Chemical Communications* **2004**, (22), 2532-2533.
27. Hayashi, G.; Hagihara, M.; Dohno, C.; Nakatani, K., Photoregulation of a Peptide-RNA Interaction on a Gold Surface. *Journal of the American Chemical Society* **2007,** 129, (28), 8678-8679.
28. Auernheimer, J.; Dahmen, C.; Hersel, U.; Bausch, A.; Kessler, H., Photoswitched Cell Adhesion on Surfaces with RGD Peptides. *Journal of the American Chemical Society* **2005,** 127, (46), 16107-16110.
29. Yoshida, M.; Lahann, J., Smart nanomaterials. *Acs Nano* **2008,** 2, (6), 1101-1107.
30. Jiang, W. H.; Wang, G. J.; He, Y. N.; Wang, X. G.; An, Y. L.; Song, Y. L.; Jiang, L., Photo-switched wettability on an electrostatic self-assembly azobenzene monolayer. *Chemical Communications* **2005**, (28), 3550-3552.
31. Siewierski, L. M.; Brittain, W. J.; Petrash, S.; Foster, M. D., Photoresponsive monolayers containing in-chain azobenzene. *Langmuir* **1996,** 12, (24), 5838-5844.
32. Wang, S. T.; Song, Y. L.; Jiang, L., Photoresponsive surfaces with controllable wettability. *Journal of Photochemistry and Photobiology C-Photochemistry Reviews* **2007,** 8, (1), 18-29.

33. Rosario, R.; Gust, D.; Garcia, A. A.; Hayes, M.; Taraci, J. L.; Clement, T.; Dailey, J. W.; Picraux, S. T., Lotus effect amplifies light-induced contact angle switching. *Journal of Physical Chemistry B* **2004,** 108, (34), 12640-12642.
34. Bunker, B. C.; Kim, B. I.; Houston, J. E.; Rosario, R.; Garcia, A. A.; Hayes, M.; Gust, D.; Picraux, S. T., Direct observation of photo switching in tethered spiropyrans using the interfacial force microscope. *Nano Letters* **2003,** 3, (12), 1723-1727.
35. Xia, F.; Zhu, Y.; Feng, L.; Jiang, L., Smart responsive surfaces switching reversibly between super-hydrophobicity and super-hydrophilicity. *Soft Matter* **2009,** 5, (2), 275-281.
36. Athanassiou, A.; Lygeraki, M. I.; Pisignano, D.; Lakiotaki, K.; Varda, M.; Mele, E.; Fotakis, C.; Cingolani, R.; Anastasiadis, S. H., Photocontrolled variations in the wetting capability of photochromic polymers enhanced by surface nanostructuring. *Langmuir* **2006,** 22, (5), 2329-2333.
37. Athanassiou, A.; Kalyva, M.; Lakiotaki, K.; Georgiou, S.; Fotakis, C., All-optical reversible actuation of photochromic-polymer microsystems. *Advanced Materials* **2005,** 17, (8), 988-+.
38. Higuchi, A.; Hamamura, A.; Shindo, Y.; Kitamura, H.; Yoon, B. O.; Mori, T.; Uyama, T.; Umezawa, A., Photon-modulated changes of cell attachments on poly(spiropyran-co-methyl methacrylate) membranes. *Biomacromolecules* **2004,** 5, (5), 1770-1774.
39. Edahiro, J.; Sumaru, K.; Tada, Y.; Ohi, K.; Takagi, T.; Kameda, M.; Shinbo, T.; Kanamori, T.; Yoshimi, Y., In situ control of cell adhesion using photoresponsive culture surface. *Biomacromolecules* **2005,** 6, (2), 970-974.
40. Aznar, E.; Casasus, R.; Garcia-Acosta, B.; Marcos, M. D.; Martinez-Manez, R., Photochemical and chemical two-channel control of functional nanogated hybrid architectures. *Advanced Materials* **2007,** 19, (17), 2228-+.
41. Lendlein, A.; Jiang, H. Y.; Junger, O.; Langer, R., Light-induced shape-memory polymers. *Nature* **2005,** 434, (7035), 879-882.
42. Yu, Y. L.; Ikeda, T., Photodeformable polymers: A new kind of promising smart material for micro- and nano-applications. *Macromolecular Chemistry and Physics* **2005,** 206, (17), 1705-1708.
43. Yamato, M.; Okano, T., Cell Sheet Engineering. *Mater Today* **2004,** 7, 42-47.
44. Yu, Y. L.; Nakano, M.; Ikeda, T., Directed bending of a polymer film by light - Miniaturizing a simple photomechanical system could expand its range of applications. *Nature* **2003,** 425, (6954), 145-145.
45. Lendlein, A.; Kelch, S., Shape-memory polymers. *Angewandte Chemie-International Edition* **2002,** 41, (12), 2034-2057.
46. Yoshida, M.; Langer, R.; Lendlein, A.; Lahann, J., From advanced biomedical coatings to multi-functionalized biomaterials. *Polymer Reviews* **2006,** 46, (4), 347-375.
47. Li, M. H.; Keller, P.; Li, B.; Wang, X. G.; Brunet, M., Light-driven side-on nematic elastomer actuators. *Advanced Materials* **2003,** 15, (7-8), 569-572.
48. Murthy, N.; Campbell, J.; Fausto, N.; Hoffman, A. S.; Stayton, P. S., Bioinspired pH-responsive polymers for the intracellular delivery of biomolecular drugs. *Bioconjugate Chemistry* **2003,** 14, (2), 412-419.

49. Gauthier, M.; Re´gnier, S.; Rougeot, P.; Chaillet, N., Analysis of forces for micromanipulations in dry and liquid media. *J. Micromechatronics* **2006,** 3, 389-413.
50. Dejeu, J. r. m.; Gauthier, M. l.; Rougeot, P.; Boireau, W., Adhesion Forces Controlled by Chemical Self-Assembly and pH: Application to Robotic Microhandling. *ACS Applied Materials & Interfaces* **2009,** 1, (9), 1966-1973.
51. Kizhakkedathu, J. N.; Norris-Jones, R.; Brooks, D. E., Synthesis of Well-Defined Environmentally Responsive Polymer Brushes by Aqueous ATRP. *Macromolecules* **2004,** 37, (3), 734-743.
52. Pyun, J.; Kowalewski, T.; Matyjaszewski, K., Synthesis of polymer brushes using atom transfer radical polymerization. *Macromolecular Rapid Communications* **2003,** 24, (18), 1043-1059.
53. Prucker, O.; Ruhe, J., Mechanism of radical chain polymerizations initiated by azo compounds covalently bound to the surface of spherical particles. *Macromolecules* **1998,** 31, (3), 602-613.
54. Ducker, R.; Garcia, A.; Zhang, J. M.; Chen, T.; Zauscher, S., Polymeric and biomacromolecular brush nanostructures: progress in synthesis, patterning and characterization. *Soft Matter* **2008,** 4, (9), 1774-1786.
55. Minko, S., Responsive polymer brushes. *Polymer Reviews* **2006,** 46, (4), 397-420.
56. Netz, R. R.; Andelman, D., Neutral and charged polymers at interfaces. *Physics Reports-Review Section of Physics Letters* **2003,** 380, (1-2), 1-95.
57. Tam, T. K.; Ornatska, M.; Pita, M.; Minko, S.; Katz, E., Polymer brush-modified electrode with switchable and tunable redox activity for bioelectronic applications. *Journal of Physical Chemistry C* **2008,** 112, (22), 8438-8445.
58. Motornov, M.; Tam, T. K.; Pita, M.; Tokarev, I.; Katz, E.; Minko, S., Switchable selectivity for gating ion transport with mixed polyelectrolyte brushes: approaching 'smart' drug delivery systems. *Nanotechnology* **2009,** 20, (43), 10.
59. Luzinov, I.; Minko, S.; Tsukruk, V. V., Adaptive and responsive surfaces through controlled reorganization of interfacial polymer layers. *Progress in Polymer Science* **2004,** 29, (7), 635-698.
60. Sheeney-Haj-Ichia, L.; Sharabi, G.; Willner, I., Control of the Electronic Properties of Thermosensitive Poly(N-isopropylacrylamide) and Au-Nano-particle/Poly(N-isopropylacrylamide) Composite Hydrogels upon Phase Transition. *Advanced Functional Materials* **2002,** 12, (1), 27-32.
61. Chung, J. E.; Yokoyama, M.; Okano, T., Inner core segment design for drug delivery control of thermo-responsive polymeric micelles. *Journal of Controlled Release* **2000,** 65, (1-2), 93-103.
62. Dimitrov, I.; Trzebicka, B.; Muller, A. H. E.; Dworak, A.; Tsvetanov, C. B., Thermosensitive water-soluble copolymers with doubly responsive reversibly interacting entities. *Progress in Polymer Science* **2007,** 32, (11), 1275-1343.
63. Dreher, M. R.; Simnick, A. J.; Fischer, K.; Smith, R. J.; Patel, A.; Schmidt, M.; Chilkoti, A., Temperature triggered self-assembly of polypeptides into multivalent spherical micelles. *Journal of the American Chemical Society* **2008,** 130, (2), 687-694.
64. Yamada, N.; Okano, T.; Sakai, H.; Karikusa, F.; Sawasaki, Y.; Sakurai, Y., Thermoresponsive Polymeric Surfaces - Control of Attachment and Detachment of

Cultured-cells. *Makromolekulare Chemie-Rapid Communications* **1990,** 11, (11), 571-576.
65. Sun, T. L.; Wang, G. J.; Feng, L.; Liu, B. Q.; Ma, Y. M.; Jiang, L.; Zhu, D. B., Reversible switching between superhydrophilicity and superhydrophobicity. *Angewandte Chemie-International Edition* **2004,** 43, (3), 357-360.
66. Chilkoti, A.; Dreher, M. R.; Meyer, D. E.; Raucher, D., Targeted drug delivery by thermally responsive polymers. *Advanced Drug Delivery Reviews* **2002,** 54, (5), 613-630.
67. Eliassaf, J., Aqueous-Solutions of Poly(N-Isopropylacrylamide). *Journal of Applied Polymer Science* **1978,** 22, (3), 873-874.
68. Huber, D. L.; Manginell, R. P.; Samara, M. A.; Kim, B. I.; Bunker, B. C., Programmed adsorption and release of proteins in a microfluidic device. *Science* **2003,** 301, (5631), 352-354.
69. Yamato, M.; Konno, C.; Utsumi, M.; Kikuchi, A.; Okano, T., Thermally responsive polymer-grafted surfaces facilitate patterned cell seeding and co-culture. *Biomaterials* **2002,** 23, (2), 561-567.
70. Yoshida, R.; Kaneko, Y.; Sakai, K.; Okano, T.; Sakurai, Y.; Bae, Y. H.; Kim, S. W., Positive Thermosensitive Pulsatile Drug-release using Negative Thermosensitive Hydrogels. *Journal of Controlled Release* **1994,** 32, (1), 97-102.
71. Kavanagh, C. A.; Rochev, Y. A.; Gallagher, W. A.; Dawson, K. A.; Keenan, A. K., Local drug delivery in restenosis injury: thermoresponsive co-polymers as potential drug delivery systems. *Pharmacology & Therapeutics* **2004,** 102, (1), 1-15.
72. Kikuchi, A.; Okano, T., Pulsatile drug release control using hydrogels. *Advanced Drug Delivery Reviews* **2002,** 54, (1), 53-77.
73. Kost, J.; Langer, R., Responsive polymeric delivery systems. *Advanced Drug Delivery Reviews* **2001,** 46, (1-3), 125-148.
74. Ernst, O.; Lieske, A.; Jager, M.; Lankenau, A.; Duschl, C., Control of cell detachment in a microfluidic device using a thermo-responsive copolymer on a gold substrate. *Lab on a Chip* **2007,** 7, (10), 1322-1329.
75. Yin, Z. Z.; Zhang, J. J.; Jiang, L. P.; Zhu, J. J., Thermosensitive Behavior of Poly(N-isopropylacrylamide) and Release of Incorporated Hemoglobin. *Journal of Physical Chemistry C* **2009,** 113, (36), 16104-16109.
76. Zhang, M.; Liu, L.; Zhao, H.; Yang, Y.; Fu, G.; He, B., Double-responsive polymer brushes on the surface of colloid particles. *Journal of Colloid and Interface Science* **2006,** 301, (1), 85-91.
77. Kagami, Y.; Gong, J. P.; Osada, Y., Shape memory behaviors of crosslinked copolymers containing stearyl acrylate. *Macromolecular Rapid Communications* **1996,** 17, (8), 539-543.
78. Swain, M. V., Shape Memory Behavior in Partially-stabilized Zirconia Ceramics. *Nature* **1986,** 322, (6076), 234-236.
79. Lendlein, A.; Schmidt, A. M.; Langer, R., AB-polymer networks based on oligo(epsilon-caprolactone) segments showing shape-memory properties. *Proceedings of the National Academy of Sciences of the United States of America* **2001,** 98, (3), 842-847.
80. Lendlein, A.; Langer, R., Biodegradable, elastic shape-memory polymers for potential biomedical applications. *Science* **2002,** 296, (5573), 1673-1676.

81. Rousseau, I. A.; Mather, P. T., Shape memory effect exhibited by smectic-c liquid crystalline elastomers. *Journal of the American Chemical Society* **2003,** 125, (50), 15300-15301.
82. Balzani, V.; Credi, A.; Ferrer, B.; Silvi, S.; Venturi, M., Artificial molecular motors and machines: Design principles and prototype systems. In *Molecular Machines*, Springer-Verlag Berlin: Berlin, 2005; Vol. 262, pp 1-27.
83. Schliwa, M.; Woehlke, G., Molecular motors. *Nature* **2003,** 422, (6933), 759-765.
84. Vale, R. D.; Milligan, R. A., The way things move: Looking under the hood of molecular motor proteins. *Science* **2000,** 288, (5463), 88-95.
85. Kay, E. R.; Leigh, D. A.; Zerbetto, F., Synthetic molecular motors and mechanical machines. *Angewandte Chemie-International Edition* **2007,** 46, (1-2), 72-191.
86. Balzani, V.; Credi, A.; Venturi, M., Molecular machines working on surfaces and at interfaces. *Chemphyschem* **2008,** 9, (2), 202-220.
87. Hiratani, K.; Kaneyama, M.; Nagawa, Y.; Koyama, E.; Kanesato, M., Synthesis of [1]rotaxane via covalent bond formation and Its unique fluorescent response by energy transfer in the presence of lithium ion. *Journal of the American Chemical Society* **2004,** 126, (42), 13568-13569.
88. Katz, E.; Lioubashevsky, O.; Willner, I., Electromechanics of a redox-active rotaxane in a monolayer assembly on an electrode. *Journal of the American Chemical Society* **2004,** 126, (47), 15520-15532.
89. Fioravanti, G.; Haraszkiewicz, N.; Kay, E. R.; Mendoza, S. M.; Bruno, C.; Marcaccio, M.; Wiering, P. G.; Paolucci, F.; Rudolf, P.; Brouwer, A. M.; Leigh, D. A., Three state redox-active molecular shuttle that switches in solution and on a surface. *Journal of the American Chemical Society* **2008,** 130, (8), 2593-2601.
90. Bunker, B. C.; Huber, D. L.; Kushmerick, J. G.; Dunbar, T.; Kelly, M.; Matzke, C.; Cao, J. G.; Jeppesen, J. O.; Perkins, J.; Flood, A. H.; Stoddart, J. F., Switching surface chemistry with supramolecular machines. *Langmuir* **2007,** 23, (1), 31-34.
91. Berna, J.; Leigh, D. A.; Lubomska, M.; Mendoza, S. M.; Perez, E. M.; Rudolf, P.; Teobaldi, G.; Zerbetto, F., Macroscopic transport by synthetic molecular machines. *Nature Materials* **2005,** 4, (9), 704-710.
92. Jun, S. I.; Lee, J. W.; Sakamoto, S.; Yamaguchi, K.; Kim, K., Rotaxane-based molecular switch with fluorescence signaling. *Tetrahedron Letters* **2000,** 41, (4), 471-475.
93. Willner, I.; Heleg-Shabtai, V.; Blonder, R.; Katz, E.; Tao, G.; Buckmann, A. F.; Heller, A., Electrical wiring of glucose oxidase by reconstitution of FAD-modified monolayers assembled onto Au-electrodes. *Journal of the American Chemical Society* **1996,** 118, (42), 10321-10322.
94. Katz, E.; Riklin, A.; Heleg-Shabtai, V.; Willner, I.; Bückmann, A. F., Glucose oxidase electrodes via reconstitution of the apo-enzyme: tailoring of novel glucose biosensors. *Analytica Chimica Acta* **1999,** 385, (1-3), 45-58.
95. Xiao, Y.; Patolsky, F.; Katz, E.; Hainfield, J. F.; Willner, I., Plugging into enzymes: nanowiring of redox enzymes by a gold nanoparticle *Science* **2003,** 299, 1877-1881.

96. Patolsky, F.; Weizmann, Y.; Willner, I., Long-range electrical contacting of redox enzymes by SWCNT connectors. *Angewandte Chemie-International Edition* **2004,** 43, (16), 2113-2117.
97. Flood, A. H.; Ramirez, R. J. A.; Deng, W. Q.; Muller, R. P.; Goddard, W. A.; Stoddart, J. F., Meccano on the nanoscale - A blueprint for making some of the world's tiniest machines. *Australian Journal of Chemistry* **2004,** 57, (4), 301-322.
98. Collier, C. P.; Mattersteig, G.; Wong, E. W.; Luo, Y.; Beverly, K.; Sampaio, J.; Raymo, F. i. M.; Stoddart, J. F.; Heath, J. R., A [2]Catenane-Based Solid State Electronically Reconfigurable Switch. *Science* **2000,** 289, (5482), 1172-1175.
99. Spruell, J. M.; Paxton, W. F.; Olsen, J. C.; Benitez, D.; Tkatchouk, E.; Stern, C. L.; Trabolsi, A.; Friedman, D. C.; Goddard, W. A.; Stoddart, J. F., A Push-Button Molecular Switch. *Journal of the American Chemical Society* **2009,** 131, (32), 11571-11580.
100. Cosnier, S.; Mailley, P., Recent advances in DNA sensors. *Analyst* **2008,** 133, (8), 984-991.
101. Daniels, J. S.; Pourmand, N., Label-free impedance biosensors: Opportunities and challenges. *Electroanalysis* **2007,** 19, (12), 1239-1257.
102. Odenthal, K. J.; Gooding, J. J., An introduction to electrochemical DNA biosensors. *Analyst* **2007,** 132, (7), 603-610.
103. Wang, K.; Goyer, C.; Anne, A.; Demaille, C., Exploring the motional dynamics of end-grafted DNA oligonucleotides by in situ electrochemical atomic force microscopy. *Journal of Physical Chemistry B* **2007,** 111, (21), 6051-6058.
104. Drummond, T. G.; Hill, M. G.; Barton, J. K., Electrochemical DNA sensors. *Nature Biotechnology* **2003,** 21, (10), 1192-1199.
105. Meng, F. B.; Liu, Y. X.; Liu, L.; Li, G. X., Conformational Transitions of Immobilized DNA Chains Driven by pH with Electrochemical Output. *Journal of Physical Chemistry B* **2009,** 113, (4), 894-896.
106. Georgiadis, R.; Peterlinz, K. P.; Peterson, A. W., Quantitative measurements and modeling of kinetics in nucleic acid monolayer films using SPR spectroscopy. *Journal of the American Chemical Society* **2000,** 122, (13), 3166-3173.
107. Yang, X. H.; Wang, Q.; Wang, K. M.; Tan, W. H.; Yao, J.; Li, H. M., Electrical switching of DNA monolayers investigated by surface plasmon resonance. *Langmuir* **2006,** 22, (13), 5654-5659.
108. Immoos, C. E.; Lee, S. J.; Grinstaff, M. W., Conformationally gated electrochemical gene detection. *Chembiochem* **2004,** 5, (8), 1100-1103.
109. Chow, D.; Nunalee, M. L.; Lim, D. W.; Simnick, A. J.; Chilkoti, A., Peptide-based biopolymers in biomedicine and biotechnology. *Materials Science & Engineering R-Reports* **2008,** 62, (4), 125-155.
110. Rant, U.; Arinaga, K.; Tornow, M.; Kim, Y. W.; Netz, R. R.; Fujita, S.; Yokoyama, N.; Abstreiter, G., Dissimilar kinetic behavior of electrically manipulated single- and double-stranded DNA tethered to a gold surface. *Biophysical Journal* **2006,** 90, (10), 3666-3671.
111. Rant, U.; Arinaga, K.; Fujita, S.; Yokoyama, N.; Abstreiter, G.; Tornow, M., Electrical manipulation of oligonucleotides grafted to charged surfaces. *Organic & Biomolecular Chemistry* **2006,** 4, (18), 3448-3455.

112. Rant, U.; Arinaga, K.; Fujita, S.; Yokoyama, N.; Abstreiter, G.; Tornow, M., Dynamic electrical switching of DNA layers on a metal surface. *Nano Letters* **2004,** 4, (12), 2441-2445.
113. Kelley, S. O.; Barton, J. K.; Jackson, N. M.; McPherson, L. D.; Potter, A. B.; Spain, E. M.; Allen, M. J.; Hill, M. G., Orienting DNA helices on gold using applied electric fields. *Langmuir* **1998,** 14, (24), 6781-6784.
114. Rant, U.; Arinaga, K.; Scherer, S.; Pringsheim, E.; Fujita, S.; Yokoyama, N.; Tornow, M.; Abstreiter, G., Switchable DNA interfaces for the highly sensitive detection of label-free DNA targets. *Proceedings of the National Academy of Sciences of the United States of America* **2007,** 104, (44), 17364-17369.
115. Mao, Y. D.; Liu, D. S.; Wang, S. T.; Luo, S. N.; Wang, W. X.; Yang, Y. L.; Qi, Q. Y.; Lei, J., Alternating-electric-field-enhanced reversible switching of DNA nanocontainers with pH. *Nucleic Acids Research* **2007,** 35, (5), 8.
116. Wang, S. T.; Liu, H. J.; Liu, D. S.; Ma, X. Y.; Fang, X. H.; Jiang, L., Enthalpy-driven three-state switching of a superhydrophilic/superhydrophobic surface. *Angewandte Chemie-International Edition* **2007,** 46, (21), 3915-3917.
117. Liedl, T.; Olapinski, M.; Simmel, F. C., A surface-bound DNA switch driven by a chemical oscillator. *Angewandte Chemie-International Edition* **2006,** 45, (30), 5007-5010.
118. Mao, Y. D.; Chang, S.; Yang, S. X.; Ouyang, Q.; Jiang, L., Tunable non-equilibrium gating of flexible DNA nanochannels in response to transport flux. *Nature Nanotechnology* **2007,** 2, (6), 366-371.
119. Balamurugan, S.; Obubuafo, A.; Soper, S. A.; Spivak, D. A., Surface immobilization methods for aptamer diagnostic applications. *Analytical and Bioanalytical Chemistry* **2008,** 390, (4), 1009-1021.
120. Mok, W.; Li, Y. F., Recent Progress in Nucleic Acid Aptamer-Based Biosensors and Bioassays. *Sensors* **2008,** 8, (11), 7050-7084.
121. Song, S. P.; Wang, L. H.; Li, J.; Zhao, J. L.; Fan, C. H., Aptamer-based biosensors. *Trac-Trends in Analytical Chemistry* **2008,** 27, (2), 108-117.
122. Rodriguez, M. C.; Kawde, A. N.; Wang, J., Aptamer biosensor for label-free impedance spectroscopy detection of proteins based on recognition-induced switching of the surface charge. *Chemical Communications* **2005**, (34), 4267-4269.
123. Huang, S. X.; Chen, Y., Ultrasensitive fluorescence detection of single protein molecules manipulated electrically on Au nanowire. *Nano Letters* **2008,** 8, (9), 2829-2833.
124. Yasutomi, S.; Morita, T.; Imanishi, Y.; Kimura, S., A molecular photodiode system that can switch photocurrent direction. *Science* **2004,** 304, (5679), 1944-1947.
125. Yasutomi, S.; Morita, T.; Kimura, S., pH-Controlled switching of photocurrent direction by self-assembled monolayer of helical peptides. *Journal of the American Chemical Society* **2005,** 127, (42), 14564-14565.
126. Simnick, A. J.; Lim, D. W.; Chow, D.; Chilkoti, A., Biomedical and biotechnological applications of elastin-like polypeptides. *Polymer Reviews* **2007,** 47, (1), 121-154.

127. Chilkoti, A.; Christensen, T.; MacKay, J. A., Stimulus responsive elastin biopolymers: applications in medicine and biotechnology. *Current Opinion in Chemical Biology* **2006,** 10, (6), 652-657.
128. Meyer, D. E.; Chilkoti, A., Purification of recombinant proteins by fusion with thermally-responsive polypeptides. *Nature Biotechnology* **1999,** 17, (11), 1112-1115.
129. Hyun, J.; Lee, W. K.; Nath, N.; Chilkoti, A.; Zauscher, S., Capture and release of proteins on the nanoscale by stimuli-responsive elastin-like polypeptide "switches". *Journal of the American Chemical Society* **2004,** 126, (23), 7330-7335.
130. Gao, D.; McBean, N.; Schultz, J. S.; Yan, Y. S.; Mulchandani, A.; Chen, W. F., Fabrication of antibody arrays using thermally responsive elastin fusion proteins. *Journal of the American Chemical Society* **2006,** 128, (3), 676-677.
131. Na, K.; Jung, J.; Kim, O.; Lee, J.; Lee, T. G.; Park, Y. H.; Hyun, J., "Smart" biopolymer for a reversible stimuli-responsive platform in cell-based biochips. *Langmuir* **2008,** 24, (9), 4917-4923.

CHAPTER 2

SURFACE MODIFICATIONS: BIOMOLECULAR INTERACTIONS AND CHEMICAL VAPOR DEPOSITION POLYMERIZATION

Some of the material in this chapter has been adapted with minor modifications from the following article which is being submitted for publication:

Ross, A.M. and Lahann, J. "Surface Engineering the Cellular Microenvironment via Patterning and Gradients," In Preparation.

2.1 BIOMOLECULAR INTERACTIONS WITH SYNTHETIC SURFACES

The previous chapter highlighted surface modification approaches based on switchable surfaces and detailed their uses in biotechnology. Biomolecular interactions with synthetic surfaces are important in a variety of biotechnology fields including medical device implants, sensors, and tissue engineering.[1] The extent of these interactions can impact medical device performance/lifetime, modulate cell form and function, and indicate disease states. Both physical and chemical factors impact these interactions and surfaces may be tuned to generate a wide array of biochemical and topographical properties. In particular, the influence of molecular motifs, surface roughness, topography, and hydrophilicity/hydrophobicity of polymeric surfaces generated by chemical vapor deposition (CVD) polymerization are investigated in this dissertation research.

2.2 OBJECTIVES OF THIS WORK

This dissertation research focuses on surface modifications with reactive polymer coatings for sensing, tissue engineering, and "click" chemistry applications. Within the broad framework of surface modifications for biomedical applications, this work aims to:

1. Fabricate and evaluate polymeric substrates as platforms for spatially-resolved, quantitative, biomolecular sensing arrays.

Hypothesis: Reactive CVD coatings may be made sufficiently thin to display functionality (discernment of physiologically relevant biomolecular concentrations) as a sensor in a commonly utilized label-free analytical tool

2. Develop reactive polymer coatings as platforms for thiol-based "click" chemistry reactions.

Hypothesis: Use of reactive CVD coatings extends the utility of thiol-based"click" chemistry reactions by increasing the number of available substrates

3. Create and characterize polymers as defined environments for human pluripotent stem cell culture.

Hypothesis: Altering the physico-chemical properties of cell culture substrates influences stem cell morphology and function

Surface modification strategies described in the following chapters enhance the materials toolbox for scientists and engineers engaged in biomaterials design.

2.3 CHEMICAL VAPOR DEPOSITION POLYMERIZATION

Chemical vapor deposition (CVD) polymerization is a versatile materials platform. Originally pioneered by Gorham et al., this process occurs under vacuum (~0.3 mbar) and consists of sublimating a monomer, decomposing the monomer at high

temperature to create free radicals, and then spontaneous polymerization onto a substrate typically maintained at or below ambient temperature.[2] In this instance, the precursor material is a functionalized [2.2]paracyclophane which is converted into poly(*p*-xylylene) (PPX) as a result of the CVD process. The CVD system consists of sublimation and pyrolysis zones as well as a deposition chamber. A depiction of the CVD set-up and process is provided in **Figure 2.1**. The substrate in the deposition chamber is rotated at a defined rate throughout the deposition process to ensure a homogenous coating. CVD polymerization of [2.2]paracyclophanes and its derivatives do not require a catalyst or an initiator and results in thin, conformal coatings.[3] Because the process is solvent-free, potential impurities in the solvent cannot contaminate the polymerization process.[4] Furthermore, polymerization is substrate independent as free radicals from the CVD monomers are adsorbed onto the surface, becoming polymer chains as they are propagated. However, the monomers can be desorbed from the surface and back into the atmosphere, thus limiting the propagation rate.[5] By maintaining the substrate at or below room temperature, temperature sensitive materials such as paper or low-temperature microelectromechanical systems (MEMS) devices may be coated with CVD films.

In general, the thickness of the coating on a given substrate decreases as substrate temperature increases, as a result of more monomers being desorbed from the surface. The thickness and properties of the films generated from this technique are dependent on the type and amount of starting material, deposition rate, rotation speed of the substrate on which the material is being deposited, as well as the pyrolysis, sublimation, and substrate temperatures. This technique is advantageous because it affords control of film composition and architecture, is accurate, highly adhesive, substrate-independent, and

solvent free. Because these surfaces are readily modified with biomolecules, CVD films have numerous applications. For example, Elkasabi et al., created a cellular transduction gradient by co-depositing two functionalized CVD films with varied reactivity towards an adenovirus that was subsequently immobilized on the surface.[6] Furthermore, a multitude of functionalized CVD films have been created and utilized for surface modification including ketones[7, 8], anhydrides[9], amines[10], esters[11], bromides[12], alkynes[13], and alcohols.[6] A listing of these functionalized coatings is provided in **Figure 2.2**. Additionally, parylenes have good elasticity, biostability and biocompatibility.[14, 15] Furthermore the FDA has already recognized PPX derivatives, such as Parylene C and Parylene N as Class VI polymers, indicating their suitability for biomedical applications. These films could be useful in applications such as microfluidic cell sensing[16, 17], microseparators for DNA[18] and proteins[19], and micro-electrical-mechanical systems (MEMS) devices.[20]

2.4 SURFACE MODIFICATION OF CHEMICAL VAPOR DEPOSITION SUBSTRATES

As technology has advanced, so has the need for micro- and nanostructured surfaces. For example, wet processing techniques are used to create patterns in organic materials for high performance optoelectronics,[21] while photolithography is used to pattern photo-sensitive hydrogels for tissue engineering applications.[22] A myriad of patterning techniques have been utilized to spatially control the immobilization of biomolecules such as proteins, DNA, and polysaccharides.[23] In general, the immobilization of biomolecules may be categorized as occurring through physisorption or covalent attachment.[24] Covalent attachment is more beneficial if long-term attachment

or stability is needed. Furthermore, physisorption may not provide the same level of molecular control as covalent attachment. As a result, covalent attachment of biomolecules has emerged as a promising technique in biomolecular patterning. However, the covalent attachment of biomolecules requires flexible binding substrates with an affinity for the biomolecules of interest. With a wide range of chemical functionalities, CVD coatings are well-suited for surface micro-nano-structuring with various ligands. Several of the techniques that have been employed in the surface modification of CVD films via micro-nanostructuring will be described in the sections that follow.

2.4.1 Soft Lithography

Soft lithography is based on the printing and molding of elastomeric stamps. [25] In this instance, the elastomeric stamp is patterned from a replica mold generated using microfabrication.[26] After the elastomeric stamp is created, it is "inked" with a molecule of interest and then brought into physical contact with a substrate. Replica molds, or masters, can be patterned with a range of geometries though the feature size is limited by the resolution of the photomask used to create the mold and the diffusion of the inks utilized.[27, 28] Elastomeric stamps are advantageous for patterning large areas simultaneously; however multiple inks may not be printed concurrently as only one ink may be coated at a time.

Microcontact printing (μCP) is a widely used soft lithographic technique that has been used to surface modify CVD coatings.[7, 9, 10] For this use, elastomeric stamps are comprised of poly (dimethylsiloxane) (PDMS) and inked with the desired linker

molecule.[29] For example, Nandivada et al., used μCP to pattern hydrazide linkers to an aldehyde functionalized CVD film.[30] Patterned hydrazide moieties served as binding partners for the subsequent immobilization of a polysaccharide, 2-α-mannobiose, via an alkyl-hydrazide linkage, which further reacted with the formyl groups on the disaccharide. Microcontact printing has also been used to pattern functionalized CVD coatings comprised of alkynes[31], pentafluorophenolesters[32], and perfluorinated ketones[7] for "click" chemistry, biomedical, and surface energy applications respectively.

2.4.2 Vapor-Assisted Micropatterning Replica Structures (VAMPIR)

Similar to microcontact printing, vapor assisted micropatterning in replica structures (VAMPIR) may be used to microengineer CVD films. With this technique, portions of the substrate are masked during the chemical vapor deposition process, generating chemical and topological surface microstructures.[33] Though seemingly straightforward, this process had to overcome several challenges including transport-limitations which may inhibit deposition into micron-sized capillaries. VAMPIR structures (or microstencils) comprised of PDMS are used to mask part of the substrate surface such that functionalized coatings are deposited in the unmasked area. Previously, this process was used to pattern poly[(*p*-xylylene-4-methyl-2-bromoisobutyrate)-*co*-(*p*-xylylene)] CVD films which can serve as an initiator coating for the polymerization of a protein resistant hydrogel. Now that areas of the substrate had been passivated, a cell adhesive protein was adsorbed to the previously masked areas, resulting in cell-adhesive and non-adhesive substrate regions. This enabled the spatially-selective culture of murine fibroblasts.[12]

More recently, VAMPIR was used to co-deposit two alkyne functionalized CVD coatings for subsequent bio-orthogonal click chemistry reactions.[34] One of the alkynes, poly[4-ethynyl-p-xylylene-co-p-xylylene] , required a copper catalyst to undergo the Huisgen 1,3 dipolar cycloaddition while the other, poly[(p-xylylene-4-methyl propiolate)-co-p-xylylene], could react under benign conditions without the copper catalyst. In this instance, the VAMPIR process facilitated the creation of a multifunctional surface which may be utilized when there is need for controlled immobilization of multiple ligands.

2.4.3 Projection Lithography

A clean room and expensive equipment are typically needed for conventional photolithographic processing. As a result, the process can be cost prohibitive if such facilities are not readily accessible. Conversely, several photolithographic techniques that obviate the need for clean room facilities have emerged including transparency-based photolithography[35] and microscope projection photolithography.[36] The benefits of photolithography include high resolution (on the order of 1μm or less) and the capability to generate varied patterns over a large surface area. Therefore, it is beneficial to have a materials platform that is compatible with projection lithography and surface topologies have been created on CVD films using this technique.

First, a photoreactive polymer, poly[4-benzoyl-*p*-xylylene-co-*p*-xylylene], is deposited via CVD onto colloidal particles.[37] Like some of the switchable materials described in Chapter 1, this functionalized coating is photoreactive. Reactivity occurs at a 365 nm wavelength and spatially resolved patches are generated via the selective illumination of the CVD-coated colloids. For this work, a digital micomirror device

(DMD) is used to mask areas of the colloid such that only photo-illuminated areas will undergo the photochemical conversion of the carbon-oxygen double bond from a single ground state to the triplet state resulting in a patterned substrate. These patterned areas may be further surface modified with biomolecules for molecular self-assembly.

2.4.4 Dip Pen Lithography

Dip pen lithography (DPN) is commonly utilized as a direct writing approach. In this method, an atomic force microscopy (AFM) probe is inked with a solution that has chemical affinity for a given surface, with patterns being generated by bringing the probe in contact with the surface.[38] Contact or tapping mode may be used to scan the inked AFM probe across the substrate surface.[39] A host of factors influence printing quality and specificity such as humidity, tip geometry, writing speed, contact time between the tip and substrate, and the material properties of the ink and substrate.[40, 41] DPN is advantageous over methods such as microcontact printing in that it allows direct writing of different molecules within a nanostructure, thereby generating complex surface architectures.[42] Additionally, a broad range of inks, from small organic molecules to biomolecules can be printed with this technique (i.e. thiols, proteins, etc).[43] Recall from Chapter 1, that DPN has been used to pattern temperature responsive elastin-like polypeptides (ELPs).[44] Furthermore, this technique has the ability to simultaneously write multiple patterns over a large surface area resulting in large pin DPN arrays being created. As a result, DPN is a viable option for high throughput patterning applications. However, this technique is limited in terms of the number of substrate/ink combinations that are compatible with the DPN process. Furthermore, silicon and gold substrates are

commonly utilized and these model substrates are not as biomedically relevant or technically useful.

Thus, Chen et al., extended the utility of DPN by enhancing the number of available binding substrates through the use of a functionalized CVD coating.[45] The substrates selected had variable material properties in terms of elasticity, roughness, and wettability. For example, elasticity ranged from soft substrates such as PDMS to hard surfaces like glass while smooth surfaces such as poly(methyl methacrylate) (PMMA) and rough surfaces such as stainless steel were evaluated. In this instance, substrates were first modified via the CVD polymerization of 4-ethynyl[2.2]paracyclophane. This alkyne functionalized CVD film is reactive with azide terminated molecules through a "click" chemistry reaction, specifically a Husigen 1,3-dipolar cycloaddition, and this was exploited to attach fluorescently labeled azide moieties. The quality of the patterning is assessed via fluorescence intensity profiles of the patterned area. DPN was successful on all of the substrate types and patterning quality was only slightly reduced on the roughest samples. Additionally, this process was evaluated as a platform for molecular self-assembly when a biotinylated azide used as the DPN ink was used to direct the self-assembly of streptavidin-conjugated gold nanoparticles.

2.5 OVERVIEW OF THE DISSERTATION

Chapter 3 describes the use of a ketone-functionalized CVD coating as a spatially-resolved binding array for a cascade of biomolecules.

Chapter 4 demonstrates the generation of multifunctional surfaces (using bromine-, bromomaleimide-, and furan-functionalized CVD coatings as the base platform) via the use of "click" chemistry and atom transfer radical polymerization.

Chapter 5 analyzes synthetic substrates currently available for the long-term culture of human pluripotent stem cells and develops design criteria for future substrates.

Chapter 6 reports the influence of the material properties of a zwitterionic hydrogel on the culture of human pluripotent stem cells.

Chapter 7 concludes the dissertation and discusses future research directions based on the findings in this work.

2.6 FIGURES AND TABLES

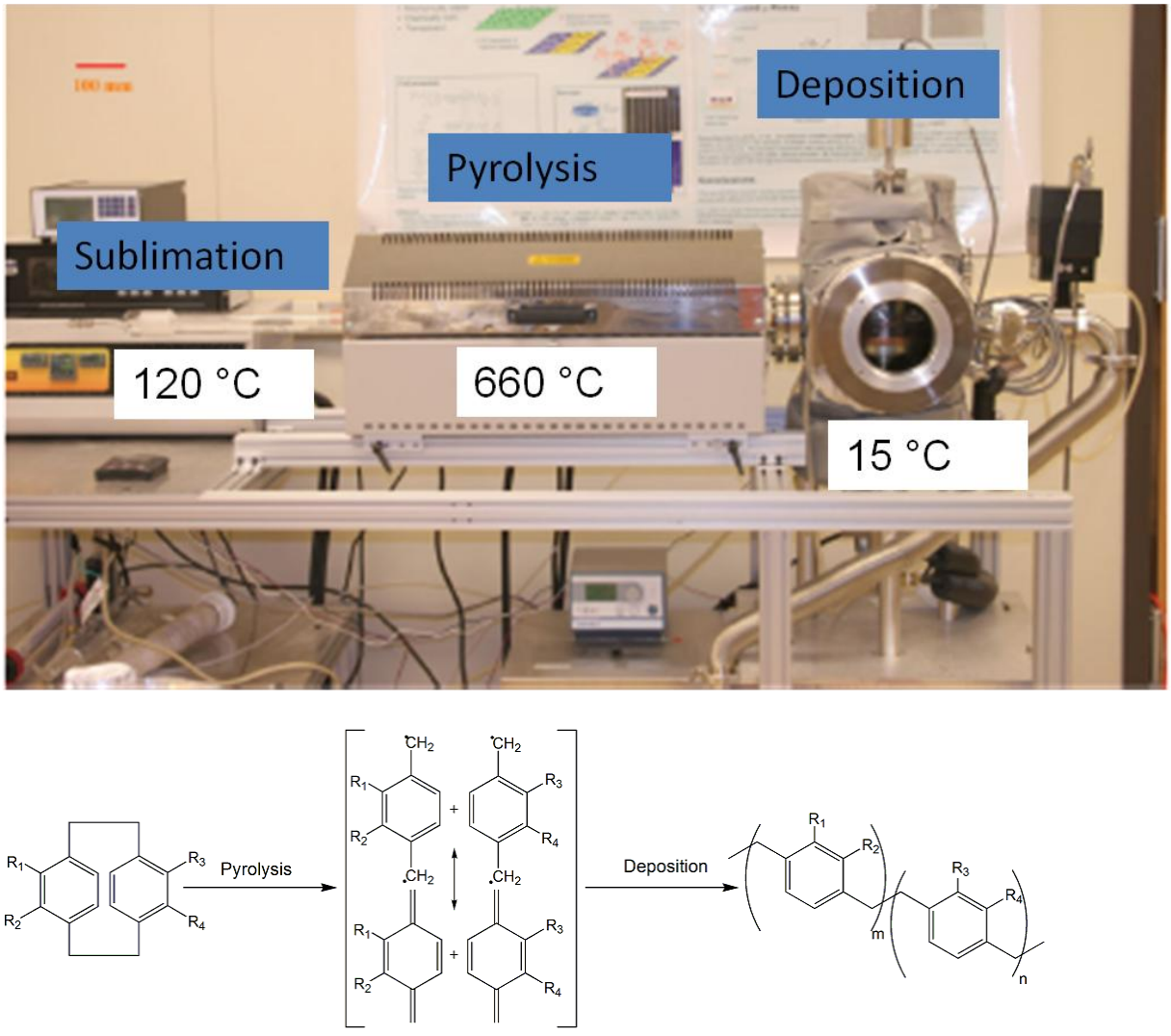

Figure 2.1. CVD set-up (top) and depiction of the CVD process (bottom).

R_1	R_2	R_3	R_4	R_1	R_2	R_3	R_4
CHO	H	H	H	CH_2OH	H	H	H
$COCH_3$	H	H	H	CH_2OCH_3	H	H	H
COC_2H_5	H	H	H	CH_2OCOCH_3	H	H	H
$COCF_3$	H	H	H	$COOCH_3$	H	H	H
COC_2F_5	H	H	H	$COOCH_3$	$COOCH_3$	$COOCH_3$	$COOCH_3$
COPh	H	H	H	$CH_2OCOPpf$	H	H	H
COPh	H	COPh	H	CH_2OCOCF_3	H	H	H
NH_2	H	H	H	Cl	H	H	H
NH_2	H	NH_2	H	Br	H	H	H
$C_5H_2NO_2Br_2$	H	H	H	Br	H	Br	H
$C_6H_5O_3$	H	H	H	COC8F17	H	H	H

Figure 2.2. Examples of functionalized CVD films available for surface engineering.

2.7 REFERENCES

1. Förch, R.; Chifen, A. N.; Bousquet, A.; Khor, H. L.; Jungblut, M.; Chu, L. Q.; Zhang, Z.; Osey-Mensah, I.; Sinner, E. K.; Knoll, W., Recent and Expected Roles of Plasma-Polymerized Films for Biomedical Applications. *Chemical Vapor Deposition* **2007,** 13, (6-7), 280-294.
2. Gorham, W. F., A New General Synthetic Method for Preparation of Linear Poly-p-xylylenes. *Journal of Polymer Science Part a-1-Polymer Chemistry* **1966,** 4, (12PA), 3027-&.
3. Lahann, J., Langer, R. , Novel poly(p-xylylenes): Thin films with tailored chemical and optical properties. *Macromolecules.* **2002,** 35, (11), 4380-4386.
4. Ozaydin-Ince, G.; Coclite, A. M.; Gleason, K. K., CVD of polymeric thin films: applications in sensors, biotechnology, microelectronics/organic electronics, microfluidics, MEMS, composites and membranes. *Reports on Progress in Physics* **2012,** 75, (1), 40.
5. Zangwill, A., *The Physics of Surfaces*. Cambridge University Press: Cambridge, 1988.
6. Elkasabi, Y. M.; Lahann, J.; Krebsbach, P. H., Cellular transduction gradients via vapor-deposited polymer coatings. *Biomaterials* **2011,** 32, (7), 1809-1815.
7. Elkasabi, Y.; Nandivada, H.; Chen, H. Y.; Bhaskar, S.; D'Arcy, J.; Bondarenko, L.; Lahann, J., Partially Fluorinated Poly-p-xylylenes Synthesized by CVD Polymerization. *Chemical Vapor Deposition* **2009,** 15, (4-6), 142-149.
8. Chen, H. Y.; Elkasabi, Y.; Lahann, J., Surface modification of confined microgeometries via vapor-deposited polymer coatings. *Journal of the American Chemical Society* **2006,** 128, (1), 374-380.
9. Lahann, J.; Balcells, M.; Rodon, T.; Lee, J.; Choi, I. S.; Jensen, K. F.; Langer, R., Reactive polymer coatings: A platform for patterning proteins and mammalian cells onto a broad range of materials. *Langmuir* **2002,** 18, (9), 3632-3638.
10. Lahann, J.; Hocker, H.; Langer, R., Synthesis of amino[2.2]paracyclophanes - Beneficial monomers for bioactive coating of medical implant materials. *Angewandte Chemie-International Edition* **2001,** 40, (4), 726-728.
11. Deng, X. P.; Eyster, T. W.; Elkasabi, Y.; Lahann, J., Bio-Orthogonal Polymer Coatings for Co-Presentation of Biomolecules. *Macromolecular Rapid Communications* **2012,** 33, (8), 640-645.
12. Jiang, X. W.; Chen, H. Y.; Galvan, G.; Yoshida, M.; Lahann, J., Vapor-based initiator coatings for atom transfer radical polymerization. *Advanced Functional Materials* **2008,** 18, (1), 27-35.
13. Nandivada, H.; Jiang, X. W.; Lahann, J., Click chemistry: Versatility and control in the hands of materials scientists. *Advanced Materials* **2007,** 19, (17), 2197-2208.
14. Greiner, A., Poly(p-xylylene)s (Structure, Properties, and Applications). In *The Polymeric Materials Encyclopedia*, CRC Press: 1996; Vol. 9, p 7171.
15. Schäfer, O.; Brink-Spalink, F.; Smarsly, B.; Schmidt, C.; Wendorff, J. H.; Witt, C.; Kissel, T.; Greiner, A., Synthesis and properties of ω-phenylalkyl-substituted poly(p-xylylene)s prepared by base-induced 1,6-dehydrohalogenation. *Macromolecular Chemistry and Physics* **1999,** 200, (8), 1942-1949.

16. Ionov, L.; Houbenov, N.; Sidorenko, A.; Stamm, M.; Minko, S., Smart microfluidic channels. *Advanced Functional Materials* **2006,** 16, (9), 1153-1160.
17. Mao, H. B.; Yang, T. L.; Cremer, P. S., Design and characterization of immobilized enzymes in microfluidic systems. *Analytical Chemistry* **2002,** 74, (2), 379-385.
18. Effenhauser, C. S.; Bruin, G. J. M.; Paulus, A.; Ehrat, M., Integrated capillary electrophoresis on flexible silicone microdevices: Analysis of DNA restriction fragments and detection of single DNA molecules on microchips. *Analytical Chemistry* **1997,** 69, (17), 3451-3457.
19. Huber, D. L.; Manginell, R. P.; Samara, M. A.; Kim, B. I.; Bunker, B. C., Programmed adsorption and release of proteins in a microfluidic device. *Science* **2003,** 301, (5631), 352-354.
20. Burns, M. A.; Johnson, B. N.; Brahmasandra, S. N.; Handique, K.; Webster, J. R.; Krishnan, M.; Sammarco, T. S.; Man, P. M.; Jones, D.; Heldsinger, D.; Mastrangelo, C. H.; Burke, D. T., An integrated nanoliter DNA analysis device. *Science* **1998,** 282, (5388), 484-487.
21. Fraleoni-Morgera, A., Fast Fabrication of Large-Area, Nanostructured Arrays from Polymers or Carbon Nanotubes by Wet-Processing. *Small* **2011,** 7, (3), 321-325.
22. Papavasiliou, G.; Songprawat, P.; Perez-Luna, V.; Hammes, E.; Morris, M.; Chiu, Y. C.; Brey, E., Three-dimensional patterning of poly(ethylene glycol) hydrogels through surface-initiated photopolymerization. *Tissue Engineering Part C-Methods* **2008,** 14, (2), 129-140.
23. Castner, D. G.; Ratner, B. D., Biomedical surface science: Foundations to frontiers. *Surface Science* **2002,** 500, (1-3), 28-60.
24. Shin, H.; Jo, S.; Mikos, A. G., Biomimetic materials for tissue engineering. *Biomaterials* **2003,** 24, (24), 4353-4364.
25. Qin, D.; Xia, Y. N.; Whitesides, G. M., Soft lithography for micro- and nanoscale patterning. *Nature Protocols* **2010,** 5, (3), 491-502.
26. Zhao, X. M.; Xia, Y. N.; Whitesides, G. M., Fabrication of three-dimensional micro-structures: Microtransfer molding. *Advanced Materials* **1996,** 8, (10), 837-&.
27. Larsen, N. B.; Biebuyck, H.; Delamarche, E.; Michel, B., Order in microcontact printed self-assembled monolayers. *Journal of the American Chemical Society* **1997,** 119, (13), 3017-3026.
28. Workman, R. K.; Manne, S., Molecular transfer and transport in noncovalent microcontact printing. *Langmuir* **2004,** 20, (3), 805-815.
29. Schmid, H.; Michel, B., Siloxane polymers for high-resolution, high-accuracy soft lithography. *Macromolecules* **2000,** 33, (8), 3042-3049.
30. Nandivada, H.; Chen, H. Y.; Lahann, J., Vapor-based synthesis of poly [(4-formyl-p-xylylene)-co-(p-xylylene)] and its use for biomimetic surface modifications. *Macromolecular Rapid Communications* **2005,** 26, (22), 1794-1799.
31. Nandivada, H.; Chen, H. Y.; Bondarenko, L.; Lahann, J., Reactive polymer coatings that "click"". *Angewandte Chemie-International Edition* **2006,** 45, (20), 3360-3363.

32. Lahann, J.; Choi, I. S.; Lee, J.; Jenson, K. F.; Langer, R., A new method toward microengineered surfaces based on reactive coating. *Angewandte Chemie-International Edition* **2001,** 40, (17), 3166-+.
33. Chen, H. Y.; Lahann, J., Vapor-assisted micropatterning in replica structures: A solventless approach towards topologically and chemically designable surfaces. *Advanced Materials* **2007,** 19, (22), 3801-+.
34. Deng, X. P.; Friedmann, C.; Lahann, J., Bio-orthogonal "Double-Click" Chemistry Based on Multifunctional Coatings. *Angewandte Chemie-International Edition* **2011,** 50, (29), 6522-6526.
35. Karp, J. M.; Yeo, Y.; Geng, W. L.; Cannizarro, C.; Yan, K.; Kohane, D. S.; Vunjak-Novakovic, G.; Langer, R. S.; Radisic, M., A photolithographic method to create cellular micropatterns. *Biomaterials* **2006,** 27, (27), 4755-4764.
36. Love, J. C.; Wolfe, D. B.; Jacobs, H. O.; Whitesides, G. M., Microscope projection photolithography for rapid prototyping of masters with micron-scale features for use in soft lithography. *Langmuir* **2001,** 17, (19), 6005-6012.
37. Chen, H. Y.; Rouillard, J. M.; Gulari, E.; Lahann, J., Colloids with high-definition surface structures. *Proceedings of the National Academy of Sciences of the United States of America* **2007,** 104, (27), 11173-11178.
38. Piner, R. D.; Zhu, J.; Xu, F.; Hong, S. H.; Mirkin, C. A., "Dip-pen" nanolithography. *Science* **1999,** 283, (5402), 661-663.
39. Wilson, D. L.; Martin, R.; Hong, S.; Cronin-Golomb, M.; Mirkin, C. A.; Kaplan, D. L., Surface organization and nanopatterning of collagen by dip-pen nanolithography. *Proceedings of the National Academy of Sciences of the United States of America* **2001,** 98, (24), 13660-13664.
40. Ginger, D. S.; Zhang, H.; Mirkin, C. A., The evolution of dip-pen nanolithography. *Angewandte Chemie-International Edition* **2004,** 43, (1), 30-45.
41. Lee, K. B.; Lim, J. H.; Mirkin, C. A., Protein nanostructures formed via direct-write dip-pen nanolithography. *Journal of the American Chemical Society* **2003,** 125, (19), 5588-5589.
42. Hong, S. H.; Zhu, J.; Mirkin, C. A., Multiple ink nanolithography: Toward a multiple-pen nano-plotter. *Science* **1999,** 286, (5439), 523-525.
43. Curran, J. M.; Stokes, R.; Irvine, E.; Graham, D.; Amro, N. A.; Sanedrin, R. G.; Jamil, H.; Hunt, J. A., Introducing dip pen nanolithography as a tool for controlling stem cell behaviour: unlocking the potential of the next generation of smart materials in regenerative medicine. *Lab on a Chip* **2010,** 10, (13), 1662-1670.
44. Hyun, J.; Lee, W. K.; Nath, N.; Chilkoti, A.; Zauscher, S., Capture and release of proteins on the nanoscale by stimuli-responsive elastin-like polypeptide "switches". *Journal of the American Chemical Society* **2004,** 126, (23), 7330-7335.
45. Chen, H. Y.; Hirtz, M.; Deng, X. P.; Laue, T.; Fuchs, H.; Lahann, J., Substrate-Independent Dip-Pen Nanolithography Based on Reactive Coatings. *Journal of the American Chemical Society* **2010,** 132, (51), 18023-18025.

CHAPTER 3

CHEMICAL-VAPOR-DEPOSITION-BASED POLYMER SUBSTRATES FOR SPATIALLY-RESOLVED ANALYSIS OF PROTEIN BINDING BY IMAGING ELLIPSOMETRY

The material in this chapter has been adapted with minor modifications from the following published article:

Ross, A.M., Zhang, D., Deng, X., Chang, SWL., Lahann, J., CVD-based Polymer Substrates for Spatially-resolved Analysis of Protein Binding by Imaging Ellipsometry, *Analytical Chemistry*, **83**, 874-880, (2011).

3.1 INTRODUCTION

Specific interactions between proteins and surface-bound ligands are important in controlling most biological events that may occur at a synthetic materials surface including protein adsorption, cell adhesion, and cell proliferation.[1, 2] Thus, quantitative analysis of protein adsorption or binding of biomacromolecules to surface-immobilized recognition sites has been an area of intense research, and a plethora of different methods have been investigated.[3] Among the most widely used methods are fluorometry,[4] enzyme-linked immunosorbent assay (ELISA),[5] radiometry,[6] and photoluminescence analysis.[7] Although widely used in current biology, these methods require cumbersome assay optimization (ELISA) or are associated with the need for diverse labels prior to detection, such as fluorescent, radioactive, or photoluminescent groups.[8] Such labels

require additional chemical or biological reactions and separation steps. In addition, chemical modification changes the properties of the target molecules.[9] Thus, label-free analytical tools, such as quartz crystal microbalance (QCM), microelectromechanical-system (MEMS)-based sensors, or surface plasmon resonance (SPR) spectroscopy, have increasingly attracted attention in the biological community.[10, 11]

In spite of the undoubted success of these methods in recent years, the spatially defined quantitative analysis of biomolecule/surface interactions remains elusive.[12] In principle, ellipsometry, and more specifically imaging ellipsometry in surface plasmon resonance conditions, is well positioned to overcome these limitations.[13] Surface plasmon resonance enhanced ellipsometry (SPREE) imaging[14] has enhanced sensitivity, as compared to conventional surface plasmon resonance methods, because it provides phase information – in addition to intensity.[15] Outputs in this configuration are the ellipsometric parameters delta (Δ) and psi (ψ), where ψ is analogous to the reflectivity intensity provided by conventional SPR spectroscopy.[15] Phase information, provided by the parameter Δ in this work, has been found to be more sensitive, **(**10^{-7}-10^{-8} refractive index unit versus 10^{-5}-10^{-6} refractive index unit for conventional SPR spectroscopy),[16, 17] to biomolecular interactions than reflective intensity alone, because the phase changes abruptly in response to variations in the bulk refractive index of the medium and thus is associated with higher signal-to-noise ratio.[18] Imaging ellipsometry can deliver spatially-resolved, quantitative data, is sufficiently sensitive for many biological questions (adsorption thickness detection in the picometer range), and can be easily used in aqueous environments. So far, progress with imaging ellipsometry for biological questions has been hampered by the availability of flexible binding substrates for protein

immobilization. Self-assembled monolayers of thiols on gold have been pursued in the past, but have limited stability and shelf-life.[19] Dextran matrixes have also been utilized, but require chemical modification in situ, typically N-hydroxysuccinimide (NHS) and 1-ethyl-3-[3-(dimethylamino)propyl] carbodiimide (EDC) chemistry.[20] Star-PEGs[21] and dendrimers[22] are other surface modification strategies that have been employed to study protein and DNA interactions for biomedical and bioanalytical applications. Recently, self-assembled gold fusion proteins were employed as recognition elements for antibody detection.[23]

Vapor-based reactive polymer coatings have the potential to function as versatile, yet chemically well-defined binding substrates, when deposited on Au-coated substrates. These reactive coatings are made by chemical vapor deposition polymerization of functionalized [2.2]paracyclophanes, and are known as poly-*p*-xylylenes. Functionalized poly-*p*-xylylenes containing aldehydes,[24] amines,[25] anhydrides,[26] or active esters,[27-29] have been used to immobilize a wide range of biomolecules.[29-31] In addition, chemical vapor deposition (CVD) based reactive coatings can be micro- and nanostructured with a number of well established patterning methods, including microcontact printing,[32] vapor-assisted micropatterning,[33] supramolecular nanostamping,[34] and photolithography.[35] In this study, we demonstrate on the basis of a representative model coating, poly[4-(pentafluoropropionyl)-*p*-xylylene-*co*-*p*-xylylene] (PPX-COC_2F_5), that reactive coatings can be deposited as sufficiently thin, yet pinhole-free coatings, that support label-free, spatially-controlled and quantitative studies of protein binding cascades for immobilization studies via imaging surface plasmon resonance enhanced ellipsometry.

As such, CVD coatings are novel substrates for studying biomolecular-surface interactions, when quantitative and spatial information is desired.

3.2 EXPERIMENTAL METHODS

3.2.1 Chemical Vapor Deposition Polymerization

Polymer coatings were prepared using a custom-designed CVD system comprised of three working sections; a sublimation zone, a pyrolysis zone, and a deposition zone.[36] In this instance, the starting material was a [2.2]paracyclophane functionalized with trifluoropropionyl groups (COC_2F_5).[37] The sublimation and pyrolysis temperatures were 120°C and 660°C for all samples. To generate different polymer thicknesses, the amount of starting material was varied and ranged from 3-13 mg with more material being utilized for thicker films. Gold-coated SPREE slides from Nanofilm (Germany) served as the substrate for polymer deposition. These slides were placed on a rotating sample holder to ensure homogenous surface coverage during deposition, and the holder was maintained at 13°C. Fourier transform infrared (FT-IR) spectroscopy was utilized to confirm polymer structure and ellipsometry was used to determine film thicknesses. Analysis of the polymer structure was undertaken with a Thermo Nicolet 6700 spectrometer (Waltham, MA) with an 85° grazing angle and 128 scans for each sample at a resolution of $4cm^{-1}$. All thicknesses were determined with a Nanofilm EP3 imaging ellipsometer at a 532 nm wavelength with an angle of incidence of 60° and polarizer range of 15°. Both ellipsometric parameters, delta and psi, were utilized in a thickness

model and the refractive index of the polymer was assumed to be 1.41 as determined by optical modeling.

3.2.2 Electrochemical Impedance Spectroscopy

The presence and quality of the polymer films was confirmed via electrochemical impedance spectroscopy (EIS).[38] Impedance samples consisted of a conducting section and a CVD-coated surface area. The base substrate, prior to CVD deposition was silicon coated with gold. Electrochemical analysis was carried out using a three electrode electrochemical cell where the CVD sample served as the working electrode, a saturated calomel electrode [SCE] functioned as the reference electrode, and the platinum mesh was operated as the counter electrode. Phosphate buffered saline (PBS) acted as the electrolyte solution. Impedance measurements were taken with a Gamry PC14/300 potentiostat and utilized EIS300 software (Warminster, PA). The applied potential had an ac amplitude of 10 mV root measure square (rms) and a frequency range from 1 to 100,000 Hz, with a dc bias of 0 mV with respect to the SCE. The amplitude and phase angle of the current response were recorded at 10 points per decade in frequency.

3.2.3 Atomic Force Microscopy

The surface roughness of the thin films was assessed by atomic force microscopy (AFM). AFM was conducted in tapping mode in air at room temperature. A Nanoscope IIIa from Digital Instruments/Veeco (Plainview, NY) using an EV scanner (15 μm x 15 μm maximum scan size) was used in the analysis. NSC15 cantilevers (MikroMasch, San

Jose, CA) with spring constants ranging from 20 N/m to 75 N/m and resonance frequencies of 265-400 kHz served as the AFM tips. Each image depicted herein represents a 5 μm x 5 μm scan size at a scan rate of 1 Hz.

3.2.4 Surface Modification of CVD Coatings

Surface modification of the CVD-coated Au slide prior to SPREE analysis consisted of several surface modification steps, as outlined in **Figure 3.1**. Briefly, poly(dimethylsiloxane) (PDMS) stamp with a 400 by 400 micron square array was utilized to microcontact print a CVD-coated Au slide.[26] To increase the hydrophilicity of the stamp, the surface was oxidized via UV ozone treatment for 25 minutes (UV-Ozone Cleaner, model 342, Jelight Co. Inc., Irvine, CA). The inking solution for the PDMS stamp consisted of 2 mg of biotin-LC-hydrazide (Pierce, Rockford, IL) dissolved in 1 ml of absolute ethanol. The stamp was inked and dried in a stream of air before being placed in contact with the CVD-coated Au slides. Contact was maintained for 3-5 minutes and the stamp removed. To limit non-specific adsorption, the patterned surface was further modified with poly(ethylene glycol) (PEG) hydrazide (MW=10,000 g/mol from Laysan Bio, Arab, AL) for 12-16 h and subsequently rinsed several times with deionized water.

3.2.5 Monitoring of Surface Reactions by Imaging Surface Plasmon Resonance Enhanced Ellipsometry

An imaging null-ellipsometer (EP^3 Nanofilm, Germany) equipped with a fluid cell, utilizing the Kretschmann configuration,[39] was employed in the analysis of protein

and antibody interactions with the CVD-coated Au surfaces. Filtered and degassed phosphate buffered saline served as the sampling medium for all experimental steps. The experimental setup consisted of a laser beam, a flow cell, a 60° SF-10 prism, and two syringe pumps (one to pump the buffer solution and the other to pump solutions of biomolecules). The syringe pumps were attached to a y-connector with two needles to prevent mixing of the buffer and the biomolecular solution before transport to the flow cell. Ellipsometric measurements were taken at 10 s intervals with a 10x magnification objective at a wavelength of 532 nm and an angle of incidence of 60°. The field of view was 0.5 mm^2. Prior to and following biomolecular exposure, the surface was rinsed with PBS. The initial PBS rinse established a baseline signal for the surface and subsequent washing removed biomolecules that were non-specifically adsorbed. Flow rates were constant at 50 µL/min for all buffer and analyte solutions. The biomolecules of interest were streptavidin labeled with a tetramethylrhodamine isothiocyanate (TRITC) fluorophore (Pierce, Rockford, IL), a biotinylated fibrinogen antibody (abcam, Cambridge, MA), and fibrinogen labeled with a fluorescein isothiocyanate (FITC) fluorophore (Invitrogen, San Diego, CA). The analyte concentrations were 40, 20, and 333 µg/ml for streptavidin, biotinylated antibody, and fibrinogen, respectively. Each analyte was exposed to the surface for 20 min. Ellipsometric signal changes for each step of the cascade were determined by subtracting the reference signal (area coated with PEG) from the analyte signal. Though many of the techniques used to study biomolecular adsorption do not measure protein density directly, they have means of correlating sensor outputs with changes in mass. [40] SPREE sensing is similar in that the surface density of the adsorbed protein can be determined, if optical parameters of the

protein and buffer as well as the adsorbed thickness are known. This relation is given by the de Feijter equation[41]:

$\sigma = d_p*(n_p-n_b)*(d_n/d_c)^{-1}$ (1)

where σ is the surface density, d_p is the thickness of the protein layer, n_p is the refractive index of the protein, n_b is the refractive index of the buffer, and dn/dc is the refractive index increment of the molecules. In this work, n_p was 1.45,[42] n_b was 1.33,[43] and d_n/d_c is 0.183 cm^3/g.[44] The change in Δ can be correlated with thickness changes. An optical model of the sensing cascade was utilized to determine the expected change in Δ per nanometer of adsorbed molecule by taking the slope of the fit in the linear regime. The inverse of this value was then multiplied by the change in Δ observed in the SPREE sensogram to determine the layer thickness. Thus, the surface density of the biomolecules in this instance was determined using optical modeling in conjunction with equation (1). In addition to SPREE imaging, fluorescence microscopy was employed to provide further confirmation of the biomolecular immobilization steps. Samples were rinsed three times with PBS and three times with a solution of PBS containing Tween 20 (0.02%, w/v) and bovine serum albumin (0.1 %, w/v) prior to fluorescence imaging.

3.3 RESULTS AND DISCUSSION

3.3.1 CVD Polymerization and Chemical/Electrical Characterization

Ultra-thin films of poly[4-(pentafluoropropionyl)-p-xylylene-co-p-xylylene] were conformally deposited onto gold-coated SPREE substrates by CVD polymerization. The chemical structure of the films was confirmed by grazing angle FT-IR spectroscopy and was in agreement with previously reported polymers.[23] Deposition of the reactive coating

resulted in characteristic vibrational bands at 1712 cm^{-1}, which is indicative of the carbonyl stretch. The bands at 1066, 1232, and 1352 cm^{-1} can be assigned to the C-F stretches (**Figure 3.2A**). The FT-IR spectra also revealed systematic changes in the intensity of characteristic vibrational bands with increasing amounts of starting material, which ranged from 3 to 13 mg in this study. We attributed the increase in signal intensity to an increased film thickness. This finding provided initial evidence that the amount of starting material can be utilized to control the thickness of the resulting polymer films. Further evidence was obtained by ellipsometry. On the basis of a Cauchy model assuming a refractive index of 1.41 for the polymer film (as determined from optical fitting) and a refractive index of 0.7 for the gold layer (provided by the manufacturer), the film thickness of coatings deposited under identical conditions with 3, 4.5, 6.5, 10, and 13 mg of starting material were determined to be 3, 10, 20, 40, and 60 nm, respectively.

Because the CVD films were utilized as reactive interfaces for a cascade of biomolecular immobilization reactions, it is highly desirable that the thin films are pinhole-free. The reason is that the presence of pinholes in the films may be an indication of incomplete coverage and will result in an undefined substrate for binding studies. To confirm complete coverage of the substrate, polymer films with a range of different thicknesses were studied by EIS. This level of coverage is indicated by the electrochemical permeability of an electrode, which should be significantly different from that of the base substrate after a polymer has been deposited. The impedance technique is limited to the assessment of 95% surface coverage.[45] As shown in **Figure 3.2B**, the impedance increases from 1.5 kohm to 17 kohm after deposition of a 3 nm thick CVD film. At a surface coverage of at least 95%, pinholes are not likely to adversely

impact SPREE sensing. As the thickness of the CVD films is further increased, the electrochemical impedance increases accordingly. Further analysis revealed a linear correlation between film thickness and impedance. Physically, this is expected, as the film is a dielectric between two conductors (the metal substrate and the electrolyte) and the impedance of the system is directly proportional to the distance between the two conductors, i.e., the thickness of the polymer film. Additional support for films having few, if any pinholes, was provided by imaging ellipsometry which has a 1 μm lateral resolution. This technique did not reveal any pinholes and imaging indicated that substrate patterning was consistent across the substrate.

3.3.2 Surface Roughness

For ultra-thin films, the morphology and roughness of the surface may change with surface thickness. Additionally, the roughness of the sensor interface may also play a role in ellipsometric sensing on functionalized CVD coatings. In fact, the surface roughness has been shown to be an important factor in protein adsorption.[46, 47] Because an important aspect of this work is to investigate the role of film thickness on the usefulness of CVD films for biomolecular sensing, it was necessary to ascertain that surface roughness did not significantly vary among polymer coatings of different thicknesses. **Figure 3.3** shows AFM images for samples coated with 3, 10, and 60 nm thick CVD films. In spite of the significant thickness differences of these samples, only slight morphological differences were observed. The 3 nm coating had sharper growth cones, while the plateau size increased with increasing amount of deposited polymer. However, the rms roughness values, which were 2.0, 1.8, and 1.9 nm for 3, 10, and 60 nm

films, did not vary significantly. On the basis of the AFM study, we concluded that differences in surface morphology and roughness can be neglected and should not affect SPREE sensing.

3.3.3 Microfluidic SPREE imaging

Surface plasmon resonance spectroscopy is a real time, in situ optical technique to study biomolecule interactions on model substrates.[48] Typical substrates include gold, self-assembled monolayers (SAMs), or thiol-modified dextrans on gold, and silver.[49, 50] Here, we tested the feasibility of using vapor-deposited polymer coatings as biomolecular immobilization layer. Samples for SPREE imaging studies were prepared as shown in **Figure 3.1**. Syringe pumps were utilized to deliver the buffer and analyte solutions to the sensor surface at a steady flow rate of 50 μL/min and the experimental set-up is depicted in **Figure 3.4A**. Analyte exposure of the reactive CVD coatings consisted of a cascade of biomolecules, starting with streptavidin labeled with a rhodamine fluorophore. Streptavidin is a 53 kDa protein that was selected because of its high-affinity interaction with the vitamin biotin.[51] The second component in the cascade was a biotinylated antibody that specifically recognized the blood plasma protein fibrinogen. Here, the biotin served as the recognition element for the protein streptavidin previously bound to the sensor surface. The antibody acted as a recognition element for the final target of the binding cascade, which was fibrinogen labeled with fluorescein fluorophores. Fibrinogen is a large, 340 kDa, protein that plays an important role in blood clotting and blood surface interactions.[52] In fact, several studies have demonstrated relationships between fibrinogen concentration and disease states, such as esophageal,[53] lung, and colon

cancer,[54] making it a relevant model molecule for ellipsometric sensing. To reduce nonspecific binding of proteins, we modified the unreacted background regions with poly(ethylene glycol). The second inset in **Figure 3.4A** displays each component of the system architecture from the base substrate to the final protein layer. In each experiment, patterned areas were compared to a non-reactive background. As seen in **Figure 3.4B**, the patterned area was distinguishable from the background on the basis of thickness differences. Bound protein was reported as the difference in adsorbed protein between binding areas and the protein-resistant background.

In this study, CVD thicknesses of 3, 10, 20, 40, and 60 nm were assessed. A representative surface response for each step in the cascade for both reference and analyte areas is presented in SPREE sensograms for a 10 nm film in **Figure 3.5**. The change in the ellipsometric signal after each analyte exposure indicates that the surface is reactive and that the analytes of interest interact with the CVD array. Analyte adsorption is evident on the order of minutes and adsorption is also independently confirmed by fluorescence microscopy. The density of the adsorbed biomolecules was found to be approximately 122, 46 and 11 ng/cm^2 for TRITC-streptavidin, biotinylated fibrinogen antibody, and FITC fibrinogen, respectively on films 20 nm or less. In the corresponding microscopy images provided in **Figure 3.4C**, the patterned array is readily apparent for both, the first step in the cascade, binding of TRITC-streptavidin to surface-immobilized biotin, and the final step in the cascade, FITC-fibrinogen binding to antibody molecules presented at the surface. Evidence of a height dependence on technique sensitivity is highlighted in **Figure 3.6**, which compares the ellipsometric response for each step in the cascade as a function of sensor film thickness. From the graphs, it is apparent that there is

an upper bound to the useful range of CVD thickness for sensing with SPREE imaging. The thinnest films (3 nm and 10 nm thickness range) have a significantly larger response ($p < 0.05$) than the thicker films (≥20 nm) for each step in the cascade. A substantial difference is also observed between the thicker films for the first step of the cascade and the 40 nm and 60 nm films as compared to the 20 nm films in the second step of the cascade. The similarity of the ellipsometric response to fibrinogen for the thicker films (≥20 nm) likely results from reduced detection sensitivity as binding occurs further from the sensor surface as a consequence of previous immobilization steps.[55] Even at the end of a 3-step binding cascade the sensor was able to detect concentrations of fibrinogen at a level of 333 μg/mL, which is about an order of magnitude lower than the average blood plasma levels of 2-4 mg/mL. [56]

Platforms for SPREE imaging studies can be utilized to obtain a wide range of data for surface-ligand interactions. These include, but are not limited to, determining concentration of molecules, kinetics of binding, relative binding patterns, and the specificity of binding.[55] Like dextran matrixes and thiols, CVD substrates are well suited for this purpose. However, CVD films have better stability and shelf-life as compared to thiols as indicated by the long term maintenance of functional groups at the film surface as seen in **Figure 3.7**. In addition to long-term stability, the advantage of the CVD platform is that it is spatially-resolved and has range of functionalities which can be incorporated onto the same surface via numerous modification techniques. This is advantageous for high throughput screening and assay optimization. In this work, fibrinogen at a concentration of 333 μg/ml was detected after a cascade of biomolecules. However, the authors do not purport this value to be the detection limit of the platform.

The detection limit of the platform is influenced not only by the concentration of the biomolecule but also its size and binding affinity.[57]

3.4 CONCLUSIONS

Herein, we described a new binding platform for ellipsometric binding studies, which uses vapor-based reactive polymer coatings as a biomolecular immobilization substrate. These novel substrates may be advantageous in that CVD coatings provide a broad range of surface chemistries. The antigen-antibody sensor showed the ability to sense a cascade of biomolecules. Furthermore, the impact of CVD film thickness on the signal intensity was determined. From this analysis, a desirable range of CVD thicknesses for ellipsometric studies was established to be less than 20 nm. The surface response was fairly rapid, occurring on the order of minutes, indicating the potential for high throughput use. Thus, it is feasible to utilize CVD reactive polymers as a platform for imaging surface plasmon resonance enhanced ellipsometry, and the ease with which these films can be modified make them attractive for a plethora of sensing applications.

3.5 FIGURES AND TABLES

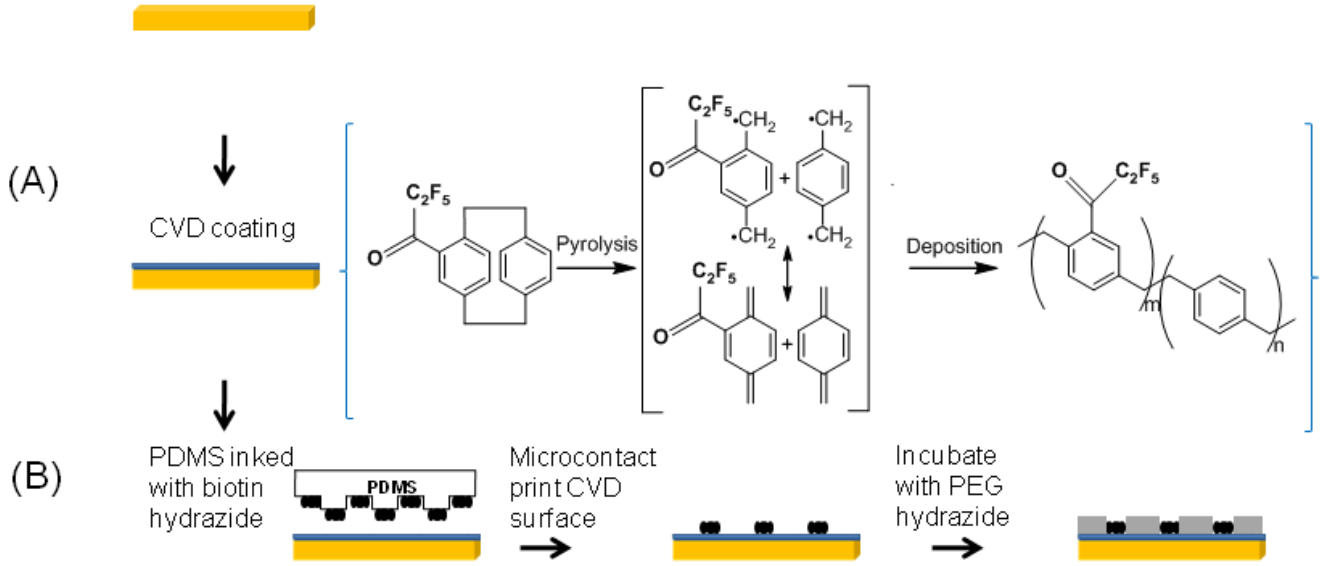

Figure 3.1. Schematic diagram of sample preparation and analysis of biomolecular binding. (A) CVD film deposited to a desired thickness on Au-coated SPREE slide. (B) Immobilization of biotin containing ligand on the CVD surface and PEG hydrazide incubation to limit nonspecific adsorption.

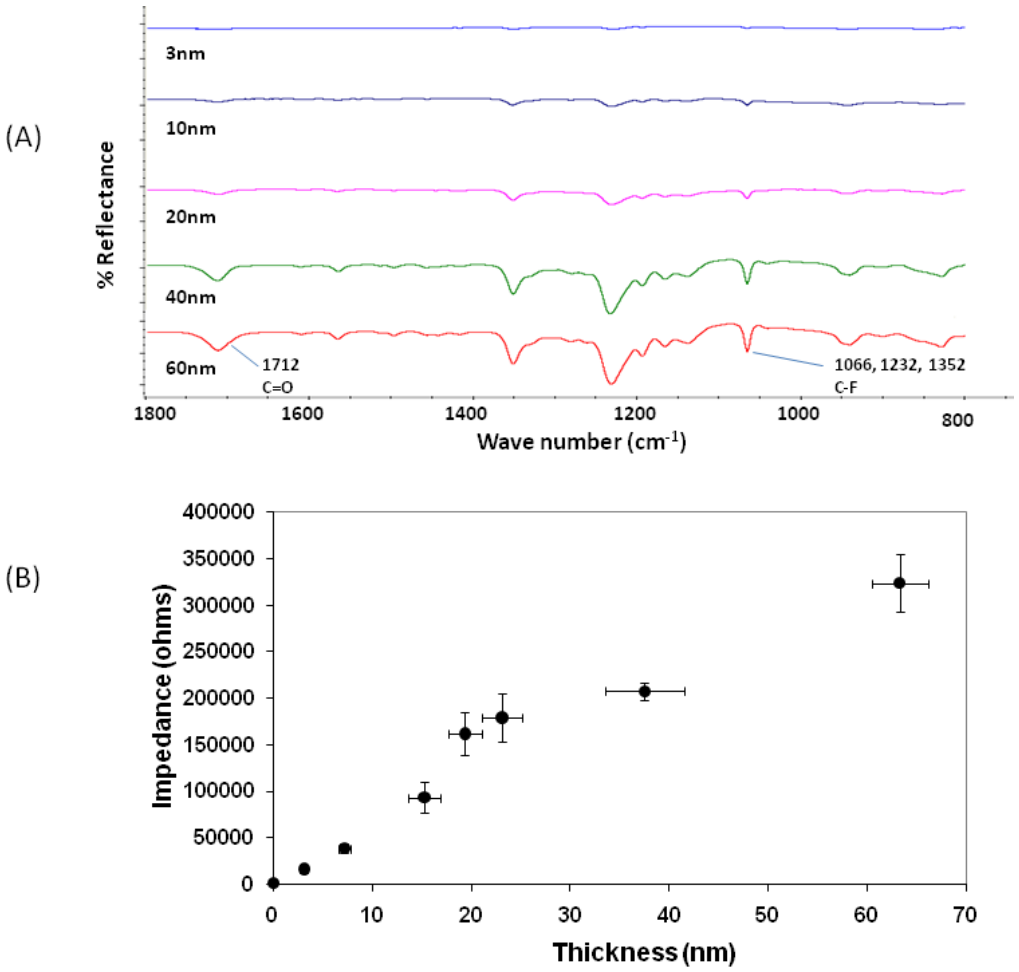

Figure 3.2. The presence of thin CVD films was confirmed by means of FTIR and electrochemical impedance. (A) FTIR spectroscopy of CVD films at various thicknesses. Characteristic carbonyl and C-F stretches are apparent. (B) Impedance output of the CVD film as a function of film thickness (n=3 per thickness).

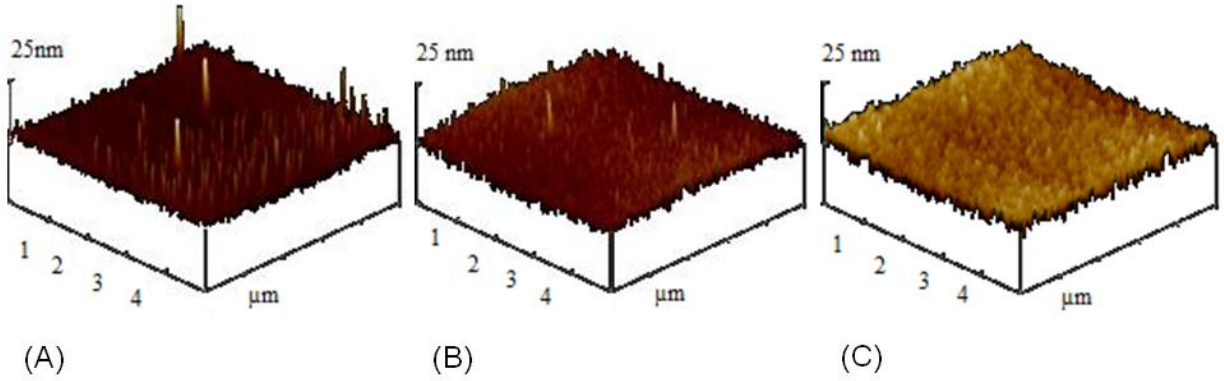

Figure 3.3. Surface roughness analysis using atomic force microscopy in tapping mode. (A) 3 nm thick film with surface roughness Rms = 2 nm (B) 10nm film with surface roughness Rms = 1.8 nm (C) 60 nm film with surface roughness Rms = 1.9 nm in 3D representations.

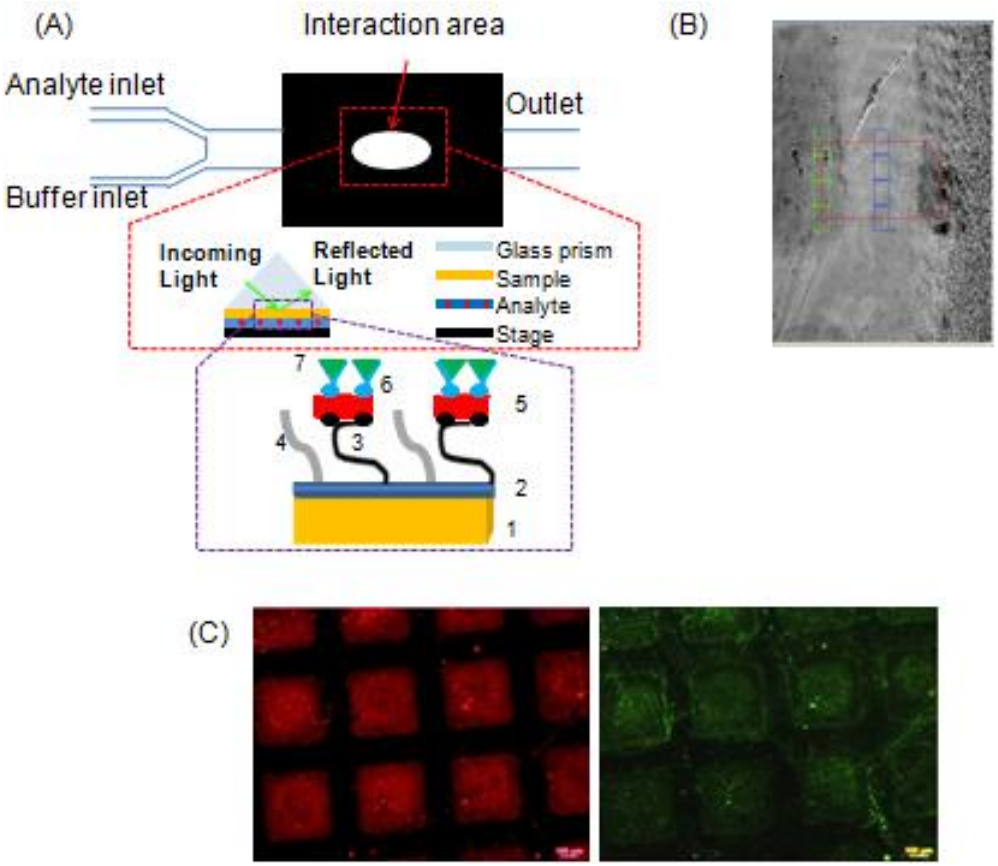

Figure 3.4.SPREE analysis set-up and fluorescence microscopy. (A) SPREE imaging was utilized to analyze biomolecular interactions with the CVD surface. Experimental set-up consisted of an inlet for buffer and analyte flow and the fluids were delivered by syringe pumps to the interaction area. The second inset is a schematic of the sample architecture with each component represented numerically as follows: 1. Au coated SPREE slide 2. $PPXCOC_2F_5$ 3. Biotin hydrazide long chain 4. 10k PEG hydrazide 5. Streptavidin TRITC 6. Biotinylated Fibrinogen Antibody 7. Fibrinogen FITC (B) Prior to analysis, portions of the sample patterned with biotin hydrazide and unpatterned areas reacted with PEG hydrazide were selected for data collection (C) Secondary confirmation of protein binding via fluorescence microscopy. The left image is the rhodamine channel which indicates the binding of streptavidin TRITC and the right image is the fluorescein channel which indicates binding of fibrinogen FITC.

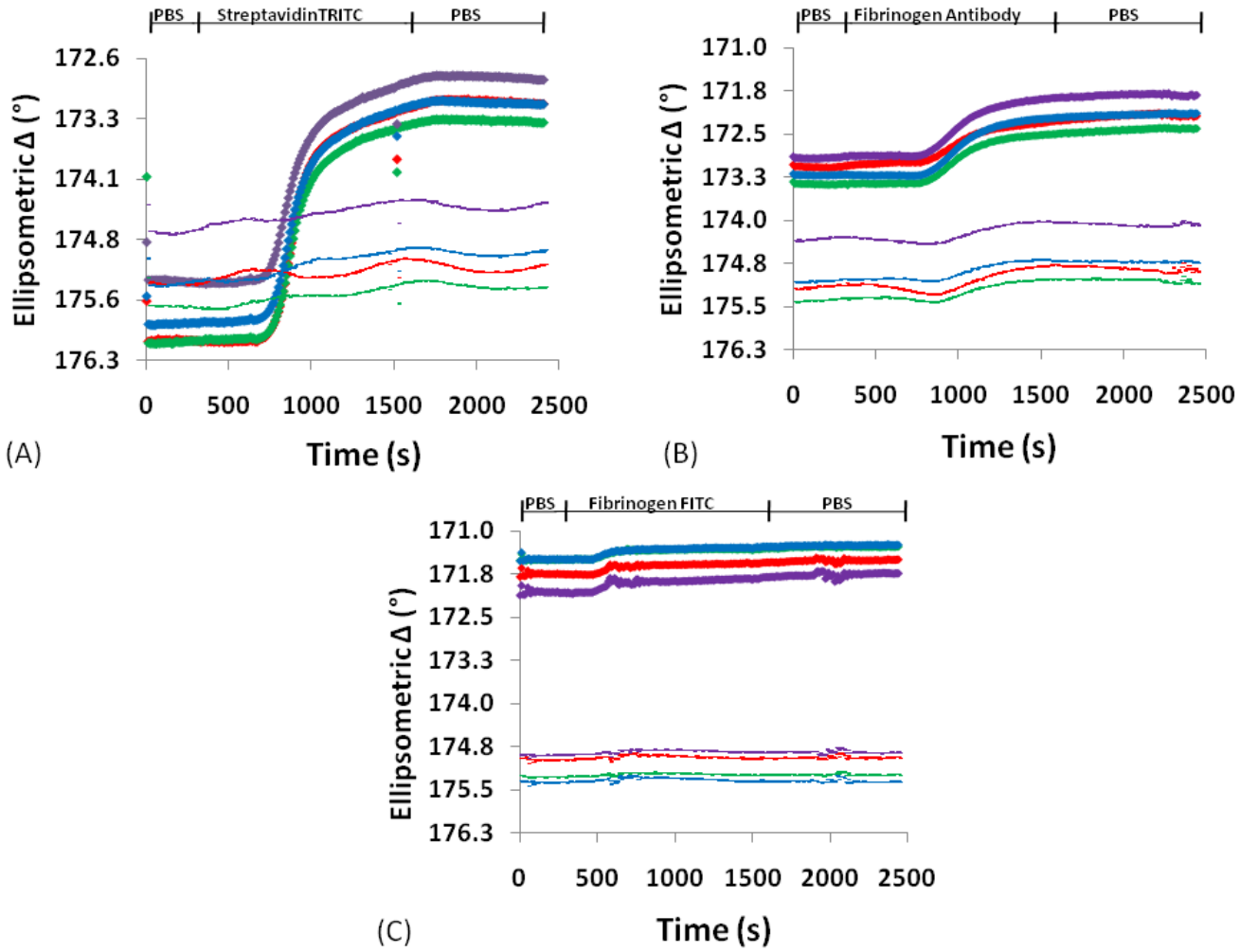

Figure 3.5.The patterned CVD surface was exposed to a cascade of biomolecules. Because the surface is patterned, an internal reference (unpatterned area) is utilized. Biomolecular immobilization is indicated by a change in ellipsometric delta signal. Thin lines on the graphs indicate the reference signal while the thick lines indicate the signal from the patterned area. Representative SPREE sensograms for a 10nm CVD film in response to sequential analyte exposure of (A) streptavidin TRITC, followed by (B) fibrinogen antibody, and then (C) fibrinogen FITC.

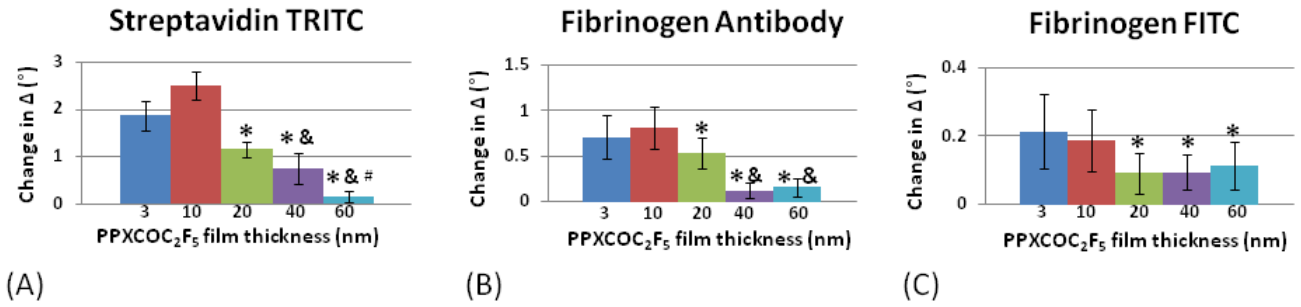

Figure 3.6. The change in ellipsometric delta is the signal difference between the patterned and unpatterned areas and is provided for each step of the biomolecular cascade for various film thicknesses. (A) Plot of streptavidin TRITC ellipsometric delta as a function of CVD film thickness (B) Plot of fibrinogen antibody ellipsometric delta as a function of CVD film thickness (C) Plot of fibrinogen FITC ellipsometric delta as a function of CVD film thickness. Error bars indicate the standard deviation of the mean of 3 samples. Symbols indicate a significant difference ($p<0.05$) between CVD thicknesses with * representing comparison to 3 and 10 nm films, & representing comparisons to 20 nm films, and # representing comparisons to 40 nm films.

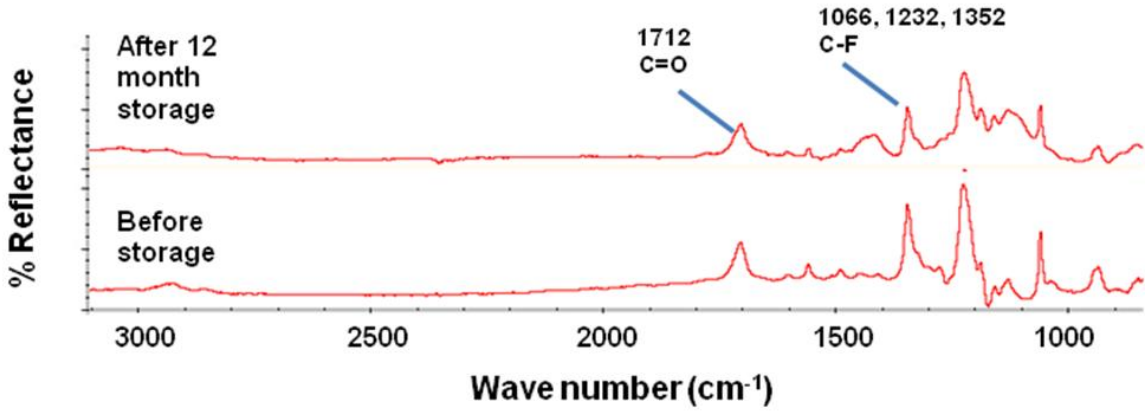

Figure 3.7.The stability of the CVD film after storage in air for 12 months was confirmed by FTIR. Characteristic carbonyl and C-F stretches are apparent.

3.6 REFERENCES

1. Anderson, J. M.; Rodriguez, A.; Chang, D. T., Foreign body reaction to biomaterials. *Seminars in Immunology* **2008,** 20, (2), 86-100.
2. Wilson, C. J.; Clegg, R. E.; Leavesley, D. I.; Pearcy, M. J., Mediation of biomaterial-cell interactions by adsorbed proteins: A review. *Tissue Engineering* **2005,** 11, (1-2), 1-18.
3. Davis, C. B.; Shamansky, L. M.; Rosenwald, S.; Stuart, J. K.; Kuhr, W. G.; Brazill, S. A., Independently-addressable micron-sized biosensor elements. *Biosensors & Bioelectronics* **2003,** 18, (10), 1299-1307.
4. Uniewicz, K. A.; Ori, A.; Xu, R.; Ahmed, Y.; Wilkinson, M. C.; Fernig, D. G.; Yates, E. A., Differential Scanning Fluorimetry Measurement of Protein Stability Changes upon Binding to Glycosaminoglycans: A Screening Test for Binding Specificity. *Analytical Chemistry* **2010,** 82, (9), 3796-3802.
5. Yu, D. Q.; Ghosh, R., Method for Studying Immunoglobulin G Binding on Hydrophobic Surfaces. *Langmuir* **2010,** 26, (2), 924-929.
6. Yamaguchi, N.; Zhang, L.; Chae, B.-S.; Palla, C. S.; Furst, E. M.; Kiick, K. L., Growth Factor Mediated Assembly of Cell Receptor-Responsive Hydrogels. *Journal of the American Chemical Society* **2007,** 129, (11), 3040-3041.
7. Yuan, C.-X.; Tao, X.-T.; Wang, L.; Yang, J.-X.; Jiang, M.-H., Fluorescent Turn-On Detection and Assay of Protein Based on Lambda (Î›)-Shaped Pyridinium Salts with Aggregation-Induced Emission Characteristics. *The Journal of Physical Chemistry C* **2009,** 113, (16), 6809-6814.
8. Ray, S.; Mehta, G.; Srivastava, S., Label-free detection techniques for protein microarrays: Prospects, merits and challenges. *Proteomics* **2010,** 10, (4), 731-748.
9. Bally, M.; Halter, M.; Voros, J.; Grandin, H. M., Optical microarray biosensing techniques. *Surface and Interface Analysis* **2006,** 38, (11), 1442-1458.
10. Hartwell, S. K.; Grudpan, K., Flow based immuno/bioassay and trends in micro-immuno/biosensors. *Microchimica Acta* **2010,** 169, (3-4), 201-220.
11. James, T.; Mannoor, M. S.; Ivanov, D. V., BioMEMS - Advancing the frontiers of medicine. *Sensors* **2008,** 8, (9), 6077-6107.
12. Zernla, J.; Lekka, M.; Wiltowska-Zuber, J.; Budkowski, A.; Rysz, J.; Raczkowska, J., Integral geometry analysis of fluorescence micrographs for quantitative relative comparison of protein adsorption onto polymer surfaces. *Langmuir* **2008,** 24, (18), 10253-10258.
13. Arwin, H.; Poksinski, M.; Johansen, K., Enhancement in ellipsometric thin film sensitivity near surface plasmon resonance conditions. *Physica Status Solidi a-Applications and Materials Science* **2008,** 205, (4), 817-820.
14. Fabre, R. M.; Talham, D. R., Stable Supported Lipid Bilayers on Zirconium Phosphonate Surfaces. *Langmuir* **2009,** 25, (21), 12644-12652.
15. Klenkar, G.; Brian, B.; Ederth, T.; Stengel, G.; Hook, F.; Piehler, J.; Liedberg, B., Addressable adsorption of lipid vesicles and subsequent protein interaction studies. *Biointerphases* **2008,** 3, (2), 29-37.
16. Nelson, S. G.; Johnston, K. S.; Yee, S. S., High sensitivity surface plasmon resonace sensor based on phase detection. *Sensors and Actuators B: Chemical* **1996,** 35, (1-3), 187-191.

17. Schasfoort, R. B. M.; Tudos, A. J., *Handbook of Surface Plasmon Resonance* The Royal Society of Chemistry Cambridge, 2008.
18. Nabok, A.; Tsargorodskaya, A., The method of total internal reflection ellipsometry for thin film characterisation and sensing. *Thin Solid Films* **2008,** 516, (24), 8993-9001.
19. Scarano, S.; Mascini, M.; Turner, A. P. F.; Minunni, M., Surface plasmon resonance imaging for affinity-based biosensors. *Biosensors and Bioelectronics* **2009,** 25, (5), 957-966.
20. Lofas, S.; Malmqvist, M.; Ronnberg, I.; Stenberg, E.; Liedberg, B.; Lundstrom, I., Bioanalysis with Surface-Plasmon Resonance *Sensors and Actuators B-Chemical* **1991,** 5, (1-4), 79-84.
21. Gasteier, P.; Reska, A.; Schulte, P.; Salber, J.; Offenhausser, A.; Moeller, M.; Groll, J., Surface grafting of PEO-Based star-shaped molecules for bioanalytical and biomedical applications. *Macromolecular Bioscience* **2007,** 7, (8), 1010-1023.
22. Benters, R.; Niemeyer, C. M.; Wohrle, D., Dendrimer-activated-solid supports for nucleic acid and protein microarrays. *Chembiochem* **2001,** 2, (9), 686-694.
23. Park, T. J.; Hyun, M. S.; Lee, H. J.; Lee, S. Y.; Ko, S., A self-assembled fusion protein-based surface plasmon resonance biosensor for rapid diagnosis of severe acute respiratory syndrome. *Talanta* **2009,** 79, (2), 295-301.
24. Nandivada, H.; Chen, H. Y.; Lahann, J., Vapor-based synthesis of poly [(4-formyl-p-xylylene)-co-(p-xylylene)] and its use for biomimetic surface modifications. *Macromolecular Rapid Communications* **2005,** 26, (22), 1794-1799.
25. Kashima, Y.; Munakata, T.; Matoba, A., InGaAsP multiple quantum well edge-emitting light-emitting diode showing low coherence characteristics using selective-area metalorganic vapor phase epitaxy. *Optical Review* **1997,** 4, (1A), 69-71.
26. Lahann, J.; Langer, R., Novel poly(p-xylylenes): Thin films with tailored chemical and optical properties. *Macromolecules* **2002,** 35, (11), 4380-4386.
27. Lahann, J.; Balcells, M.; Lu, H.; Rodon, T.; Jensen, K. F.; Langer, R., Reactive Polymer Coatings: A First Step toward Surface Engineering of Microfluidic Devices. *Analytical Chemistry* **2003,** 75, (9), 2117-2122.
28. Jiang, X. W.; Chen, H. Y.; Galvan, G.; Yoshida, M.; Lahann, J., Vapor-based initiator coatings for atom transfer radical polymerization. *Advanced Functional Materials* **2008,** 18, (1), 27-35.
29. Lahann, J.; Choi, I. S.; Lee, J.; Jenson, K. F.; Langer, R., A new method toward microengineered surfaces based on reactive coating. *Angewandte Chemie-International Edition* **2001,** 40, (17), 3166-3169.
30. Lahann, J.; Hocker, H.; Langer, R., Synthesis of amino[2.2]paracyclophanes - Beneficial monomers for bioactive coating of medical implant materials. *Angewandte Chemie-International Edition* **2001,** 40, (4), 726-728.
31. Himabindu, N.; Hsien-Yeh, C.; Lidija, B.; Joerg, L., Reactive Polymer Coatings that "Click". *Angewandte Chemie International Edition* **2006,** 45, (20), 3360-3363.
32. Lahann, J.; Balcells, M.; Rodon, T.; Lee, J.; Choi, I. S.; Jensen, K. F.; Langer, R., Reactive polymer coatings: A platform for patterning proteins and mammalian cells onto a broad range of materials. *Langmuir* **2002,** 18, (9), 3632-3638.

33. Chen, H. Y.; Lahann, J., Vapor-assisted micropatterning in replica structures: A solventless approach towards topologically and chemically designable surfaces. *Advanced Materials* **2007,** 19, (22), 3801-3808.
34. Thévenet, S.; Chen, H. Y.; Lahann, J.; Stellacci, F., A Generic Approach Towards Nanostructured Surfaces Based on Supramolecular Nanostamping on Reactive Polymer Coatings. *Advanced Materials* **2007,** 19, (24), 4333-4337.
35. Chen, H. Y.; Lahann, J., Fabrication of discontinuous surface patterns within microfluidic channels using photodefinable vapor-based polymer coatings. *Analytical Chemistry* **2005,** 77, (21), 6909-6914.
36. Lahann, J., Vapor-based polymer coatings for potential biomedical applications. *Polymer International* **2006,** 55, (12), 1361-1370.
37. Elkasabi, Y.; Yoshida, M.; Nandivada, H.; Chen, H. Y.; Lahann, J., Towards multipotent coatings: Chemical vapor deposition and biofunctionalization of carbonyl-substituted copolymers. *Macromolecular Rapid Communications* **2008,** 29, (11), 855-870.
38. Ganesh, V.; Lakshminarayanan, V., Self-Assembled Monolayers of Alkanethiols on Gold Prepared in a Hexagonal Lyotropic Liquid Crystalline Phase of Triton X-100/Water System. *Langmuir* **2006,** 22, (4), 1561-1570.
39. Raether, H., Surface-plasmons on Smooth and Rough Surfaces and on Gratings *Springer Tracts in Modern Physics* **1988,** 111, 1-133.
40. Goda, T.; Miyahara, Y., Detection of Microenvironmental Changes Induced by Protein Adsorption onto Self-Assembled Monolayers using an Extended Gate-Field Effect Transistor. *Analytical Chemistry* **2010,** 82, (5), 1803-1810.
41. Defeijter, J. A.; Benjamins, J.; Veer, F. A., Ellipsometry as a Tool to Study Adsorption Behavior of Synthetic Biopolymers at Air-Water Interface. *Biopolymers* **1978,** 17, (7), 1759-1772.
42. Beketov, G. V.; Shirshov, Y. M.; Shynkarenko, O. V.; Chegel, V. I., Surface plasmon resonance spectroscopy: prospects of superstrate refractive index variation for separate extraction of molecular layer parameters. *Sensors and Actuators B: Chemical* **1998,** 48, (1-3), 432-438.
43. Topolancik, J.; Vollmer, F., Photoinduced transformations in bacteriorhodopsin membrane monitored with optical microcavities. *Biophysical Journal* **2007,** 92, (6), 2223-2229.
44. Ball, V.; Ramsden, J. J., Buffer dependence of refractive index increments of protein solutions. *Biopolymers* **1998,** 46, (7), 489-492.
45. Rehak, M.; Hall, E. A. H., Examination of bilayer lipid membranes for 'pin-hole' character. *Analyst* **2004,** 129, (11), 1014-1025.
46. Rechendorff, K.; Hovgaard, M. B.; Foss, M.; Zhdanov, V. P.; Besenbacher, F., Enhancement of protein adsorption induced by surface roughness. *Langmuir* **2006,** 22, (26), 10885-10888.
47. Lord, M. S.; Foss, M.; Besenbacher, F., Influence of nanoscale surface topography on protein adsorption and cellular response. *Nano Today* **2010,** 5, (1), 66-78.
48. Homola, J., Present and future of surface plasmon resonance biosensors. *Analytical and Bioanalytical Chemistry* **2003,** 377, (3), 528-539.

49. Green, R. J.; Frazier, R. A.; Shakesheff, K. M.; Davies, M. C.; Roberts, C. J.; Tendler, S. J. B., Surface plasmon resonance analysis of dynamic biological interactions with biomaterials. *Biomaterials* **2000,** 21, (18), 1823-1835.
50. Homola, J., Surface plasmon resonance sensors for detection of chemical and biological species. *Chemical Reviews* **2008,** 108, (2), 462-493.
51. Turková, J., Oriented immobilization of biologically active proteins as a tool for revealing protein interactions and function. *Journal of Chromatography B: Biomedical Sciences and Applications* **1999,** 722, (1-2), 11-31.
52. Marchant, R. E.; Barb, M. D.; Shainoff, J. R.; Eppell, S. J.; Wilson, D. L.; Siedlecki, C. A., Three dimensional structure of human fibrinogen under aqueous conditions visualized by atomic force microscopy. *Thrombosis and Haemostasis* **1997,** 77, (6), 1048-1051.
53. Hiroya, T.; Shunji, I.; Yuko, K.; Atsushi, S.; Takashi, O.; Yoh, I.; Kiyoshi, K.; Masaki, K.; Sumio, M., Pretreatment plasma fibrinogen level correlates with tumor progression and metastasis in patients with squamous cell carcinoma of the esophagus. *Journal of Gastroenterology and Hepatology* **2007,** 22, (12), 2222-2227.
54. Wojtukiewicz, M. Z.; Zacharski, L. R.; Moritz, T. E.; Hur, K.; Edwards, R. L.; Rickles, F. R., Prognostic-significance of blood-coagulation tests in carcinoma of the lung and colon. *Blood Coagulation & Fibrinolysis* **1992,** 3, (4), 429-437.
55. Liedberg, B.; Lundström, I.; Stenberg, E., Principles of biosensing with an extended coupling matrix and surface plasmon resonance. *Sensors and Actuators B: Chemical* **1993,** 11, (1-3), 63-72.
56. Wolberg, A. S., Thrombin generation and fibrin clot structure. *Blood Reviews* **2007,** 21, (3), 131-142.
57. Fan, X. D.; White, I. M.; Shopoua, S. I.; Zhu, H. Y.; Suter, J. D.; Sun, Y. Z., Sensitive optical biosensors for unlabeled targets: A review. *Analytica Chimica Acta* **2008,** 620, (1-2), 8-26.

CHAPTER 4

CHEMICAL-VAPOR-DEPOSITION-BASED SURFACE MODIFICATION STRATEGIES FOR THE GENERATION OF MULTIFUNCTIONAL SURFACES VIA "CLICK" CHEMISTRY

The material in this chapter has been adapted with minor modifications from the following article which is being submitted for publication:

Ross, A.M., Durmaz, H., Cheng, K., Friedmann, C., Oh, J., Deng, X., Lahann, J., "CVD-Based Surface Modification Strategies for the Generation of Multifunctional Surfaces via "Click" Chemistry", In preparation.

4.1 INTRODUCTION

4.1.1 "Click" Chemistry

Ideally, surface-mediated assembly involves substrates with high reactivity and efficient reactions kinetics.[1] "Click" chemistry refers to a broad class of reactions utilized to create defined surface chemistries on the micron- and nanoscale.[2] Developed by Sharpless et al., it has a wide range of applications in chemistry, materials, and biology.[3] Relevant "click" reactions, including those that utilize functionalized paracyclophanes as a reactive partner which will be further described herein.

4.1.1.1 Diels Alder Reactions

A commonly utilized "click" chemistry is the Diels Alder reaction. This reaction consists of [4 +2] cycloaddition reaction between a diene which is electron rich and a

dienophile which is electron poor resulting in the formation of a stable cyclohexene adduct.[4] It has been used to modify peptides and proteins[5] and for the surface functionalization of organic and inorganic surfaces and nanostructures.[6, 7] The Diels Alder reaction is advantageous in that it is thermally reversible and is not metal catalyzed.

4.1.1.2 Copper Catalyzed Cycloaddtion Reactions

One of the most prominent click reactions is the Cu^{I}-catalyzed Huisgen 1,3-dipolar cycloaddition of terminal alkynes and azides (CuAAC). Examples of its use include the functionalization of single-walled carbon nanotubes[8] and the surface modification of nanodiamond nanoparticles.[9] However, this chemistry may be limited in biomedical applications as copper is toxic to cells.[10] Therefore it would be advantageous to use copper-less "click" chemistries for surface modifications that involve biomolecules.[11, 12]

4.1.1.3 Thiol-based "Click" Reactions

In an effort to move away from metal-catalyzed "click" reactions, particularly for biomedical uses, thiol "click" chemistries have recently emerged as a group of chemical reactions with attractive attributes for surface modifications in biomedical applications as they are not copper catalyzed. Several classes of thiol "click" chemistries exist including nucleophilic thiol-"click" chemistries and thiol-radical "click" chemistries.[13] Nucleophilic, thiol-"click" chemistries are largely influenced by the substrate and its susceptibility to attack which further impacts the rate at which these reactions occur.

Within this class of "click" chemistries, thiol-halogen nucleophilic substitution reactions are of particular interest. Thio-bromo "click" chemistries fall under this reaction class and have been utilized in dendrimer synthesis and the generation of glycopolymers.[14] The aforementioned uses are applicable in biomedical fields such as drug delivery and tissue engineering. Moreover, due to the large number of functionalized thiols currently available including biotinylated-[15], carboxyl-[16], and azide-terminated[17] thiols can also serve as a platform for additional surface modification/self-assembly.

4.1.2 "Click" Chemistry and Controlled Radical Polymerizations

The utility of thiol-click chemistries is enhanced when they are utilized in conjunction with other surface modification techniques. Controlled radical polymerizations (CRPs) are attractive for surface modification because they allow for tight control of polymer polydispersity, i.e. yielding polymers of a narrow molecular weight distribution, and are applicable to a wide range of monomers and solvents. [18, 19] Some of the most commonly utilized CRPs are atom transfer radical polymerization (ATRP),[20] nitroxide-mediated polymerization (NMP),[21] and reversible addition-fragmentation transfer (RAFT) polymerization.[22] Of these, ATRP is especially attractive, because it is water and impurity tolerant in addition to having relatively low polymerization temperatures.[23] The wide applicability of "click" chemistries and CRPs make their combination appealing. In particular, investigators have utilized "click" chemistries in conjunction with RAFT polymerization to generate alkyne functionalized polymer brushes that could be utilized in a host of post polymerization processes [24]

Furthermore, Opsteen et al., utilized ATRP and successive click reactions in the generation of modular block copolymers.[25]

So far, many of the efforts have primarily focused on the combinatorial use of "click" chemistry and CRP to generate functionalized polymers. However, this combination is also of value to the materials science community as a means of generating multifunctional surfaces and this particular application will be highlighted in this chapter. In particular, chemical vapor deposition polymers have a host of functional groups, including those used to initiate ATRP, namely poly[(*p*-xylylene-4-methyl-2-bromoisobutyrate)-*co*-(*p*-xylylene)] (PPX-EB) which may be exploited.[23] Chemical vapor deposition polymerization enhances the versatility of thiol-based "click" chemistries and ATRP as it can be applied to a wide range of substrates. Further highlighted herein, is the CVD polymerization of two novel paracyclophanes 4-(3,4-dibromomaleimide)[2.2]paracyclophane and [2.2]paracyclophane-4-furan which are also used for "click" chemistries. In this work, the generation of a multifunctional surface is demonstrated via a combination of "click" chemistry and atom transfer radical polymerization on reactive CVD coatings. Specifically, the thiol chemistry is extended beyond noble metal substrates to include silicon, copper, and glass slides. Additionally, this platform is showcased as a means of creating complex architectures for biomedical and self-assembly applications.

4.2 EXPERIMENTAL METHODS

4.2.1 Synthesis of Functionalized Paracyclophanes

4.2.1.1 Synthesis of 4-(3,4-dibromomaleimide)[2.2]paracyclophane

Triphenylphosphine (1.05 g, 4.01 mmol) was dissolved in 100 mL of anhydrous THF and cooled to -78°C in a dry ice/acetone bath. The solution was stirred at this temperature for 30 min under nitrogen atmosphere. Diisopropyl azodicarboxylate (0.79 mL, 4.01 mmol) was added dropwise to the solution over 5 min and stirred for 30 min. 4-(hydroxymethyl)[2.2]paracyclophane (1.05 g, 4.41 mmol) was dissolved in 5 mL of THF and added dropwise to the mixture over 10 min. Finally, neopentyl alcohol (0.176 g, 2.0 mmol) and 3,4-dibromomaleimide (1.02 g, 4.01 mmol) were added to the mixture, respectively. The reaction mixture was stirred at -78 ^{o}C for 2 h and then overnight at room temperature. The solvent was removed in vacuo yielding yellow oil which was purified by column chromatography over silica gel eluting with ethyl acetate/hexane (1:4) afforded yellow solid. The solid was taken to a beaker and diethyl ether (20 mL) was added and stirred at room temperature for 1 h filtered and washed several times with diethyl ether. Yellow powder was obtained after drying. R_f = 0.55 (1:4, ethyl acetate/hexane). Yield (0.7 g, 37%). ^{1}H NMR (400 MHz, $CDCl_3$) 6.8-6.2 (m, 7H, Ar*H*), 4.71 (d, 1H, ArC*H*$_2$N), 4.51 (d, 1H, ArC*H*$_2$N), 3.65 (m, 1H, ArC*H*$_2$C*H*$_2$Ar), 3.2-2.8 (m, 7H, ArC*H*$_2$C*H*$_2$Ar). ^{13}C NMR (100 MHz, $CDCl_3$, δ): 163.5, 140.3, 139.5, 139.2, 137.9, 135.3, 134.5, 133.7, 133.5, 133.1, 132.6, 132.2, 129.4, 129.2, 41.5, 35.2, 34.9, 34.6, 33.3.

4.2.1.2 Synthesis of [2.2]paracyclophane-4-furan

4-(hydroxymethyl)[2.2]paracyclophane (0.65 g, 2.73 mmol) was dissolved in 20 mL of CH_2Cl_2 under nitrogen atmosphere. 2-Furoic acid (0.33 g, 3.0 mmol), and DMAP (0.067 g, 0.54 mmol) were added to the solution in that order. After stirring 5 min at room temperature, DCC (0.62 g, 3.0 mmol) dissolved in 5 mL of CH_2Cl_2 was added to the mixture. Reaction mixture was stirred overnight at room temperature and filtered to remove urea by-product. The solvent was evaporated and the crude product was purified by column chromatography over silica gel eluting with ethyl acetate/ hexane (4:1) to give **12** as a white solid. R_f = 0.41 (1:4, ethyl acetate/hexane). Yield (0.55 g, 61%). ^{1}H NMR (400 MHz, $CDCl_3$) 7.56 (d, 2H, C*H* of furan), 7.21 (d, 2H, C*H* of furan), 6.8-6.3 (m, 8H, C*H* of furan and Ar*H*), 5.29 (d, 1H, ArCH_2OC=O), 5.09 (d, 1H, ArCH_2OC=O), 3.41 (m, 1H, ArCH$_2$CH_2Ar), 3.2-2.8 (m, 7H, ArCH_2CH_2Ar). ^{13}C NMR (100 MHz, $CDCl_3$, δ): 158.7, 146.4, 144.6, 140.1, 139.5, 139.2, 138.4, 135.1, 133.9, 133.8, 133.2, 133.1, 133.0, 132.2, 129.7, 118.0, 111.8, 65.6, 35.2, 34.9, 34.5, 32.9.

4.2.2 Chemical Vapor Deposition Polymerization

A custom chemical vapor deposition system composed of a sublimation zone, pyrolysis zone, and deposition zone was used to generate polymer coatings.[26] For this particular work, CVD coatings of [2.2]paracyclophane-4-methyl 2-bromoisobutyrate (PPX-EB), parylene N (PPX-N), [2.2]paracyclophane-4-furan (PPX-Furan), and 4-(3,4-dibromomaleimide)[2.2]paracyclophane (PPX-BrMal) are generated. PPX-EB was sublimed at 120°C, underwent pyrolysis at 540-550°C, and was deposited at 15°C onto gold, silicon, copper, or glass substrates via spontaneous polymerization. Pressure was

maintained at 0.3 mbar and the deposition occurred on a rotating sample holder that was held at 15°C. Polymerization conditions for PPX-N and PPX-Furan were the same as that for PPX-EB except for the pyrolysis temperature which were 660°C and 510°C respectively. For the polymerization of the PPX-BrMal, 120°C, 750°C, and 23°C were used as the sublimation, pyrolysis, and deposition temperatures respectively and the pressure was constant at 0.3 mbar. Patterning of the CVD coatings was accomplished via a vapor-assisted micropatterning in replica structures (VAMPIR) technique which has been previously described.[27] Briefly, PDMS was spin-coated at 1000 rpm for 45 seconds onto a patterned silicon wafer. The PDMS coating was baked overnight at 60°C and then mechanically removed from the patterned wafer resulting in a structure consisting of 300 μm squares. At this point the, patterned PDMS was placed in conformal contact with PPX-N coated substrates of silicon, gold, glass, or copper and polymerization of the functionalized paracyclophanes was undertaken in accordance with the previously mentioned CVD processing conditions as displayed in **Figure 4.3**.

4.2.3 Surface Analysis: FT-IR, XPS, Ellipsometry

Fourier transform infrared spectroscopy (FT-IR) was utilized to confirm film presence after CVD. It also served to confirm the successful polymerization of poly(OEGMA) after thiol patterning. In all instances, a Nicolet 6700 spectometer with a resolution of $4cm^{-1}$ and 85° grazing angle was utilized. A total of 128 scans were taken for each sample. X-ray photoelectron microscopy (XPS) was used to assess the composition of the homopolymer before and after surface modification. Specifically, data were recorded with an Axis Ultra X-ray photoelectron spectrometer (Kratos Analyticals,

UK) outfitted with a monochromatized Al Ka X-ray source at a power of 150 kW. Both survey and high resolution spectra were taken at 160 eV and 20 eV respectively. Information on film thickness and visualization of surface patterning was provided by a multi-wavelength imaging null-ellipsometer (EP^3 Nanofilm, Germany). Thickness was determined by fitting ellipsometric delta and psi with fixed values of the real and refractive index of the CVD coating (n=1.6 and k=0). Measurements were taken at an angle of incidence of 60° for gold, 65° for copper, and 70° for silicon. A CCD camera incorporated into the ellipsometer was used to capture images and the field of view was 0.5 mm^2.

4.2.4 Thiol or Maleimide Immobilization

The thiols of interest, perfluorodecanethiol (PFC10) (Sigma Aldrich, St. Louis, MO) or biotin-PEG-thiol (Nanocs, New York, NY), were immobilized on the CVD-coated substrates by an incubation reaction or via microcontact printing. A biotin-PEG-maleimide (Nanocs, New York, NY) or *N*-(4,4,5,5,6,6,7,7,8,8,9,9,9-Tridecafluorononyl)maleimide (TFMal) (Sigma Aldrich, St. Louis, MO) was used in the surface modification of the PPX-Furan.

4.2.3.1 PPX-EB

For the surface modification of the PPX-EB, a solution comprised of 10 mM of PFC10 was then combined with a 21 mM solution of triethylamine (Et_3N) in acetonitrile and a drop of dithiothreitol (DTT). Here, the DTT served as a reducing agent to prevent the creation of disulfide bonds. The reaction for incubated substrates was allowed to

proceed for 16 mins and then rinsed with ethanol and deionized water as seen in **Figure 4.1**. Patterning of the PPX-EB coatings via microcontact printing consisted of placing a PDMS stamp into physical contact with the CVD-coated substrate as shown in **Figure 4.2**. The PDMS stamp was comprised of a 100 by 400 micron patterned array. A solution containing the thiol of interest, Et_3N, and DTT was vortexed and then used as the ink for the PDMS stamp. Before placing it in contact with the CVD substrate, the stamp was inked and dried in a stream of nitrogen. Contact was maintained for 3-5 mins and then the samples rinsed with ethanol and deionized water.

4.2.3.2 PPX-BrMal & PPX-Furan

The surface modification of PPX-BrMal and PPX-Furan was undertaken on both patterned and homogenous substrates. For PPX-BrMal, PFC10 (10 mM in ethanol) or biotin-PEG-thiol (10 mM in deionized water) were immobilized onto the substrates via a 12.5 h solution reaction. After reaction, substrates were rinsed with deionized water and/or ethanol as appropriate. The PPX-Furan substrates were reacted for 48-72 h with TFMal (1 mg/mL in ethanol) or biotin-PEG-maleimide (1 mg/mL in deionized water) in order to immobilize the maleimide.

4.2.5 Atom Transfer Radical Polymerization: Surface Modification of PPX-EB

Atom transfer radical polymerization (ATRP) was an additional surface modification method for the PPX-EB substrates utilized in this study. In this work, an aqueous solution of poly(ethylene glycol methacrylate) was purified via column chromatography prior to polymerization. Once purified, a solution of OEGMA

(OEGMA/deionized water, 1:1, v:v) and 2'2 bipyridyl (5.13 mg/mL) were stirred in a schlenk flask at room temperature for 10 mins. Then the solution was degassed 2 times via freeze-pump-thaw cycles. This solution was frozen again and the catalyst complex, consisting of CuBr (1.5mg/mL) and $CuBr_2$ (0.73 mg/mL), was added and the flask placed under vacuum to repeat the pump-thaw process. Then a final freeze-pump thaw cycle was completed. At this juncture, the mixture was stirred as it was warmed to room temperature resulting in a reddish-brown solution. Scintillation vials were degassed via 3 vacuum-argon purge cycles and then placed into an argon purged glove bag along with the solution. This solution was then distributed into 20 ml scintillation vials that contained the CVD substrates. The ATRP reaction was allowed to proceed for 30 mins, after which CVD substrates were rinsed with deionized water and dried.

4.2.6 Protein Immobilization & Visualization

A fluorescently labeled protein, streptavidin TRITC, was incubated on surfaces containing an immobilized thiol or maleimide. For PPX-EB the analyte concentration was 40 µg/mL and its buffer consisted of PBS, tween (0.01% w/v), and BSA (0.2% w/v). The protein concentration for PPX-BrMal and PPX-Furan substrates was decreased to 1:100 dilution of 40 µg/mL concentration, however the buffer remained the same. After one hour of protein exposure, CVD substrates were rinsed 3 times with PBS, buffer, and deionized water and were then dried prior to fluorescence imaging. Protein immobilization was visualized via fluorescence microscopy on a Nikon Eclipse 80i.

4.3 RESULTS AND DISCUSSION

4.3.1 Characterization of Vapor-Deposited Substrates

Approximately 30-50 nm polymeric coatings of PPX-EB, PPX-BrMal, and PPX-Furan were generated and served as the base for subsequent surface modifications. Coating thickness is determined by ellipsometry on the basis of an n_k fix model assuming a refractive index of approximately 1.6 for the functionalized polymer films which is determined from optical fitting. In particular, the PPX-EB coating was selected, because it contains a bromo group, which can be substituted with a thiol via thio-bromo "click" chemistry (as a result of a nucelophilic addition) or can serve as an initiator for copper catalyzed polymerization reactions. Maleimide is known to be highly reactive with thiols[28] and bromomaleimides have been shown to be even more reactive.[29] Thus a PPX-BrMal was investigated and in this instance thiol immobilization is facilitated via a Michael addition "click" reaction between the thiol and the maleimide functionality and a thio-bromo "click" reaction between the thiol and the bromine functionality. A Diels Alder "click" reaction is exploited in the immobilization of maleimide to PPX-Furan. Prior to surface modification, the presence of the expected surface functional groups was confirmed via FT-IR and XPS. For all of the coatings, FT-IR revealed characteristic bands from 2800-3300 cm^{-1} indicating the presence of C-H symmetric and asymmetrtic bands. In addition, bands at 1730 cm^{-1} and from 1000-1300 cm^{-1} are indicative of the C=O bond and the C-O-C stretches respectively as seen in **Figure 4.4**. Furthermore, the coating compositions were confirmed via XPS as spectra indicative of O_{1S}, C_{1S}, N_{1S}, and Br_{3p} are evident as appropriate in the survey spectra in **Figures 4.5-4.7A**. The atomic compositions of the novel coatings, PPX-BrMal and PPX-Furan, were compared to the

theoretical values. Theoretical composition values were calculated based on the structure of each polymer. PPX-BrMal consisted of 82.17 atom% oxygen, 7.95 atom % carbon, 3.82 atom % bromine, and 3.87 atom % nitrogen. This compares well with the theoretical values of the PPX-BrMal coating of 80.77 atom% oxygen, 7.69 atom % carbon, 7.69 atom % bromine, 3.85 atom % nitrogen. The atomic composition found for PPX-Furan also compared favorably to theoretical values. PPX-Furan was comprised of 85.84 atom % carbon and 12.73 atom % oxygen which aligns well with the theoretical values of 88 atom% carbon and 12 atom % oxygen.

4.3.2 Surface Modification: Thiol Immobilization and Atom Transfer Radical Polymerization

Several methods were utilized to confirm thiol or maleimide immobilization. First, for substrates in which PFC10 had been homogenously immobilized, XPS was utilized. Since fluorine is readily apparent in XPS, a thiol containing 17 fluorine atoms was selected for immobilization because the signal from the thiol is readily distinguishable from that of the CVD coatings which should not have fluorine. From the XPS survey spectra in **Figure 4.5** and **Figure 4.6**, it is apparent that there is an increase in the fluorine signal on the PPX-EB and PPX-BrMal coatings after immbolization of the perfluorinated thiol demonstrating successful immobilization via the various thio-"clicks." XPS also confirmed the immobilization of TFMal onto PPX-Furan as fluorine atoms are apparent after TFMal exposure as shown in **Figure 4.7**.

These initial findings served as a proof of concept for CVD coatings as a platform for "click" chemistries that are not metal-catalyzed and the focus was then shifted to spatio-selective immobilization of thiol or maleimide moieties for the generation of

multifunctional surfaces. For PPX-EB, a grid pattern consisting of 100 μm lines separated by 400 μm squares were generated via microcontact printing (where the thiols were only printed on the lines) while 300 μm square patterns (functionalized PPX's only inside the squares) were generated via VAMPIR. Imaging ellipsometry is utilized to confirm patterning. Specifically, an imaging ellipsometric map of the patterned thiol on the PPX-EB coating was taken and patterning is apparent as thickness differences between the thiol and its background are displayed in the delta map provided in **Figure 4.8A**. A line scan of the delta map indicates a step height difference between the patterned thiol and the background PPX-EB coating. In addition, an imaging ellipsometry thickness map is used to indicate the spatio-selective deposition of PPX-BrMal and PPX-Furan into the 300 μm squares as indicated in **Figure 4.8B** and **Figure 4.8C** which display thicknesses of approximately 12 nm and 2 nm respectively. Furthermore, imaging elliposmetry is used to demonstrate pattern persistence on PPX-EB after further surface functionalization via PEGMA ATRP. PEGMA is primarily patterned in the squares as the bromine initiating groups for the ATRP are no longer available on the lines because they have been replaced by the thiol as a result of the thio-bromo "click." A line scan of the ellipsometric thickness map in **Figure 4.9B** displays a 3 nm difference between the thiol and the PEGMA layer when an n_k fix model assuming an n of 1.45 and 1.52 for the thiol and PEGMA respectively is used. Evidence of PEGMA presence is also provided by the FT-IR spectra in **Figure 4.9A** as there is a shift in the C-H stretch around 2900 cm^{-1}, C-O stretch around 1735 cm^{-1}, and the C-O-C stretch around 1220 cm^{-1} which also aligns well with previously reported data. [23]

4.3.3 Protein Binding

In the previous section, surfaces presenting multiple functional groups were generated. Specifically for PPX-EB substrates, a thiol was patterned in a PEGMA background. PEGMA may be utilized to passivate a surface for protein and biomolecular adsorption and this property may be exploited for the selective immobilization of proteins.[30] For the VAMPIR patterned PPX-BrMal and PPX-Furan, the base PPX-N coating was used as a non-reactive background for the selective immobilization of thiols and maleimides respectively. At this point, a fluorescently labeled protein, streptavidin TRITC, was spatio-selectively adsorbed onto the thiol patterned lines (PPX-EB), thiol patterned squares (PPX-BrMal), or maleimide patterned squares (PPX-Furan) as adsorption to the background was inhibited by the non-reactive backgrounds. As evidenced by the fluorescent micrographs in **Figure 4.10**, the rhodamine labeled streptavidin binds to the patterned lines or squares as appropriate and has little non-specific adsorption to the non-reactive background. Streptavidin has a strong affinity, with a dissociation constant K(d) on the order of 4*10^(-14) for the vitamin biotin, and is in fact the strongest non-covalent interaction known.[31] As a result, it is one of the most commonly utilized affinity pairs in molecular, cellular, and immunological assays.[32] Therefore, the adsorption of streptavidin to the patterned lines and squares could be utilized for susbsequent immobilization of various biotinylated moieties. For example, biotinylated Au nanoparticles or biotinylated antibodies could be immobilized to the adsorbed streptavidin creating areas of distinct roughness or chemoselectivity respectively which could be exploited in cellular or biomolecular studies.

4.4 CONCLUSIONS

In this chapter, vapor-deposited substrates as a new platform for "click" chemistries which are not copper catalyzed and that utilize thiols are demonstrated thereby expanding the number and type of substrates that may be utilized. Furthermore, selective patterning of the surfaces via microcontact printing enabled spatial control and allowed for the simultaneous presentation of multiple functional groups on the same surface. Reactivity of the thiols, maleimiedes, and non-reactive backgrounds is clearly demonstrated via a host of characterization techniques. This platform provides another means for generating complex surface architectures using a bottoms-up approach. This work has applications in molecular self-assembly, biomolecular patterning, and spatio-selective cell culture.

4.5 FIGURES AND TABLES

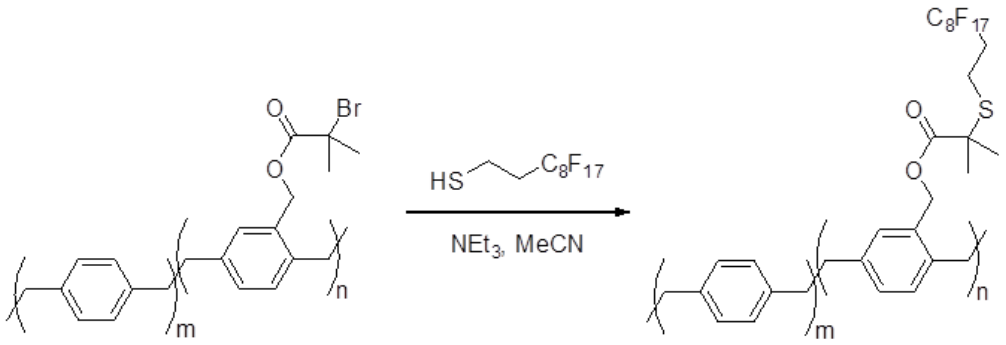

Figure 4.1. Reaction schemes for thio-bromo "click" chemistry with CVD substrates. A perfluorinated thiol is immobilized onto PPX-EB via thio-bromo "click" chemistry.

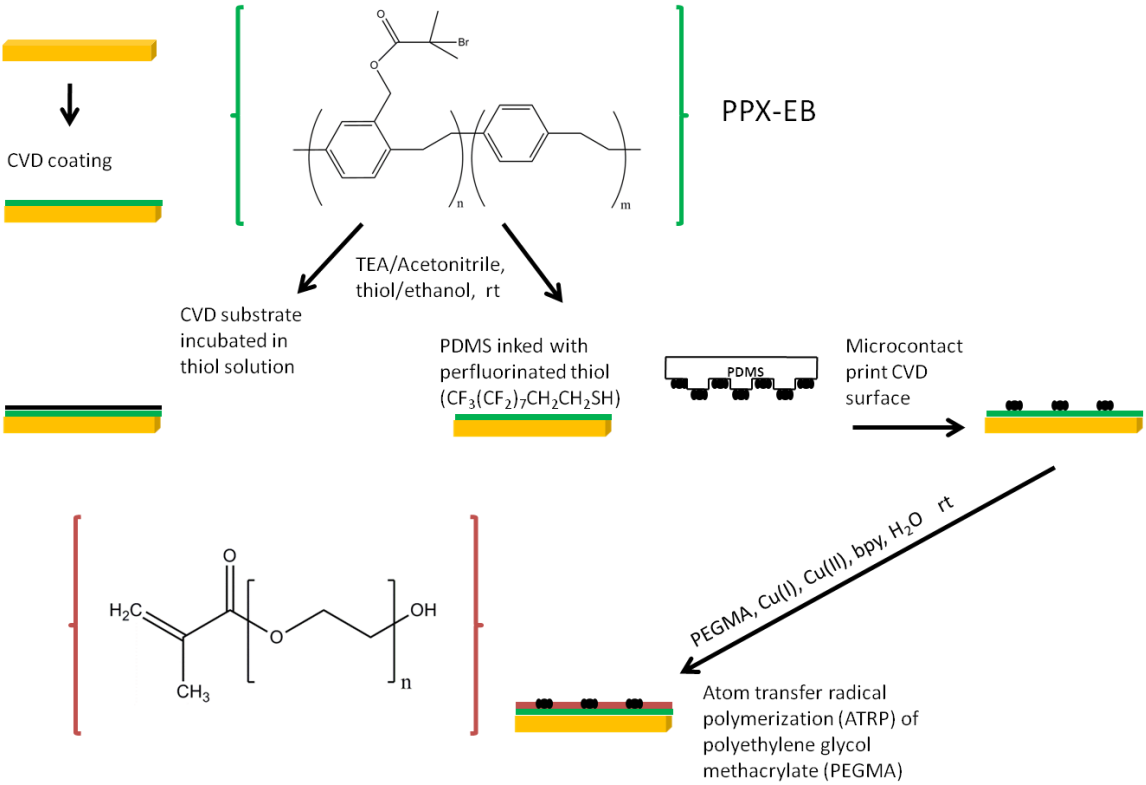

Figure 4.2. Schematic diagram of patterned PPX-EB sample preparation.

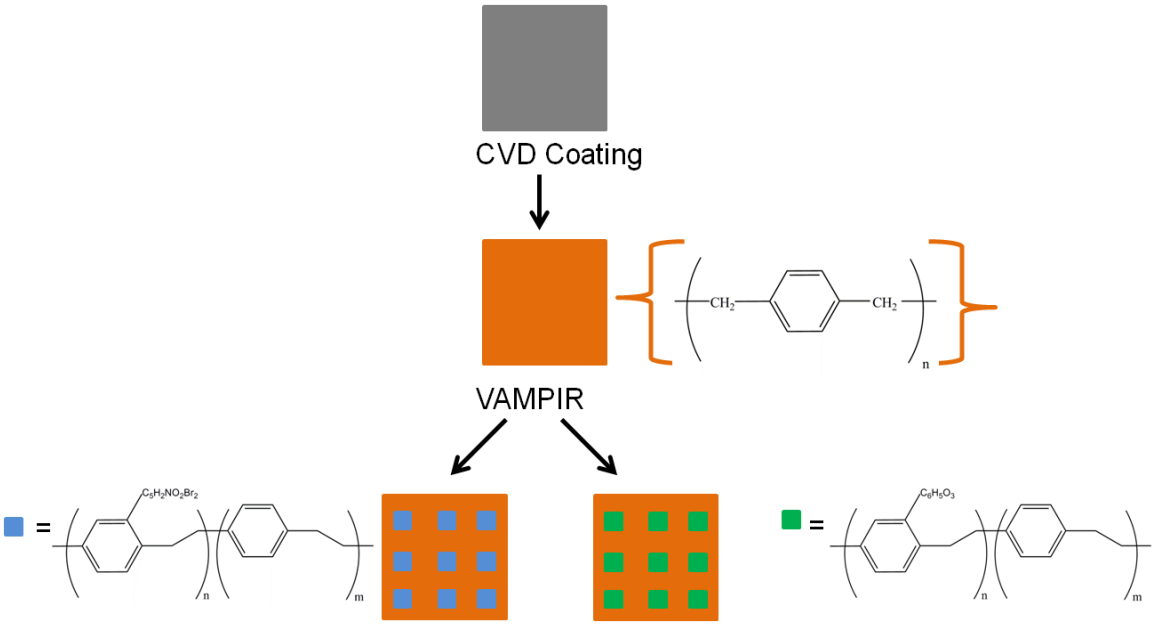

Figure 4.3. Schematic diagram of patterned PPX-BrMal and PPX-Furan sample preparation.

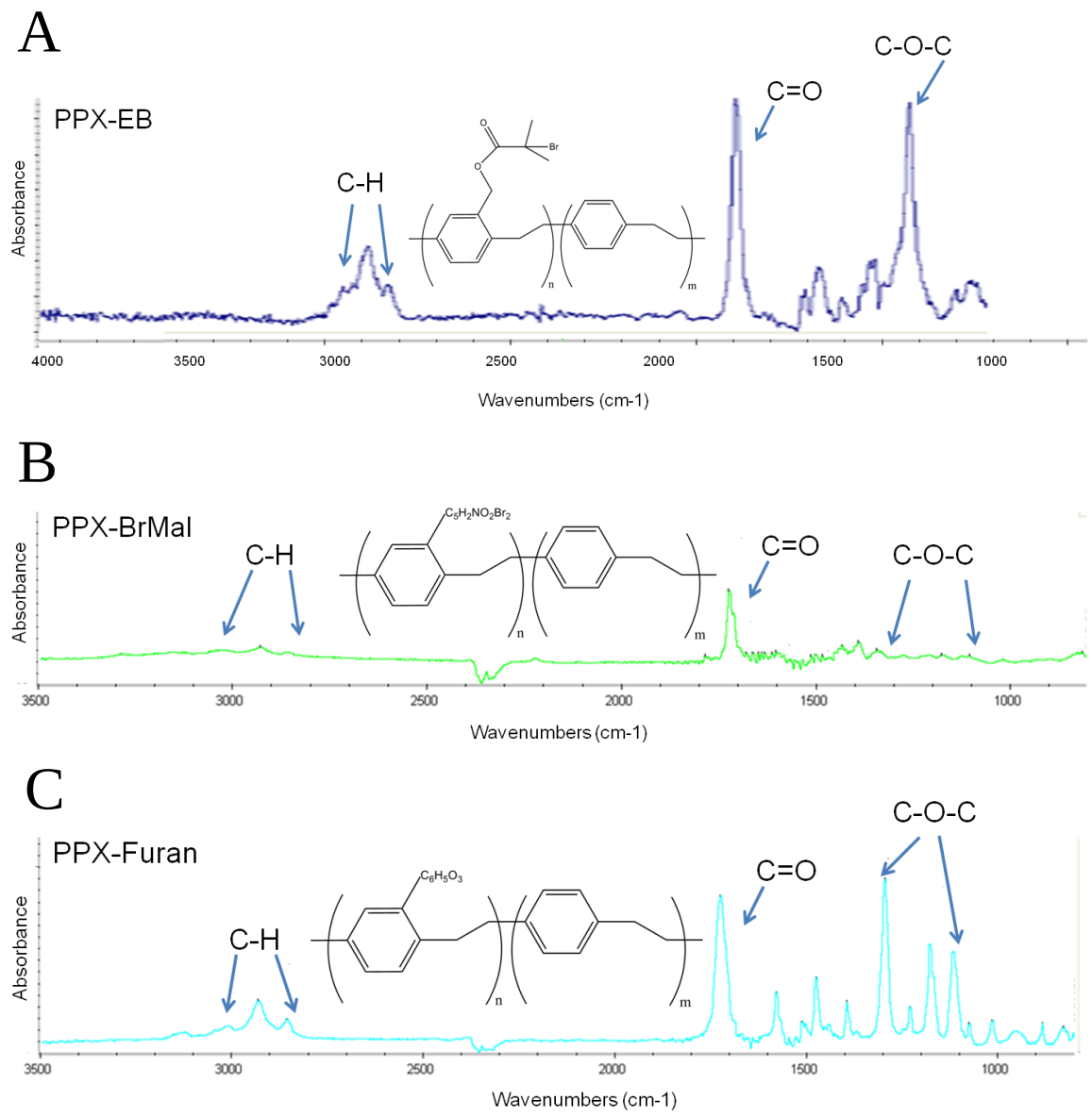

Figure 4.4. FT-IR of the functionalized paracyclophanes after CVD.

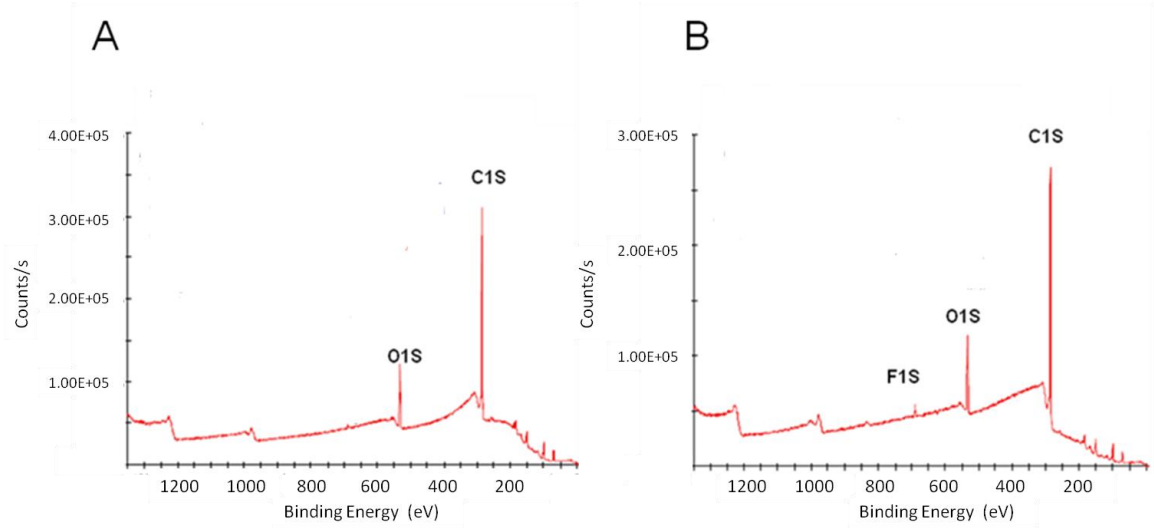

Figure 4.5. X-ray photoelectron spectroscopy of the PPX-EB coating. (A) PPX-EB coating before perfluorinated thiol immobilization. (B) PPX-EB coating after perfluorinated thiol immobilization via thio-bromo "click" chemistry

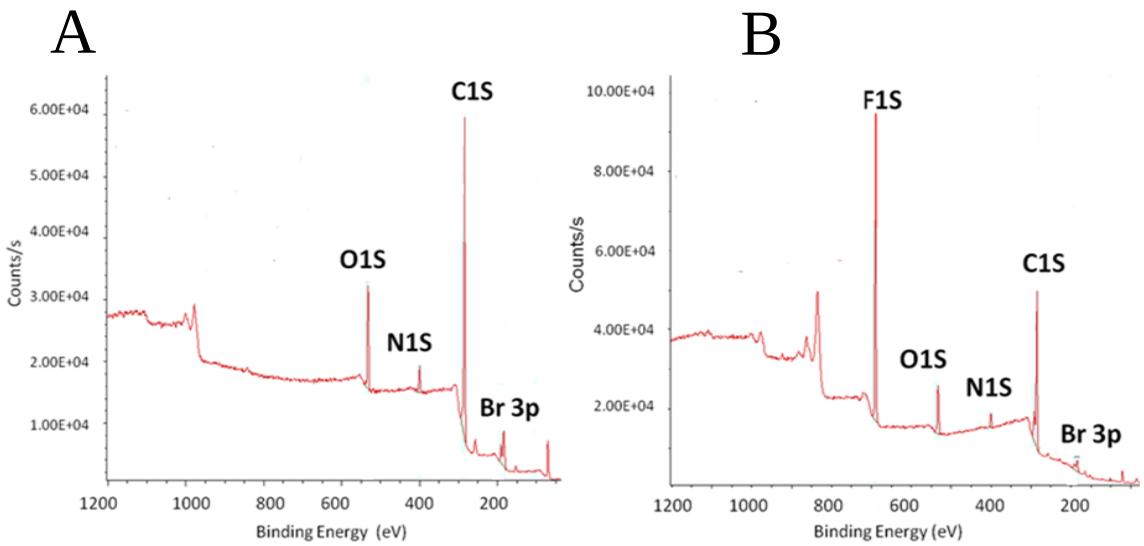

Figure 4.6. X-ray photoelectron spectroscopy of the PPX-BrMal coating. (A) PPX-BrMal coating before perfluorinated thiol immobilization. (B) PPX-BrMal coating after perfluorinated thiol immobilization

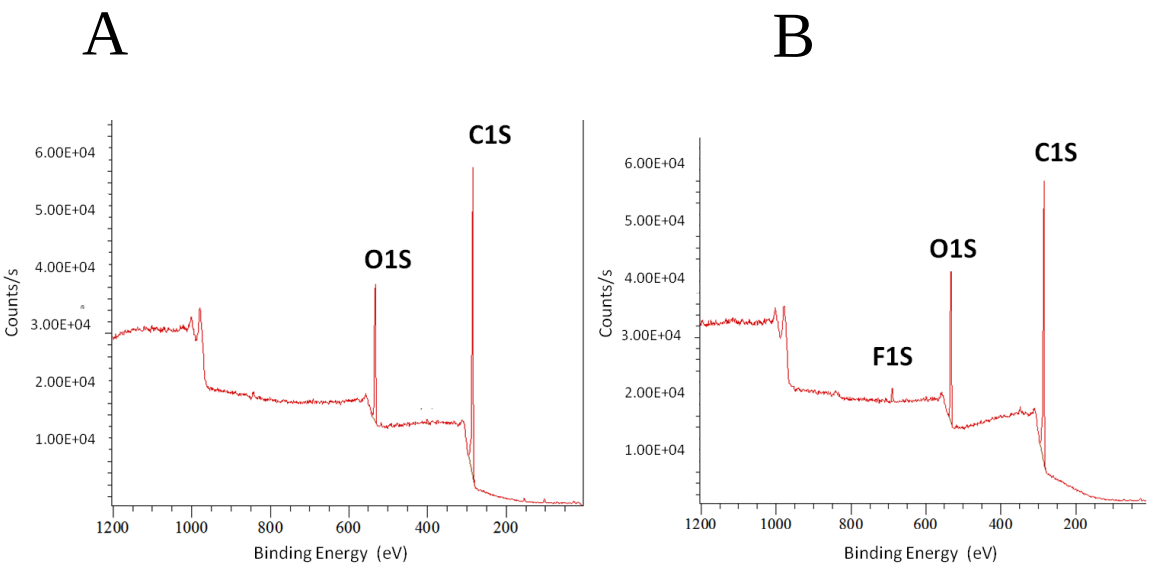

Figure 4.7. X-ray photoelectron spectroscopy of the PPX-Furan coating. (A) PPX-Furan coating before TFMal immobilization. (B) PPX-Furan coating after TFMal immobilization

A

B

C

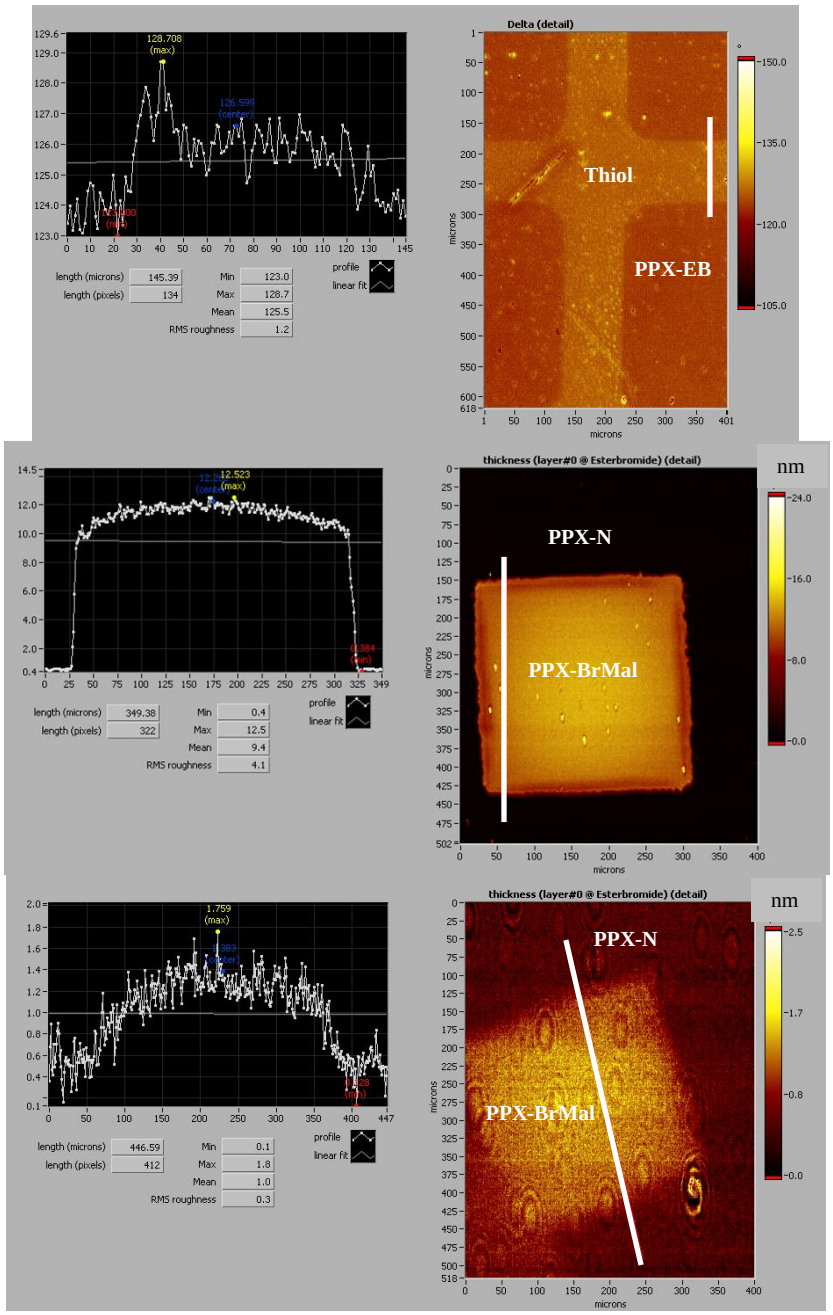

Figure 4.8. Patterning of functionalized PPX. (A) Imaging ellipsometry delta map of thiol (line) immobilization onto PPX-EB via microcontact printing. Imaging ellipsometry thickness map of PPX-BrMal VAMPIR (B) and PPX-Furan (C) onto a PPX-N background.

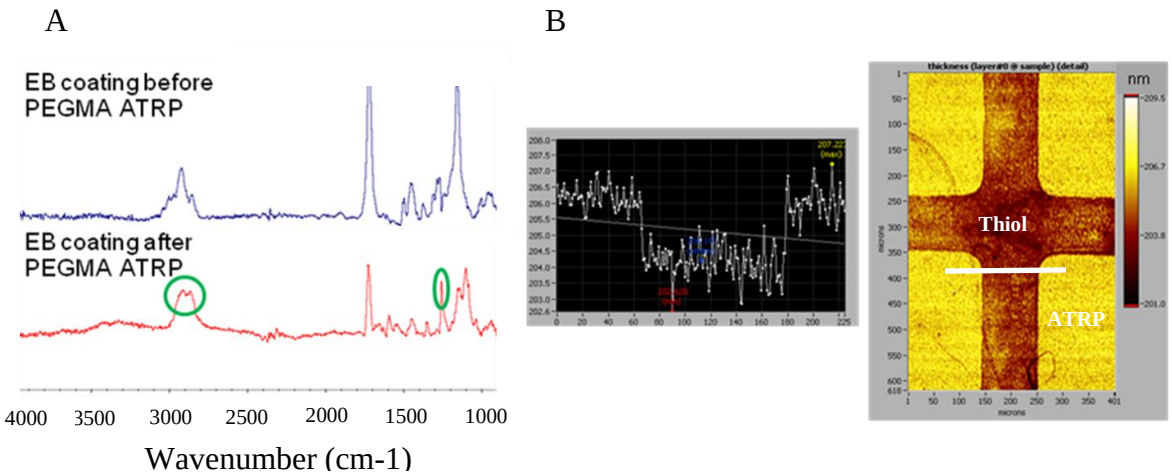

Figure 4.9. Surface analysis on patterned CVD substrates after the ATRP of poly(OEGMA). (A.) FT-IR of patterned before and after ATRP. (B.) Imaging ellipsometry thickness map of perfluorinated thiol (line) in a PEGMA background (squares) following ATRP.

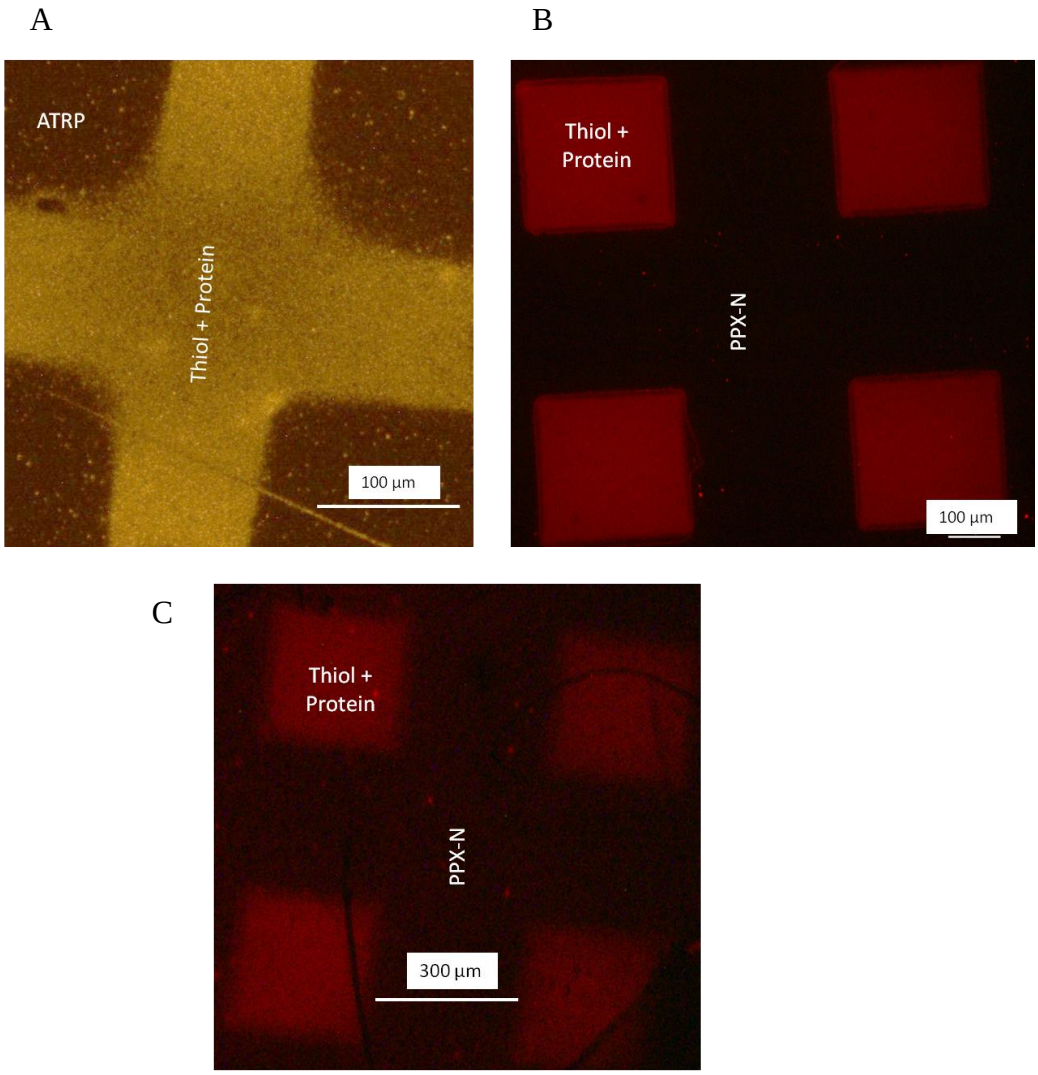

Figure 4.10. Fluorescence microscopy of thiol-patterned substrates after exposure to an aqueous solution of fluorescenctly-labeled streptavidin. (A) Micro-contact printing of thiol (lines) on PPX-EB in a passivated PEGMA background (B) VAMPIR of PPX-BrMal (squares) (C) VAMPIR of PPX-Furan (squares)

4.6 REFERENCES

1. Nandivada, H.; Chen, H. Y.; Bondarenko, L.; Lahann, J., Reactive polymer coatings that "click"". *Angewandte Chemie-International Edition* **2006,** 45, (20), 3360-3363.
2. Nandivada, H.; Jiang, X. W.; Lahann, J., Click chemistry: Versatility and control in the hands of materials scientists. *Advanced Materials* **2007,** 19, (17), 2197-2208.
3. Kolb, H. C.; Finn, M. G.; Sharpless, K. B., Click chemistry: Diverse chemical function from a few good reactions. *Angewandte Chemie-International Edition* **2001,** 40, (11), 2004-+.
4. Nicolaou, K. C.; Snyder, S. A.; Montagnon, T.; Vassilikogiannakis, G., The Diels-Alder reaction in total synthesis. *Angewandte Chemie-International Edition* **2002,** 41, (10), 1668-1698.
5. Hackenberger, C. P. R.; Schwarzer, D., Chemoselective Ligation and Modification Strategies for Peptides and Proteins. *Angewandte Chemie-International Edition* **2008,** 47, (52), 10030-10074.
6. Goodall, G. W.; Hayes, W., Advances in cycloaddition polymerizations. *Chemical Society Reviews* **2006,** 35, (3), 280-312.
7. Nebhani, L.; Barner-Kowollik, C., Orthogonal Transformations on Solid Substrates: Efficient Avenues to Surface Modification. *Advanced Materials* **2009,** 21, (34), 3442-3468.
8. Li, H. M.; Cheng, F. O.; Duft, A. M.; Adronov, A., Functionalization of single-walled carbon nanotubes with well-defined polystyrene by "click" coupling. *Journal of the American Chemical Society* **2005,** 127, (41), 14518-14524.
9. Barras, A.; Lyskawa, J.; Szunerits, S.; Woisel, P.; Boulcherroub, R., Direct Functionalization of Nanodiamond Particles Using Dopamine Derivatives. *Langmuir* **2011,** 27, (20), 12451-12457.
10. Inglis, A. J.; Barner-Kowollik, C., Ultra Rapid Approaches to Mild Macromolecular Conjugation. *Macromolecular Rapid Communications* **2010,** 31, (14), 1247-1266.
11. Debets, M. F.; van der Doelen, C. W. J.; Rutjes, F.; van Delft, F. L., Azide: A Unique Dipole for Metal-Free Bioorthogonal Ligations. *Chembiochem* **2010,** 11, (9), 1168-1184.
12. Deng, X. P.; Friedmann, C.; Lahann, J., Bio-orthogonal "Double-Click" Chemistry Based on Multifunctional Coatings. *Angewandte Chemie-International Edition* **2011,** 50, (29), 6522-6526.
13. Hoyle, C. E.; Lowe, A. B.; Bowman, C. N., Thiol-click chemistry: a multifaceted toolbox for small molecule and polymer synthesis. *Chemical Society Reviews* **2010,** 39, (4), 1355-1387.
14. Becer, C. R.; Hoogenboom, R.; Schubert, U. S., Click Chemistry beyond Metal-Catalyzed Cycloaddition. *Angewandte Chemie-International Edition* **2009,** 48, (27), 4900-4908.
15. Gau, J. J.; Lan, E. H.; Dunn, B.; Ho, C. M.; Woo, J. C. S., A MEMS based amperometric detector for E-Coli bacteria using self-assembled monolayers. *Biosensors & Bioelectronics* **2001,** 16, (9-12), 745-755.

16. Scotchford, C. A.; Gilmore, C. P.; Cooper, E.; Leggett, G. J.; Downes, S., Protein adsorption and human osteoblast-like cell attachment and growth on alkylthiol on gold self-assembled monolayers. *Journal of Biomedical Materials Research* **2002,** 59, (1), 84-99.
17. Sommer, W. J.; Weck, M., Facile Functionalization of Gold Nanoparticles via Microwave-Assisted 1,3 Dipolar Cycloaddition. *Langmuir* **2007,** 23, (24), 11991-11995.
18. Braunecker, W. A.; Matyjaszewski, K., Controlled/living radical polymerization: Features, developments, and perspectives. *Progress in Polymer Science* **2007,** 32, (1), 93-146.
19. Davis, K. A.; Matyjaszewski, K., Statistical, gradient, block, and graft copolymers by controlled/living radical polymerizations. *Statistical, Gradient, Block and Graft Copolymers by Controlled/Living Radical Polymerizations* **2002,** 159, 1-169.
20. Kamigaito, M.; Ando, T.; Sawamoto, M., Metal-catalyzed living radical polymerization. *Chemical Reviews* **2001,** 101, (12), 3689-3745.
21. Hawker, C. J.; Bosman, A. W.; Harth, E., New polymer synthesis by nitroxide mediated living radical polymerizations. *Chemical Reviews* **2001,** 101, (12), 3661-3688.
22. Barner-Kowollik, C.; Davis, T. P.; Heuts, J. P. A.; Stenzel, M. H.; Vana, P.; Whittaker, M., RAFTing down under: Tales of missing radicals, fancy architectures, and mysterious holes. *Journal of Polymer Science Part a-Polymer Chemistry* **2003,** 41, (3), 365-375.
23. Jiang, X. W.; Chen, H. Y.; Galvan, G.; Yoshida, M.; Lahann, J., Vapor-based initiator coatings for atom transfer radical polymerization. *Advanced Functional Materials* **2008,** 18, (1), 27-35.
24. Ranjan, R.; Brittain, W. J., Combination of living radical polymerization and click chemistry for surface modification. *Macromolecules* **2007,** 40, (17), 6217-6223.
25. Opsteen, J. A.; Van Hest, J. C. M., Modular synthesis of ABC type block copolymers by "click" chemistry. *Journal of Polymer Science Part a-Polymer Chemistry* **2007,** 45, (14), 2913-2924.
26. Lahann, J., Vapor-based polymer coatings for potential biomedical applications. *Polymer International* **2006,** 55, (12), 1361-1370.
27. Chen, H. Y.; Lahann, J., Vapor-assisted micropatterning in replica structures: A solventless approach towards topologically and chemically designable surfaces. *Advanced Materials* **2007,** 19, (22), 3801-+.
28. Ghosh, S. S.; Kao, P. M.; McCue, A. W.; Chappelle, H. L., Use of Maleimide-Thiol Coupling Chemistry for Efficient Syntheses of Oligonucleotide-Enzyme Conjugate Hybridization Probes. *Bioconjugate Chemistry* **1990,** 1, (1), 71-76.
29. Tedaldi, L. M.; Smith, M. E. B.; Nathani, R. I.; Baker, J. R., Bromomaleimides: new reagents for the selective and reversible modification of cysteine. *Chemical Communications* **2009**, (43), 6583-6585.
30. Benhabbour, S. R.; Sheardown, H.; Adronov, A., Protein resistance of PEG-functionalized dendronized surfaces: Effect of PEG molecular weight and dendron generation. *Macromolecules* **2008,** 41, (13), 4817-4823.
31. Green, N. M., Avidin and Streptavidin. *Methods in Enzymology* **1990,** 184, 51-67.

32. Holmberg, A.; Blomstergren, A.; Nord, O.; Lukacs, M.; Lundeberg, J.; Uhlen, M., The biotin-streptavidin interaction can be reversibly broken using water at elevated temperatures. *Electrophoresis* **2005,** 26, (3), 501-510.

CHAPTER 5

ANALYSIS AND CRITERIA FOR THE DESIGN AND USE OF SYNTHETIC SUBSTRATES FOR HUMAN PLURIPOTENT STEM CELL CULTURE

The material in this chapter has been adapted with minor modifications from the following published article:

Ross A.M., Nandivada H., Ryan A.L., and Lahann J. Synthetic substrates for long-term stem cell culture, *Polymer*, **53**, 2533-2539, (2012).

5.1 INTRODUCTION

The cellular environment is complex and plays an important role in cellular properties and processes. [1] For example, environmental cues have been shown to influence cell adhesion, proliferation, and gene expression. [2, 3] As a result, cell-material interactions are an integral part of *in vitro* cell studies and investigators have used synthetic biomaterials to mimic the cellular microenvironment in terms of its physiochemical properties. [4, 5] However, the influence of a single substrate property, such as surface chemistry, wettability, and roughness, is difficult to assess, because these properties may be interconnected and work synergistically to garner a particular cellular response. [6] In addition to proliferation and gene expression, environmental cues also impact the differentiation of stem cells. [7-9] Human pluripotent stem cells (hPSCs), due to their ability to differentiate into multiple cell types, have a myriad of applications in the

healthcare industry. [10, 11] Potential uses include cures/treatments for diseases such as heart failure and diabetes as well as drug safety and efficacy testing. [12-14]

Feeder layers of mouse embryonic fibroblasts (mEFs) and Matrigel™, an undefined gelatinous protein mixture secreted by mouse carcinoma cells, are currently utilized in hPSC culture. [15] Matrigel™ is typically placed on the cell culture substrate prior to cell seeding in order to generate a thin monolayer that serves as a complex, extracellular matrix (ECM). Although hPSCs show therapeutic promise, one of the major hurdles inhibiting clinical adoption is the use of this Matrigel™ culture system as it results in batch-to-batch variation, uses xenogenous factors which warrant immunogenic concerns, and is not suitable for large-scale hPSC expansion. [16] Synthetic substrates are a promising alternative for prolonged hPSC culture as they address many of these issues. Because synthetic surfaces are generated from defined materials and processes, there is little variation between batches and thus has greater potential for scale-up. [17] More importantly, eliminating the need for animal byproducts eradicates concerns regarding immunogenicity. [18]

This feature article highlights new developments in the use of synthetic biomaterials as substrates in the long-term culture of hPSCs. In particular, a zwitterionic polymeric system developed in our lab is described in terms of its fabrication, efficacy, and stability. This synthetic substrate is then compared to synthetic culture systems generated by other research groups that have demonstrated efficacy in maintaining prolonged hPSC culture. In this instance, substrates are assessed in terms of desired criteria for hPSC culture systems and provide a framework for examining challenges in the design and fabrication of substrates for expanding hPSCs.

5.2 HYDROGELS AND STEM CELLS

In an attempt to replace poorly defined biological matrices, numerous materials have been studied as potential stem cell substrates including electroactive polymers, tissue culture plastic, and self-assembled monolayers of alkanethiols. [19-21] Recent work in our group has focused on the use of hydrogels as a platform for stem cell culture. To that end, synthetic cell culture substrates are generated via surface-initiated graft polymerization of chemically defined polymers. In particular, various methacrylates were grafted onto tissue culture polystyrene (TCPS) dishes. Synthesis occurs in an oxygen-free glass reaction vessel. Briefly, the reaction vessel was degassed via a vacuum-argon purge cycle, which is completed three times. Simultaneously, the solvent, comprised of ethanol and deionized water in a volumetric ratio of 1:4, was degassed via vacuum for 40 min. Then the degassed solvent and the monomer of interest are added to the reaction vessel and heated such that the temperature range was between 76 and 82 °C. Tight temperature control is important for effective polymerization. Prior to monomer synthesis, free radicals must be created on the TCPS dishes by UV ozone plasma treatment. Later, these free radicals enable the polymerization of the monomers of interest. Once the reaction reached the desired temperature, TCPS dishes were added to the reaction vessel and polymerization proceeds for 2.5 h (**Figure 5.1**).

After the reaction is complete and the reaction vessel has been cooled to at least 60 °C, the dishes were removed and rinsed overnight in a 1% saline solution that was maintained at 50 °C to remove any excess monomer. Subsequent rinsing steps with 1% saline and deionized water ensure that any unreacted monomer has been eliminated. [22] Because the influence of hydrogel structure on hESCs was unknown, a total of six

methacrylate derivatives were generated for cell screening. Specifically, poly[carboxybetaine methacrylate] (PCBMA), poly[[2-(methacryloyloxy)ethyl]trimethylammonium chloride] (PMETAC), poly[poly(ethylene glycol) methyl ether methacrylate] (PPEGMA), poly[2-hydroxyethyl methacrylate] (PHEMA), poly[3-sulfopropyl methacrylate] (PSPMA), and poly[2-(methacryloyloxy)ethyl dimethyl-(3-sulfopropyl)ammonium hydroxide] (PMEDSAH) were characterized in terms of their material properties and by the ability of hESCs to adhere and maintain an undifferentiated state on these surfaces (**Figure 5.2**). [23]

Of the hydrogels assessed, only the zwitterionic PMEDSAH was able to support undifferentiated hESCs from two cell lines (BG01 and H9) for long-term passage (passage number ≥25) as indicated by hESC gene expression, karyotype, and embryoid body formation (**Figure 5.3**). Results from the synthetic substrates were compared to Matrigel™, which served as a control and no significant difference was noted. As a proof of concept, a commonly utilized media from animal-derived products, mouse embryonic fibroblast-conditioned media (MEF-CM), was used in this initial screening study. However, since the ultimate goal of our work is to make a more chemically defined system with enhanced clinical relevance, subsequent studies focused on the behavior of hESCs on PMEDSAH-coated dishes using media which lacked non-human animal products or in serum-free, defined media.

5.2.1 Storage and Sterility of PMEDSAH Coatings

Maintenance of material properties after prolonged storage and exposure to common sterilization methods are important aspects of making synthetic stem cell

substrates commercially viable. The stability of the PMEDSAH coating was investigated in an accelerated six-week storage study. In this instance, PMEDSAH-coated dishes were stored at three different conditions (all at room temperature) – (1) ambient, (2) inert (in a glove-bag under nitrogen atmosphere) and (3) vacuum (in a desiccator attached to a vacuum pump). Fourier transform infrared spectroscopy (FT-IR) and/or X-ray photoelectron spectroscopy (XPS) was used to assess the stability of the film. Elemental analysis of XPS samples exposed to the various storage conditions after six weeks were compared to those values previously reported in literature (**Table 5.1**). [23]

XPS indicates little difference between samples stored under air and nitrogen. However, vacuum conditions cause slight differences in the overall composition. FT-IR spectroscopy of samples stored under ambient conditions (in air at room temperature) revealed characteristic bands at 1732.9 cm^{-1} and 1208.4 cm^{-1} for carbonyl and sulfonate groups (**Figure 5.4**). Characteristic stretches were readily apparent in air and thus a difference under inert conditions is not expected.

The compatibility of PMEDSAH-coated dishes towards common sterilization methods, particularly e-beam- and gamma-radiation, was also investigated. E-beam- and gamma-radiation were selected because these methods are widely accepted for the sterilization of biomedical products, and unlike ethylene oxide treatments, no residual chemicals are left behind after processing. [24] PMEDSAH-coated dishes were exposed to three different levels of e-beam-radiation (10, 20 and 50 kGy) and gamma-radiation (8-15, 22-40, 45-75 kGy) respectively. The effect of radiation on the coatings was then investigated by XPS and FT-IR. The material composition of samples after radiation was compared to the values previously reported in literature (**Table 5.2**). [23] Overall, XPS

indicates that radiation does not cause a significant difference in the PMEDSAH coatings. This is further confirmed by FT-IR analysis as characteristic carbonyl, 1732.9cm^{-1}, and sulfonate, 1208.4cm^{-1}, bands are evident for each radiation type and level (**Figure 5.5**).

5.2.2 PMEDSAH and Human Embryonic Stem Cells in Xenofree/Defined Media

We further extended our work by culturing BG01 and H9 cells on PMEDSAH-coated dishes using a commercially available xenofree media, or media that lacks non-human animal products, but was instead conditioned with human cell serum. Matrigel™ was also used as a control. PMEDSAH substrates were shown to maintain pluripotency through 15 passages as evidenced by cell-population doubling times, hESC cell markers, and karyotyping. Not only were these culture conditions more clinically relevant in terms of the media utilized, but they also resulted in enhanced cell adhesion; at least for one of the hESC lines. In particular, hESC aggregate adhesion for H9 cells was significantly higher at each passage for cells grown on PMEDSAH in human cell-conditioned media (hCCM), 86 ± 6 %, than in MEF-conditioned media, 15 ± 2 %, (**Figure. 5.6**).

Finally, we explored the ability of PMEDSAH-coated substrates to promote the undifferentiated growth of hESCs in defined media conditions using two commercially available serum-free media, StemPro™ and mTeSR™. Attempts to passage H9 hESCs on PMEDSAH-coated dishes in mTeSR™ were unsuccessful and the focus was shifted to the StemPro™ media. These culture conditions led to the successful proliferation of undifferentiated H9 cells on PMEDSAH substrates throughout 10 passages while BG01 cells were maintained for 3 passages. The undifferentiated nature of the H9 cells was

confirmed via staining for hESC pluripotency markers and the directed differentiation of the cells into three specific lineages as specified by immunofluorescence and gene expression (**Figure. 5.7**). In subsequent culture, pluripotency could be maintained for up to 25 passages under these conditions.

5.3 EMERGENCE OF ALTERNATIVE SYNTHETIC CULTURE SYSTEMS AND BENCHMARKING

Due to the limitations associated with undefined matrices, more defined stem cell culture systems have been investigated. After our initial publication based on PMEDSAH, [23] other synthetic polymers have shown the ability to maintain stem cells in the undifferentiated state for numerous passages including another methacrylate containing polymer, hit 9, and an anhydride containing polymer poly(methyl vinyl ether-alt-maleic anhydride) (PMVE-alt-MA) (**Figure 5.8**). [25, 26] Hit 9 is fabricated through the use of photopolymerization while PMVE-alt-MA is generated by free radical polymerization. The aforementioned systems are entirely polymeric, but materials that have attached biomolecules, such as peptides, have also been identified. In particular, Synthemax™ (Corning) consists of an acrylate polymer with covalently immobilized amine-containing peptides on the surface (**Figure 5.8**). [27] Polymers are not the only materials of choice, as GKKQRFRHRNRKG, a heparin-binding peptide, has been conjugated to self-assembled alkanethiol monolayers and subsequently utilized for stem cell culture (**Figure 5.8**). [28] Synthetic biomolecules such as recombinant proteins and synthetic peptides have also served as substrates in cell culture. For example, a human recombinant protein, specifically laminin-511, has been generated to facilitate long-term hPSC culture (**Figure 5.8**). [29] Furthermore, synthetic peptides designed to engage specific

integrins involved in cell adhesion have been evaluated for hESC culture and initial results demonstrate their ability to support hESC adhesion and proliferation, though efficacy for prolonged culture has yet to be realized. [30] Creating new materials is not the only approach to generating synthetic culture systems. Polystyrene is a commonly used tissue culture plastic and it may be augmented to enhance prolonged stem cell culture. Recently, Saha et al., exposed polystyrene surfaces to short-wavelength UV in different doses to generate distinct surface chemistries. [31] Surfaces displaying particular amounts of carboxylic acid/ester and nitrogen-containing moieties were shown to promote long-term culture of pluripotent stem cells.

The ideal stem culture platform would support long-term expansion (≥20 passages) of undifferentiated stem cells, maintain efficacy in defined/xenofree media, has compatibility with common sterilization techniques, results from a process that is scalable, reusable, relatively inexpensive, and demonstrates efficacy for multiple stem cell lines and types. [32-34] Though several strategies other than grafting of PMEDSAH exist for prolonged stem cell culture, they are not without their limitations. In particular, PMEDSAH, Synthemax™, GKKQRFRHRNRKG, and recombinant laminin-511 have demonstrated efficacy for 10 or more passages of hESC culture in xenofree/defined media. This is significant as a large number of stem cells are required for many therapeutic applications and immunogenicity concerns abound with stem cell work. [35, 36] Thus it is advantageous for a substrate platform to work in xenofree media.

In order to ensure clinical applicability, culture substrates should be compatible with common batch sterilization techniques such as e-beam- and gamma-radiation. The data presented in the previous section indicates compatibility of these methods for

PMEDSAH coated substrates. However, radiation-based sterilization has not been demonstrated for some of its counterparts. In particular, sterilization data is not available for GKKQRFRHRNRKG, human recombinant laminin-511, and hit 9. Additionally, large-scale radiation sterilization is likely to degrade peptide and protein containing culture systems. [37] Reusability is also an issue for peptide based systems, Synthemax™ and GKKQRFRHRNRKG, as well as the recombinant laminin-511 system since they cannot be reused because peptides/proteins are subject to degradation by metalloproteinases secreted by the cultured cells. [38, 39] Degradation will lead to increased costs for end users as more culture substrates will be needed for a given task. The inclusion of peptides and recombinant proteins in the technologies also increases system costs as the peptides and proteins alone may be cost prohibitive. [40] Currently, Synthemax™ is the only commercially available synthetic stem cell culture platform and at a cost of $75 per 6-well plate, pricing may hinder access. Several stem cell types have clinical applicability including hESCs, human induced pluripotent stem cells (hiPSCs), and human mesenchymal stem cells (hMSCs). Thus in order to enhance wide-spread applicability, it is desirable for a cell culture system to promote long-term, undifferentiated culture for numerous stem cell lines and types. To date, PMEDSAH, Synthemax™, GKKQRFRHRNRKG, recombinant laminin-511, hit 9, and PMVE-alt-MA have all demonstrated efficacy with multiple stem cell types or stem cell lines. **Table 5.3** that follows provides a comparison of the synthetic substrates described in this work, relative to one another and to Matrigel™ the current gold standard for stem cell culture in defined media conditions.

It is apparent that many efforts have been focused on maintaining hPSCs in the undifferentiated state in long-term culture. However, ultimately these hPSCs will be directed to specific cell lineages for various applications in tissue engineering and regenerative medicine. Therefore, a number of important studies have attempted directed differentiation of hPSCs. [41, 42] Recently, hMSCs derived from hESCs have been encapsulated into poly(ethylene glycol)-based (PEG-based) hydrogels containing ECM proteins. [43] In this instance, stem cells were cultured for up to 6 weeks in media conditions designed to direct cells to chondrogenic or osteogenic lineages. Results indicated that the type of ECM protein contained within the hydrogel influenced the degree to which differentiation markers were expressed. Others have tuned the mechanical properties of materials to guide differentiation. For example, hESCs were cultured on poly(dimethylsiloxane) substrates with augmented stiffness to determine the influence of this material property on the differentiation of hESCs. [44] The authors found that stiffness impacted primary germ layer differentiation and terminal differentiation to an osteogenic lineage. Increasing substrate stiffness from 0.041 MPa to 2.7 MPa led to an upregulation of mesodermic markers in the early stages and to enhanced osteogenic differentiation in the terminal stages. Systematic studies on the role of stem cells and stem cell sourcing are essential in developing clinically relevant bone. [45]

5.4. CONCLUSIONS

The generation of synthetic substrates for sustained pluripotent stem cell culture in defined and xenofree media is a significant step in the use of hPSCs in therapeutics as well as basic research. At this juncture, polymeric and peptide-based materials have been utilized to maintain hPSCs in an undifferentiated state. However, the mechanism(s) of

action that result in the success of these substrates for prolonged culture have not been elucidated. Future work will aim to illuminate the influence and interaction of material parameters such as surface chemistry, hydrophilicity/hydrophobicity, stiffness, etc on stem cell maintenance. Doing so will enhance the design of biomaterials for stem cell applications. Recently, a majority of research has focused on hESCs, however an optimal substrate would be compatible with multiple cell types and therefore future work will assess the efficacy of these substrates for the long-term culture of numerous cell types. Efficacy and immunogenicity are not the only considerations as cost also impacts technology adoption. Going forward, cost effective materials and processes such as those used to generate our groups' zwitterionic hydrogel will need to be explored.

5.5 FIGURES AND TABLES

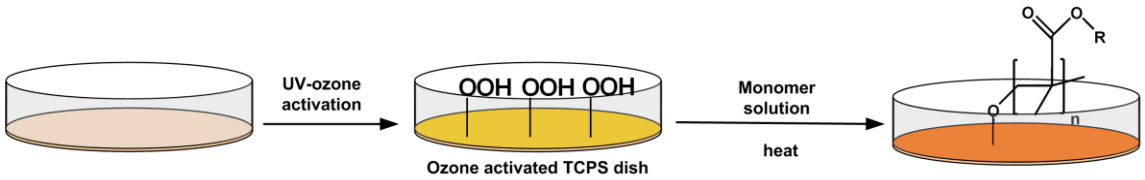

Figure 5.1.Schematic depicting the graft-polymerization process used to fabricate the polymer coatings. UV ozone was utilized to activate the tissue culture polystyrene dishes and then methacrylate-based monomers were subsequently polymerized on the surface. Reproduced from[23] with permission.

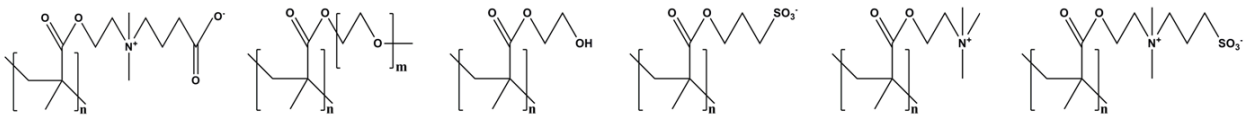

	PCBMA	PPEGMA	PHEMA	PSPMA	PMETAC	PMEDSAH
Contact Angle	71.6 ± 4.8	63.3 ± 3.1	56.0 ± 3.7	50.2 ± 4.1	40.5 ± 5.7	17.1 ± 1.1
Reduced Elastic Modulus (GPa)	3.3 ± 0.1	3.9 ± 0.1	3.0 ± 0.5	3.0 ± 0.1	3.3 ± 0.1	2.5 ± 0.1
Cell-aggregate adhesion (%)	0	5 ± 1	12 ± 1	14 ± 2	8 ± 1	15 ± 1
Number of passages	0	1	2	2	2	25

Figure 5.2. Long-term culture of H9 hESCs on methacrylate-derivative coatings with mouse embryonic fibroblast (MEF)-conditioned media. Table provides information about substrate properties (contact angle, reduced elastic modulus (GPa) (mean ± s.d.)) and cell behavior (initial hESC aggregate adhesion (mean ± s.e.m.) and number of passages achieved) on each polymer coating. Reproduced from [23] with permission.

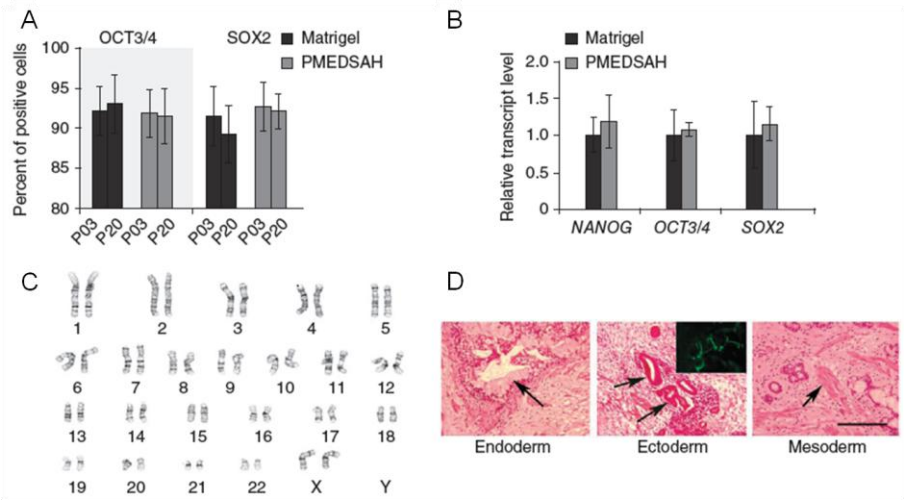

Figure 5.3. Cellular characterization of hESCs cultured on PMEDSAH substrates in MEF-CM. (A) Percentage (mean ± s.e.m.) of hESCs expressing OCT3/4 and SOX2 at passages 3 (P03) and 20 (P20). (B) Relative transcript levels of NANOG, OCT3/4 and SOX2 from hESCs cultured on PMEDSAH and Matrigel™. (C, D) After 25 passages, hESCs cultured on PMEDSAH (C) maintained a normal karyotype and (D) retained pluripotency as demonstrated by teratoma formation in immunosuppressed mice. Hematoxylin and eosin-stained paraffin sections indicating endoderm (goblet-like cells at arrow), ectoderm (neuroepithelial aggregates at arrow; and cells expressing neuron-restricted protein β-III tubulin in inset) and mesodermal derivatives (cartilage, connective tissue and muscle at arrow). Scale bar, 200 μm. Reproduced from [23] with permission.

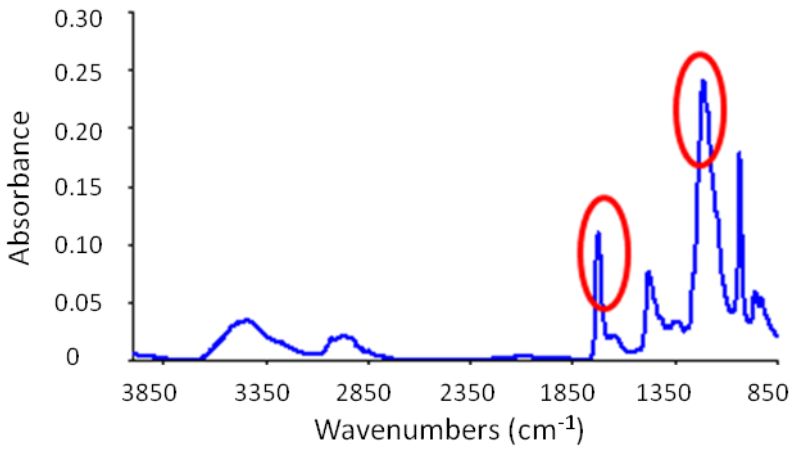

Figure 5.4. FT-IR of PMEDSAH coatings stored for six weeks under ambient conditions.

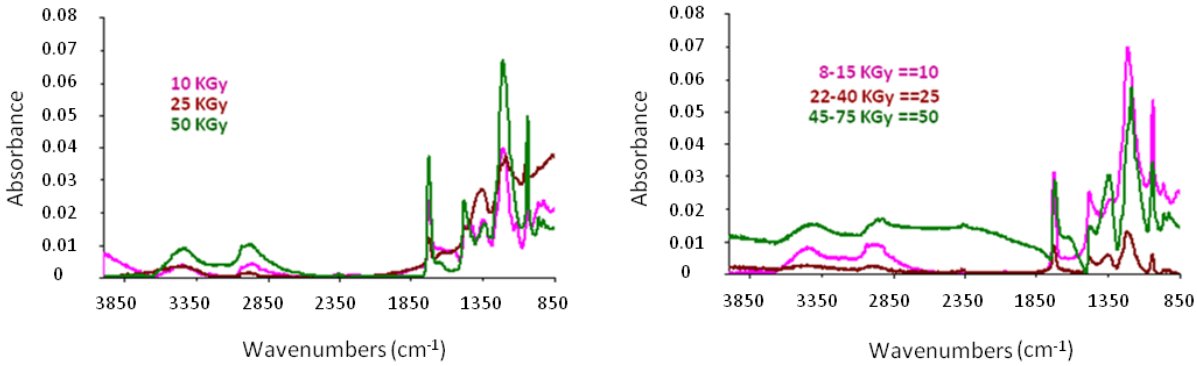

Figure 5.5. FT-IR of PMEDSAH coatings after exposure to various levels of e-beam- (left) and gamma- (right) radiation.

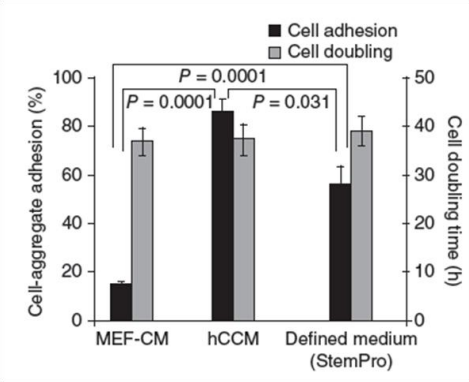

Figure 5.6. PMEDSAH culture efficacy of hESCs in various media. Percentage (mean ± s.e.m.) of cell aggregate adhesion (number of aggregates attached with respect to total aggregates passaged) and population doubling time (twofold increase in colony area) for H9 hESCs cultured on PMEDSAH in several culture conditions. *P*-values calculated using unpaired *t*-test. Reproduced from [23] with permission.

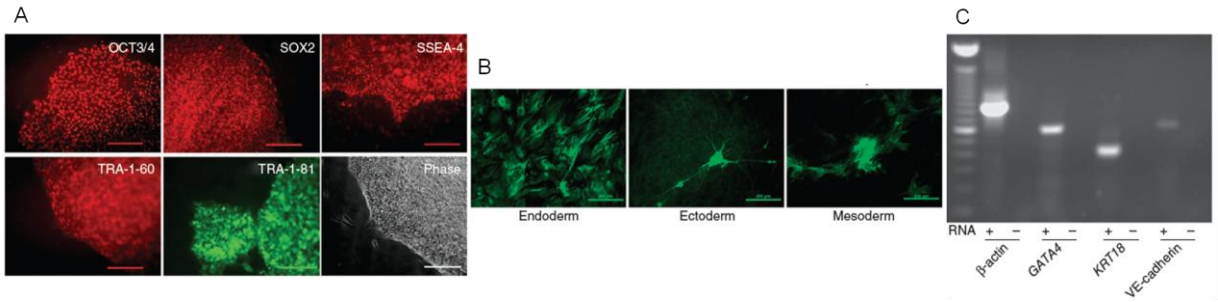

Figure 5.7. Cellular characterization of hESCs cultured on PMEDSAH substrates in StemPro™ media. (A) Fluorescence micrographs of colonies of H9 cells cultured on PMEDSAH in StemPro medium showing expression of hESC markers and a phase-contrast image. Scale bars, 200 μm. (B) Micrographs showing immunoreactivity for α-fetoprotein (endoderm), β-III tubulin (ectoderm) and smooth muscle actin (mesoderm) indicating the pluripotent state of H9 cells cultured on PMEDSAH in StemPro™ medium. Scale bars, 200 μm. (C) RT-PCR analysis of RNA from embryoid bodies showing expression of endoderm (*GATA4*), ectoderm (*KRT18*) and mesoderm derivatives (*VE-cadherin*; also known as *CDH5*). Reproduced from [23] with permission.

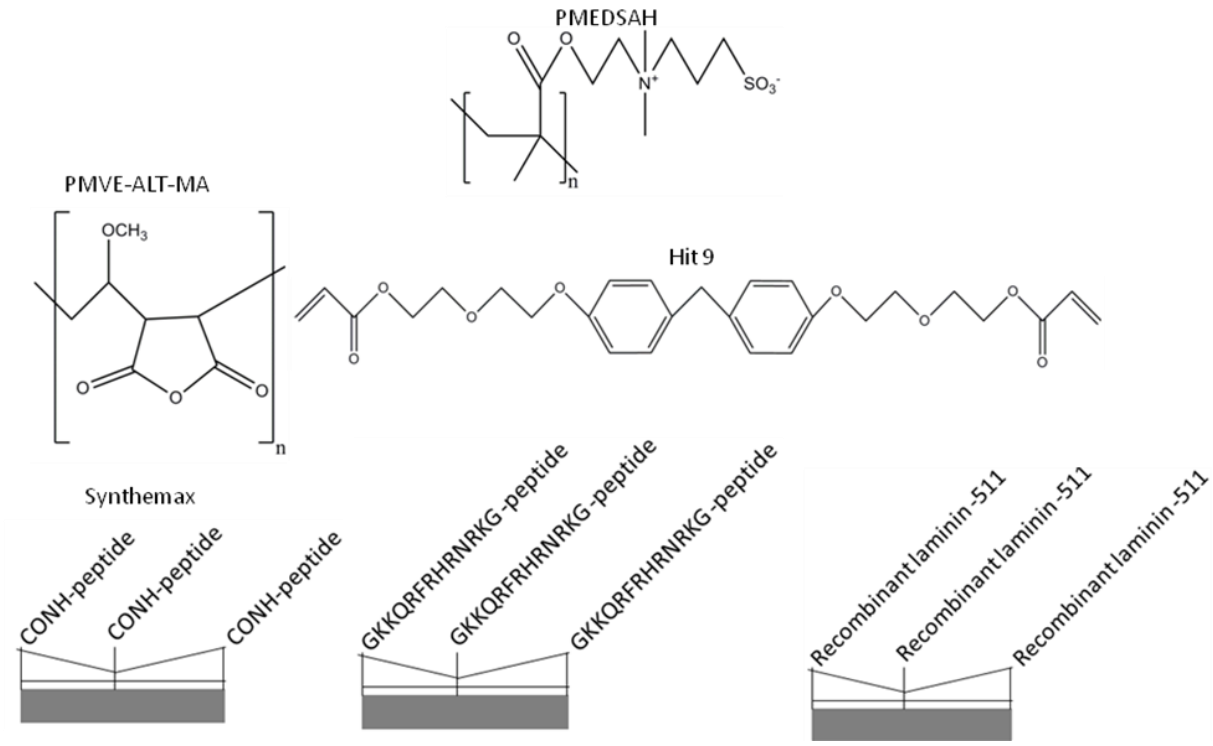

Figure 5.8. Synthetic stem cell culture materials used for long-term maintenance of hPSCs.

Table 5.1. XPS of PMEDSAH-coated substrates after 6 weeks of storage under various environmental conditions, as compared to samples that were not stored.

Storage conditions

	experimental		
element	air	vaccum	nitrogen
C 1s	74.1	79.4	74.6
O 1s	17.3	18.3	20.8
N 1s	3.8	0.9	1.8
S 2p	4.8	1.4	2.8

element	theoretical	from Nature biotech
C 1s	61.1	72.7
O 1s	27.8	20.9
N 1s	5.6	3.2
S 2p	5.6	3.2

Table 5.2. XPS of PMEDSAH-coated substrates after batch sterilization with either e-beam- or gamma-radiation as compared to unsterilized samples.

E-beam

	experimental		
element	10 KGy	25 KGy	50 KGy
C 1s	73.2	72.9	67.3
O 1s	20.8	21.4	23
N 1s	2.6	2.1	3.9
S 2p	3.5	3.7	5.9

Gamma

	experimental		
element	8-15 KGy	22-40 KGy	45-75 KGy
C 1s	70	71.6	70.6
O 1s	21.6	21.5	21.8
N 1s	3.6	3.4	3.2
S 2p	4.7	3.5	4.5

element	theoretical	from Nature biotech
C 1s	61.1	72.7
O 1s	27.8	20.9
N 1s	5.6	3.2
S 2p	5.6	3.2

Table 5.3.Comparison of synthetic substrates and Matrigel™ for long-term hPSC culture.

Substrate Type	Reusable	Passage # Tested	Prep for Cell Culture Use	Can be sterilized via large batch methods?	Relative Cost	Fabrication	Cell Type
PMEDSAH	Yes	25	Used as is	Yes. E-beam- and gamma-radiation	Inexpensive	Polymeric Grafting	hESC (several types)
Synthemax™ (Corning)	No (b/c peptide)	≥10	Used as is	Gamma radiation. Subject to degradation after gamma exposure (b/c peptide)	Expensive (b/c of peptides)	Photopolymerization & chemical conjugation of peptide via EDC/NHS	hESC (several types)
GKKQRFRHRNRKG	No (b/c peptide)	17	Used as is	Subject to degradation after gamma exposure (b/c peptide)	Expensive (b/c of peptides)	Physisorption	hiPSC and hESC
PMVE-alt-MA	Yes	5	Used as is	UVC germicidal radiation	Inexpensive	Free Radical Polymerization	hiPSC and hESC
hit 9	No (b/c of need of protein adsorption)	≥5	Yes. Requires preadsorption of ECM protein vitronectin.	Unknown	Inexpensive	Photopolymerization	hiPSC and hESC
Human recombinant laminin-511	No (b/c protein)	≥20	Used as is	Subject to degradation after gamma exposure (b/c peptide)	Expensive	Physisorption	hiPSC and hESC
Matrigel™	No	≥20	Yes	No	Expensive	Cell feeder layers	hiPSC, hESC, hMSCs, etc

5.6. REFERENCES

1. Fuchs, E.; Tumbar, T.; Guasch, G., Socializing with the neighbors: Stem cells and their niche. *Cell* **2004,** 116, (6), 769-778.
2. Ayala, R.; Zhang, C.; Yang, D.; Hwang, Y.; Aung, A.; Shroff, S. S.; Arce, F. T.; Lal, R.; Arya, G.; Varghese, S., Engineering the cell-material interface for controlling stem cell adhesion, migration, and differentiation. *Biomaterials* **2011,** 32, (15), 3700-3711.
3. Guilak, F.; Cohen, D. M.; Estes, B. T.; Gimble, J. M.; Liedtke, W.; Chen, C. S., Control of Stem Cell Fate by Physical Interactions with the Extracellular Matrix. *Cell Stem Cell* **2009,** 5, (1), 17-26.
4. Geckil, H.; Xu, F.; Zhang, X. H.; Moon, S.; Demirci, U., Engineering hydrogels as extracellular matrix mimics. *Nanomedicine* **2010,** 5, (3), 469-484.
5. Lutolf, M. P.; Hubbell, J. A., Synthetic biomaterials as instructive extracellular microenvironments for morphogenesis in tissue engineering. *Nature Biotechnology* **2005,** 23, (1), 47-55.
6. Ashton, R. S.; Keung, A. J.; Peltier, J.; Schaffer, D. V., Progress and Prospects for Stem Cell Engineering. In *Annual Review of Chemical and Biomolecular Engineering, Vol 2*, Annual Reviews: Palo Alto, 2011; Vol. 2, pp 479-502.
7. Phillips, J. E.; Petrie, T. A.; Creighton, F. P.; Garcia, A. J., Human mesenchymal stem cell differentiation on self-assembled monolayers presenting different surface chemistries. *Acta Biomaterialia* **2010,** 6, (1), 12-20.
8. Markiewicz, I.; Sypecka, J.; Domanska-Janik, K.; Wyszomirski, T.; Lukomska, B., Cellular Environment Directs Differentiation of Human Umbilical Cord Blood-Derived Neural Stem Cells In Vitro. *Journal of Histochemistry & Cytochemistry* **2011,** 59, (3), 289-301.
9. Namgung, S.; Baik, K. Y.; Park, J.; Hong, S., Controlling the Growth and Differentiation of Human Mesenchymal Stem Cells by the Arrangement of Individual Carbon Nanotubes. *Acs Nano* **2011,** 5, (9), 7383-7390.
10. Nelson, T. J.; Martinez-Fernandez, A.; Terzic, A., Induced pluripotent stem cells: developmental biology to regenerative medicine. *Nature Reviews Cardiology* **2010,** 7, (12), 700-710.
11. Xu, C. H.; Police, S.; Rao, N.; Carpenter, M. K., Characterization and enrichment of cardiomyocytes derived from human embryonic stem cells. *Circulation Research* **2002,** 91, (6), 501-508.
12. Bearzi, C.; Rota, M.; Hosoda, T.; Tillmanns, J.; Nascirnbene, A.; De Angelis, A.; Yasuzawa-Amano, S.; Trofimova, I.; Siggins, R. W.; LeCapitaine, N.; Cascapera, S.; Beltrami, A. P.; D'Alessandro, D. A.; Zias, E.; Quaini, F.; Urbanek, K.; Michler, R. E.; Bolli, R.; Kajstura, J.; Leri, A.; Anversa, P., Human cardiac stem cells. *Proceedings of the National Academy of Sciences of the United States of America* **2007,** 104, (35), 14068-14073.
13. Ramiya, V. K.; Maraist, M.; Arfors, K. E.; Schatz, D. A.; Peck, A. B.; Cornelius, J. G., Reversal of insulin-dependent diabetes using islets generated in vitro from pancreatic stem cells. *Nature Medicine* **2000,** 6, (3), 278-282.

14. Urban, V. S.; Kiss, J.; Kovacs, J.; Gocza, E.; Vas, V.; Monostori, E.; Uher, F., Mesenchymal stem cells cooperate with bone marrow cells in therapy of diabetes. *Stem Cells* **2008,** 26, (1), 244-253.
15. Nagaoka, M.; Si-Tayeb, K.; Akaike, T.; Duncan, S. A., Culture of human pluripotent stem cells using completely defined conditions on a recombinant E-cadherin substratum. *Bmc Developmental Biology* **2010,** 10, 12.
16. Valamehr, B.; Tsutsui, H.; Ho, C. M.; Wu, H., Developing defined culture systems for human pluripotent stem cells. *Regenerative Medicine* **2011,** 6, (5), 623-634.
17. Azarin, S. M.; Palecek, S. P., Development of scalable culture systems for human embryonic stem cells. *Biochemical Engineering Journal* **2010,** 48, (3), 378-384.
18. Ilic, D., Culture of human embryonic stem cells and the extracellular matrix micro environment. *Regenerative Medicine* **2006,** 1, (1), 95-101.
19. Wei, Y.; Li, B. S.; Fu, C. K.; Qi, H. X., Electroactive Conducting Polymers for Biomedical Applications. *Acta Polymerica Sinica* **2010**, (12), 1399-1405.
20. Colter, D. C.; Class, R.; DiGirolamo, C. M.; Prockop, D. J., Rapid expansion of recycling stem cells in cultures of plastic-adherent cells from human bone marrow. *Proceedings of the National Academy of Sciences* **2000,** 97, (7), 3213-3218.
21. Nakaji-Hirabayashi, T.; Kato, K.; Arima, Y.; Iwata, H., Oriented immobilization of epidermal growth factor onto culture substrates for the selective expansion of neural stem cells. *Biomaterials* **2007,** 28, (24), 3517-3529.
22. Nandivada, H.; Villa-Diaz, L. G.; O'Shea, K. S.; Smith, G. D.; Krebsbach, P. H.; Lahann, J., Fabrication of synthetic polymer coatings and their use in feeder-free culture of human embryonic stem cells. *Nature Protocols* **2011,** 6, (7), 1037-1043.
23. Villa-Diaz, L. G.; Nandivada, H.; Ding, J.; Nogueira-De-Souza, N. C.; Krebsbach, P. H.; O'Shea, K. S.; Lahann, J.; Smith, G. D., Synthetic polymer coatings for long-term growth of human embryonic stem cells. *Nature Biotechnology* **2010,** 28, (6), 581-583.
24. Lucas, A. D.; Stratmeyer, M. E., Extraction and Stability of Ethylene Oxide Residue in Medical Devices. *Biomedical Instrumentation & Technology* **2008,** 42, (1), 76-79.
25. Mei, Y.; Saha, K.; Bogatyrev, S. R.; Yang, J.; Hook, A. L.; Kalcioglu, Z. I.; Cho, S. W.; Mitalipova, M.; Pyzocha, N.; Rojas, F.; Van Vliet, K. J.; Davies, M. C.; Alexander, M. R.; Langer, R.; Jaenisch, R.; Anderson, D. G., Combinatorial development of biomaterials for clonal growth of human pluripotent stem cells. *Nature Materials* **2010,** 9, (9), 768-778.
26. Brafman, D. A.; Chang, C. W.; Fernandez, A.; Willert, K.; Varghese, S.; Chien, S., Long-term human pluripotent stem cell self-renewal on synthetic polymer surfaces. *Biomaterials* **2010,** 31, (34), 9135-9144.
27. Melkoumian, Z.; Weber, J. L.; Weber, D. M.; Fadeev, A. G.; Zhou, Y. E.; Dolley-Sonneville, P.; Yang, J. W.; Qiu, L. Q.; Priest, C. A.; Shogbon, C.; Martin, A. W.; Nelson, J.; West, P.; Beltzer, J. P.; Pal, S.; Brandenberger, R., Synthetic peptide-acrylate surfaces for long-term self-renewal and cardiomyocyte differentiation of human embryonic stem cells. *Nature Biotechnology* **2010,** 28, (6), 606-U95.

28. Klim, J. R.; Li, L. Y.; Wrighton, P. J.; Piekarczyk, M. S.; Kiessling, L. L., A defined glycosaminoglycan-binding substratum for human pluripotent stem cells. *Nature Methods* **2010,** 7, (12), 989-U72.
29. Rodin, S.; Domogatskaya, A.; Strom, S.; Hansson, E. M.; Chien, K. R.; Inzunza, J.; Hovatta, O.; Tryggvason, K., Long-term self-renewal of human pluripotent stem cells on human recombinant laminin-511. *Nature Biotechnology* **2010,** 28, (6), 611-U102.
30. Meng, Y.; Eshghi, S.; Li, Y. J.; Schmidt, R.; Schaffer, D. V.; Healy, K. E., Characterization of integrin engagement during defined human embryonic stem cell culture. *Faseb Journal* **2010,** 24, (4), 1056-1065.
31. Saha, K.; Mei, Y.; Reisterer, C. M.; Pyzocha, N. K.; Yang, J.; Muffat, J.; Davies, M. C.; Alexander, M. R.; Langer, R.; Anderson, D. G.; Jaenisch, R., Surface-engineered substrates for improved human pluripotent stem cell culture under fully defined conditions. *Proceedings of the National Academy of Sciences* **2011,** 108, (46), 18714-18719.
32. Ludwig, T. E.; Levenstein, M. E.; Jones, J. M.; Berggren, W. T.; Mitchen, E. R.; Frane, J. L.; Crandall, L. J.; Daigh, C. A.; Conard, K. R.; Piekarczyk, M. S.; Llanas, R. A.; Thomson, J. A., Derivation of human embryonic stem cells in defined conditions. *Nature Biotechnology* **2006,** 24, (2), 185-187.
33. Abraham, S.; Eroshenko, N.; Rao, R. R., Role of bioinspired polymers in determination of pluripotent stem cell fate. *Regenerative Medicine* **2009,** 4, (4), 561-578.
34. Mallon, B. S.; Park, K. Y.; Chen, K. G.; Hamilton, R. S.; McKay, R. D. G., Toward xeno-free culture of human embryonic stem cells. *International Journal of Biochemistry & Cell Biology* **2006,** 38, (7), 1063-1075.
35. Amit, M.; Shariki, C.; Margulets, V.; Itskovitz-Eldor, J., Feeder layer- and serum-free culture of human embryonic stem cells. *Biology of Reproduction* **2004,** 70, (3), 837-845.
36. Rajala, K.; Hakala, H.; Panula, S.; Aivio, S.; Pihajamaki, H.; Suuronen, R.; Hovatta, O.; Skottman, H., Testing of nine different xeno-free culture media for human embryonic stem cell cultures. *Human Reproduction* **2007,** 22, (5), 1231-1238.
37. Huebsch, N.; Gilbert, M.; Healy, K. E., Analysis of sterilization protocols for peptide-modified hydrogels. *Journal of Biomedical Materials Research Part B-Applied Biomaterials* **2005,** 74B, (1), 440-447.
38. Fonseca, K. B.; Bidarra, S. J.; Oliveira, M. J.; Granja, P. L.; Barrias, C. C., Molecularly designed alginate hydrogels susceptible to local proteolysis as three-dimensional cellular microenvironments. *Acta Biomaterialia* **2011,** 7, (4), 1674-1682.
39. Behrendtsen, O.; Alexander, C. M.; Werb, Z., Metalloproteinases Mediate Extracellular-matrix Degradation by Cells from Mouse Blastocyst Outgrowths. *Development* **1992,** 114, (2), 447-456.
40. Irwin, E. F.; Gupta, R.; Dashti, D. C.; Healy, K. E., Engineered polymer-media interfaces for the long-term self-renewal of human embryonic stem cells. *Biomaterials* **2011,** 32, (29), 6912-6919.
41. Hwang, N. S.; Varghese, S.; Zhang, Z.; Elisseeff, J., Chondrogenic differentiation of human embryonic stem cell-derived cells in arginine-glycine-aspartate modified hydrogels. *Tissue Engineering* **2006,** 12, (9), 2695-2706.

42. Zoldan, J.; Karagiannis, E. D.; Lee, C. Y.; Anderson, D. G.; Langer, R.; Levenberg, S., The influence of scaffold elasticity on germ layer specification of human embryonic stem cells. *Biomaterials* **2011,** 32, (36), 9612-9621.
43. Hwang, N. S.; Varghese, S.; Li, H. W.; Elisseeff, J., Regulation of osteogenic and chondrogenic differentiation of mesenchymal stem cells in PEG-ECM hydrogels. *Cell and Tissue Research* **2011,** 344, (3), 499-509.
44. Evans, N. D.; Minelli, C.; Gentleman, E.; LaPointe, V.; Patankar, S. N.; Kallivretaki, M.; Chen, X. Y.; Roberts, C. J.; Stevens, M. M., Substrate Stiffness Affects Early Differentiation Events In Embryonic Stem Cells. *European Cells & Materials* **2009,** 18, 1-14.
45. Gentleman, E.; Swain, R. J.; Evans, N. D.; Boonrungsiman, S.; Jell, G.; Ball, M. D.; Shean, T. A. V.; Oyen, M. L.; Porter, A.; Stevens, M. M., Comparative materials differences revealed in engineered bone as a function of cell-specific differentiation. *Nat Mater* **2009,** 8, (9), 763-770.

CHAPTER 6

INFLUENCE OF THICKNESS DEPENDENT PROPERTIES OF A ZWITTERIONIC HYDROGEL ON PLURIPOTENT STEM CELL CULTURE

Some of the material in this chapter has been adapted with minor modifications from the following published article:

Ross, A.M., Jiang, Z., Bastmeyer, M., Lahann, J., "Physical Aspects of Cell Culture Substrates: Topography, Roughness, and Elasticity", *Small* 2012, 8 (3), 336-355.

6.1 INTRODUCTION

Cellular responses to environmental cues can result in intercellular and intracellular changes in cytoskeletal organization, proliferation, cell differentiation, gene expression, and apoptosis.[1-3] In addition to the biochemical properties of the extracellular matrix (ECM),[4] cells can sense underlying substrates with respect to surface properties such as topography, wettability, roughness, elasticity, gradients, and geometrical changes.[5-8] Cellular interactions with environments occur both *in vivo* and *in vitro*. In particular, interactions with synthetic surfaces are of increasing significance, because they are utilized to mimic *in vivo* conditions for a variety of healthcare applications.[9]

Numerous methods are exploited to alter the surface properties of synthetic substrates. The topography of synthetic surfaces may be altered using a myriad of techniques, such as photolithography,[10] electron beam lithography,[11] and soft lithography.[12] These techniques alter material properties on the micron- and nano-scale

including surface roughness. For example, properties such as roughness provide adhesion and alignment cues for endothelial cells.[13] Furthermore, surface cues such as composition, roughness, and wettability determine stem cell fate.[14, 15] Self-assembled monolayers of alkanethiols with different chemical functionalities have been shown to influence the differentiation lineage of human mesenchymal stem cells, indicating the importance of surface composition on cellular responses.[16] Marletta et al., found that making poly(e-caprolactone) (PCL) thin films less rough via helium irradiation treatments induced the differentiation of human mesenchymal stem cells into an osteogenic lineage.[17] Additionally, increasing the hydrophilicity of titanium dental implants by means of plasma source ion implantation enhanced the attachment and proliferation of mesenchymal stem cell prescursor cells, C2C12 cells.[18] Human pluripotent stem cells (hPSCs), cell types that have the ability to undergo self-renewal and differentiate into numerous cell types[19-21], have a multitude of therapeutic applications including the treatment of macular degeneration[22] and osteoporosis.[23] The ability to culture these cells in an undifferentiated state in a defined microenvironment is paramount in amassing the large number of stem cells required for many therapeutic applications.[24, 25] Therefore, an understanding of how the physico-chemical environment influences stem cell behavior would be highly beneficial and synthetic substrates provide this opportunity.

Recently, our lab group identified a zwitterionic hydrogel, poly[2-(methacryloyloxy)ethyl dimethyl-(3-sulfopropyl)ammonium hydroxide] (PMEDSAH), that displayed efficacy in the long term culture of hPSCs.[26] Subsequently, this novel hydrogel was utilized in the culture of induced pluripotent stem cells (iPS). The

functionality of these iPS cells was further assessed by differentiating them into functional mesenchymal stem cells which were further differentiated into osteoblasts and then utilized to regenerate bone in a mouse model *in vivo*.[27] This hydrogel is advantageous in that it maintains stem cells in an undifferentiated state in xeno-free/defined media conditions, is compatible with common batch sterilization techniques, remains stable after prolonged storage in air, and is generated from a process that readily lends itself to scale-up.[28]

Though clinically promising since it does not use xenogenous factors, the material properties influencing hPSC culture on these synthetic substrates is not well understood. As a result, a method for generating the hydrogel that allows the decoupling of surface chemistry from material properties is investigated. Specifically, halide-containing coatings generated by chemical vapor deposition (CVD) are used to initiate the polymerization of the zwitterionic hydrogel via atom transfer radical polymerization (ATRP). Radical polymerizations like ATRP have been beneficial in biomaterials because of their widespread applicability in the generation of polymer materials.[29] In ATRP, free radical polymerization is initiated by a halogenated organic species (in this case the CVD coating) in the presence of a metal halide catalyst. Because the metal halide has numerous oxidation states, it is capable of extracting a halide from the organic species, which then initiates the free radical polymerization. Following initiation, the chain is propagated until reacting with the metal halide in its higher oxidation state reversibly terminates the free radical on the active end of the polymer chain. The resulting uniform polymer growth stems from the equilibrium provided by the catalyst which favors the dormant (polymer-halide) rather than the active (polymer-radical) state

thereby suppressing side reactions.[30] Consequently, ATRP affords control of PMEDSAH coating thickness which influences surface wettability, or how water attracts or repels on a surface. This chapter focuses on assessing the influence of PMEDSAH material properties such as coating thickness and wettability on the culture of two types of hPSCs, human mesenchymal and human embryonic stem cells.

6.2 EXPERIMENTAL METHODS

6.2.1 Chemical Vapor Deposition Polymerization

Polymer coatings were generated via a custom chemical vapor deposition system consisting of a sublimation zone, pyrolysis zone, and deposition zone. For this application, the starting materials were a [2.2]paracyclophane-4-methyl 2-bromoisobutyrate and [2.2]paracyclophane-4-methyl 2-dibromoisobutyrate. Sublimation occurred at 120°C, followed by pyrolysis at 540-550°C, after which the materials were deposited in converted form as poly[(*p*-xylylene-4-methyl-2-bromoisobutyrate)-*co*-(*p*-xylylene)] (hereafter referred to as the 50% initiator coating) and poly[(*p*-xylylene-4-methyl-2-dibromoisobutyrate)-*co*-(*p*-xylylene)] (hereafter referred to as the 100% initiator coating). Deposition occurred on gold, silicon, and tissue culture polystyrene (TCPS) plates via spontaneous polymerization (**Figure 6.1**). In this instance, gold and silicon substrates were used as surrogates for the cell culture substrates in subsequent materials characterization. The working pressure during the polymerization was 0.3 mbar and the deposition occurred on a rotating sample holder that was maintained at 15°C.

6.2.2 Surface Analysis: Fourier Transform Infrared Spectroscopy, Ellipsometry, Water Contact Angle Goniometry, and Atomic Force Microscopy

Film presence after CVD and the successful polymerization of PMEDSAH is confirmed by Fourier transform infrared spectroscopy (FT-IR). For this analysis, a Nicolet 6700 spectometer was utilized and it had a resolution of $4cm^{-1}$ and a grazing angle of 85°. A total of 128 scans were taken for each sample. Film thickness was assessed via the use of a multi-wavelength imaging null-ellipsometer (EP^3 Nanofilm, Germany). Fixed values of the real (n=1.58) and imaginary (k=0) refractive index of the polymer coatings and the ellipsometric delta and psi were used to determine film thickness. Because the refractive index of the 50% and 100% initiator coatings and the PMEDSAH hydrogel are relatively close, it can be difficult to distinguish between the two. As a result, the initiator coating+hydrogel was modeled as the initiator coating alone and the sample thickness prior to ATRP was subtracted from this value to determine the final hydrogel thickness. Measurements were taken at an angle of incidence of 60° for gold and 70° for silicon. Static water contact angles were taken using a contact angle goniometer. Three measurements were taken per sample and then averaged. The surface roughness of the PMEDSAH coatings is evaluated via atomic force microscopy (AFM) using a Dimension Icon (Bruker, Madison, WI). Measurements were taken in tapping mode at room temperature in air. An EV scanner was used in the analysis. In particular, NSC15 cantilevers (MikroMasch, San Jose, CA) with resonant frequency and spring constants of 20-75 N/m and 265-400 kHz respectively were utilized as probe tips. All surface roughness measurements were taken at 1 Hz scan rate.

6.2.3 Atom Transfer Radical Polymerization

In this instance, atom transfer radical polymerization is utilized to generate brushes of poly[2-(methacryloyloxy)ethyl dimethyl-(3-sulfopropyl)ammonium hydroxide] (PMEDSAH) (Monomoer Polymer Dajac Labs, Trevose, PA). The solvent consists of 4 parts methanol to 1 part deionized water and it is placed into a 50 mL schlenk flask for degassing. This solvent is degassed three times via freeze-pump-thaw cycles. Once the solvent is near room temperature, 10% of the total solvent volume is removed from the 50 mL flask via a needle and transferred to a 10 mL schlenk flask that has been degassed via 3 argon-vacuum cycles. The catalyst system consisting of CuCl (3.6 mg/mL), $CuCl_2$ (0.96 mg/mL), and 2'2 bipyridyl (14mg/mL) are added to the 10 mL flask. Meanwhile, PMEDSAH (0.5 g/mL) is added to the 50 mL flask. Both mixtures are stirred for 10 mins until all reactants have dissolved. It should be noted that the polymer and the catalyst system are kept in separate flasks to prevent gel formation. Once the solutions are fully mixed, the catalyst system is added to the 50 mL flask containing the PMEDSAH and this combined solution is stirred briefly. At this juncture, the 50 mL flask is placed in an argon purged glove bag and distributed into 20 ml scintillation vials containing silicon or gold CVD substrates and into 6-well plates of TCPS, with approximately 1 mL of solution being added to each vial or plate well. Before being placed in the purged glove bag, scintillation vials were degassed via 3 vacuum-argon purge cycles. The ATRP reaction was allowed to proceed for 1, 12, and 24 hrs in order to augment the brush thickness, as thickness is known to increase with increasing reaction times.[31] After ATRP, CVD substrates and TCPS plates were rinsed with 1% saline and deionized water and dried. As copper is known to be toxic to cells, it is important to

remove any residual copper from the ATRP-modified surfaces. Thus TCPS plates were further rinsed with 5 mM EDTA, and deionized water to remove any remaining copper.

6.2.4 Ultraviolet Ozone Grafted Polymerization

Previous work in our group indicated that PMEDSAH brushes generated via UV ozone grafted polymerization were capable of maintaining pluripotent stem cells in an undifferentiated state in long term culture. Therefore, grafted PMEDSAH was used as a control in this study. The process began with degassing of the 10 L reaction vessel via argon-vacuum purge 3 times. While the reaction vessel was being purged, the solvent system consisting of 4 parts deionized water and 1 part ethanol was degassed via a 40 min vacuum purge. Once the reaction vessel and solvent were purged, the solvent and PMEDSAH at 0.06 g/ ml (Sigma Aldrich, St. Louis, MO) were added to the reaction vessel and heated to between 76-82°C. Please note that the reaction temperature is important for effective polymerization. While the reaction vessel is heating up, cell culture plates are exposed to UV ozone for 25 mins in order to create free radicals on the surface that are later utilized to initiate the polymerization. After free radicals have been generated, cell culture plates are placed into the reaction vessel and the polymerization occurs over a 2.5 hr time period. Once the process is complete, TCPS plates are removed from the reaction vessel and rinsed in a 1% saline solution at 50 °C overnight prior to use.

6.2.5 Cell Culture

Both hMSCs and hESCs are evaluated. hMSCs are cultured for 7 days on the various ATRP surfaces and the cell culture work for the hMSCs was completed by

Thomas Eyster. The media utilized was comprised of the following: alpha-MEM (Gibco)+ 10% Screened FBS (Lot: 791291) + 1% Pen/Strep (Gibco, 10K units). In this instance, UV grafted PMEDSAH is utilized as a control. hMSCs were seeded at a density of 6000 cells/cm^2 and were initially fed after 24 hrs and subsequently fed every 48 hrs thereafter. hESCs are also cultured for 7 days on the various ATRP surfaces. Twenty thousand trypsinized single hESCs and approximately 100 uniformed hESC colony clusters are cultured after mechanical cutting. hESC culture was completed by Luis Villa-Diaz and Xu Qian. Cell clusters are grown in a chemically defined media, StemPro (Life Technologies, Grand Island, NY) which is supplemented with 4 ng/ml of FGF2 and are fed every 48 hrs. Furthermore, ROCK inhibitor was added to single cell culture medium at 10μM concentration once immediately after cell seeding to support the survival of dissociated hESCs. Matrigel^{TM}, the gold standard in hESC culture is used as a control.

6.2.5.1 Analysis of human pluripotent stem cell culture

The morphology, attachment, and differentiation of both cell types are evaluated. In particular, morphology is assessed by determining the average cell area. Images of the cells are taken after 7 days of culture and then ImageJ software is used to analyze the images. The area of hMSCs is found by counting the total number of cells (as indicated by the number of DAPI stains) and dividing this number by the total cell area which is measured using the ImageJ software. For hESC colonies, the colony area is calculated by using the surface area equation of an ellipse ($\pi \times a \times b/4$, where a and b are the horizontal and longitudinal diameters) and ImageJ is used to measure colony diameters. Cell attachment, for both cell types is found by counting the number of cells/colonies present

on the surface after 7 days of culture. Flow cytometry is used to quantify the extent of cell differentiation as the cells are stained with fluorescent dyes for the pluripotency markers of interest. Specifically, CD73, CD166, and CD105 are used as positive pluripotent markers for hMSCs. Hematopoietic stem cell markers CD34 and CD45 are also utilized as negative controls. Prior to flow analysis on the stained cells, cells that have not been stained are assessed in order to calibrate the baseline for subsequent measurements. A qualitative assessment of hESC differentiation is undertaken using image analysis. For this assessment, hESC colonies with holes in them or those without distinct boundaries are considered to be differentiated and the number of differentiated colonies is compared to the total number of colonies attached to the surface of interest.

6.3 RESULTS AND DISCUSSION

6.3.1 Hydrogel Characterization

In order to decouple the influence of surface chemistry from the material properties of PMEDSAH, PMEDSAH brushes are generated from ATRP using CVD initiator coatings. Two initiator coatings, one with approximately 50% initiator density and the other with 100% initiator density were assessed to determine whether initiator density has an impact on the ATRP of the hydrogel and thus the subsequent cell culture. After ATRP, FTIR was used to confirm the presence of appropriate functional groups on the surface. The presence of sulfonate, carbonyl, and hydroxyl groups at 1208 cm^{-1}, 1732 cm^{-1}, and 2800-3550 cm^{-1} indicate a successful polymerization. Both the 100% initiator and 50% initiator coatings are capable of generating PMEDSAH brushes of different thicknesses as a function of reaction time, with longer reaction times resulting in thicker

brushes. This is evidenced by the magnitude of the sulfonate (1208 cm^{-1}), carbonyl (1732 cm^{-1}), and hydroxyl (2800-3100 cm^{-1} and 3300-3550 cm^{-1}) FT-IR bands which increase with increasing brush thickness (**Figure 6.2**) and by thickness measurements via ellipsometry (**Figure 6.3A**). It appears that the kinetics of polymerization is similar irrespective of the initiator coating type.

Furthermore, the wettability of the hydrogels is augmented as a result of reaction time, with increasing reaction time leading to more hydrophobic brushes. In particular, the static water contact angle ranged from 15 ° for ~20-35 nm brushes to 65 ° for 100-120 nm brushes (**Figure 6.3B**). This transition from hydrophilic to more hydrophobic surface properties occurs as the polymer chains propagate due to chain associations.[32] As the chains propagate, more interchain and intrachain associations occur as a result of intermolecular forces, in this case the attraction of the positive and negative charges on the polymer side chains. These enhanced chain associations lead to physical crosslinks within the polymer brush and subsequently reduces water penetration resulting in more hydrophobic surface characteristics (**Figure 6.4**). In addition to wettability, surface roughness is also known to influence cell form and function. The roughness value (R_a) quantitatively depicts the degree of roughness for a given surface is widely used to describe the surface of in vitro cell culture substrates. Therefore, the surface roughness of the hydrogels was also investigated. AFM measurements indicate that irrespective of the initiator coating type or brush thickness, the surface roughness of all the ATRP-modified surfaces assessed was comparable at approximately 0.8 nm average roughness (R_a) (**Figure 6.5**). Error bars on the bar graphs represent standard deviation and difference was assessed using a two tailed student t-test of unequal variance at a significance level

of $p < 0.05$. As a result of this finding, it was concluded that any differences seen in cellular behavior on the ATRP surfaces could be attributed to wettability differences rather than roughness effects.

6.3.2 Cellular Characterization

After the surfaces were generated and fully characterized, cellular response could be assessed. Since it would be beneficial for a synthetic culture substrate to be compatible with multiple stem cell lines/types, the behavior of both hMSCs and hESCs on the synthetic surfaces is evaluated. Specifically, hMSCs and hESCs are evaluated in terms of cell attachment, morphology, and differentiation after 7 days of culture.

6.3.2.1 hMSCs

Cells are assessed on the various ATRP surfaces and UV grafted surfaces. Concerning cell attachment, more hMSCs are found on ATRP modified surfaces than on the UV grafted surfaces (**Figure 6.6**) as demonstrated at significance level of $p < 0.05$ using a two-tailed student t-test assuming unequal variances. After 7 days of culture, differences in cell morphology are apparent for the different surface treatments. In particular, hMSCs cultured on the UV grafted surfaces are larger than those on the ATRP modified surfaces (**Figure 6.7**) as indicated at a significance level of $p < 0.05$ using a two-tailed student t-test assuming unequal variances. This may occur as a result of there being fewer cells adhered on the UV grafted substrates which affords more area for spreading and thus larger cell areas on average. However, cell size on the various ATRP

modified surfaces are comparable indicating that thickness and thus corresponding wettability differences have little influence on cell morphology.

Very little difference was noted between the ATRP modified surfaces, and as such, subsequent hMSC testing utilized a single surface type and reaction time, that of the 50% initiator coating resulting in ~27 nm thick hydrogels. In addition, because the primary goal of this work is to maintain stem cells in the undifferentiated state, differentiation is analyzed via flow cytometry. Both pluripotency markers highly expressed by hMSCs (CD73, CD 166, CD105) and those minimally expressed by hMSCs (CD34, CD45) are analyzed. Flow cytometry indicated that hMSCs cultured on the ATRP modified plates, after one week of culture, displayed high expression (>99%) of protein markers commonly used to identify hMSCs as indicated by signaling of the PE fluorophore for the markers of interest (**Figure 6.8A-C**). It is also noted that there is low expression (<1%) of markers minimally expressed by hMSCs (**Figure 6.8D-E**).

6.3.2.2 hESCs

Cell colonies are assessed on the various ATRP surfaces and Matrigel^{TM} surfaces. All bar graphs generated from cell data display error bars which represent standard deviation. However, statistics could not be performed on the hESC data set due to the small sample size. An assessment of cell attachment did not show a distinction between the ATRP modified surfaces and the Matrigel^{TM} control (**Figure 6.9**). On average cell colony size on ATRP modified surfaces and the Matrigel^{TM} control is similar at approximately 5 mm^2. While very little difference is noted between the modified surfaces and the control, initial feasibility of this surface treatment for hESC culture is indicated

(**Figure 6.10**). Furthermore, average colony size between the ATRP surface treatments is comparable indicating little influence of thickness/wettability difference on hESC colony spreading after 7 days.

Differentiation of hESCs after one week of culture is evaluated qualitatively using image analysis. Qualitative analysis indicated that there may be a difference in the percentage of undifferentiated colonies on the ATRP modified surfaces as compared to the Matrigel™ control (**Figure 6.11**). Specifically, colonies cultured on the 50% initiator coatings with a PMEDSAH thickness of approximately 80 nm resulted in a slightly higher percentage of undifferentiated colonies as compared to the Matrigel™ control. Furthermore, all of the remaining ATRP modified surfaces had a colony differentiation percentage comparable to Matrigel™ indicating the ability of these surfaces to maintain hESCs in an undifferentiated state after one week of culture.

6.4 CONCLUSIONS

PMEDSAH coatings are successfully generated by ATRP as indicated by FT-IR and XPS. Additionally, the coatings generated were of varying thickness and as a result had different wettability properties as evidenced by static water contact angle measurements. Human pluripotent stem cells, specifically hESCs and hMSCs, are cultured for one week on the various ATRP surfaces indicating the ability of the surfaces to support hPSC culture. For hMSCs, there is no apparent difference in cellular attachment and morphology as a function of the thickness and wettability of the PMEDSAH coatings generated by ATRP. In addition, hMSCs did not differentiate on the PMEDSAH coatings after one week of culture as evidenced by flow cytometry. On average, the ATRP modified surfaces were on par with or better than Matrigel™ with

respect to hESC colony morphology, attachment, and differentiation. Taken together, the results of this work indicate the feasibility of PMEDSAH modified surfaces for pluripotent stem cell culture. As demonstrated in this chapter, results from this work may aid in the design of future biomaterials.

6.5 FIGURES AND TABLES

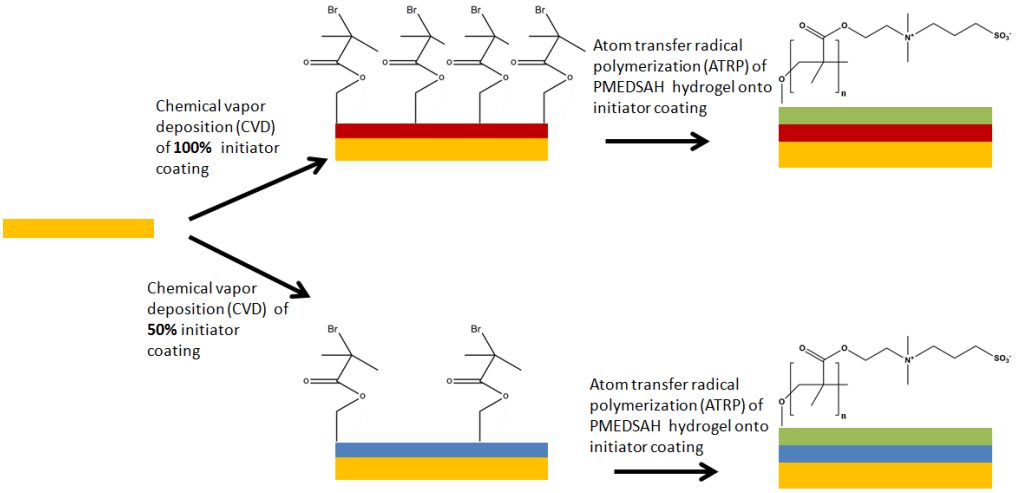

Figure 6.1.Schematic of CVD initiator coatings of different brush density.

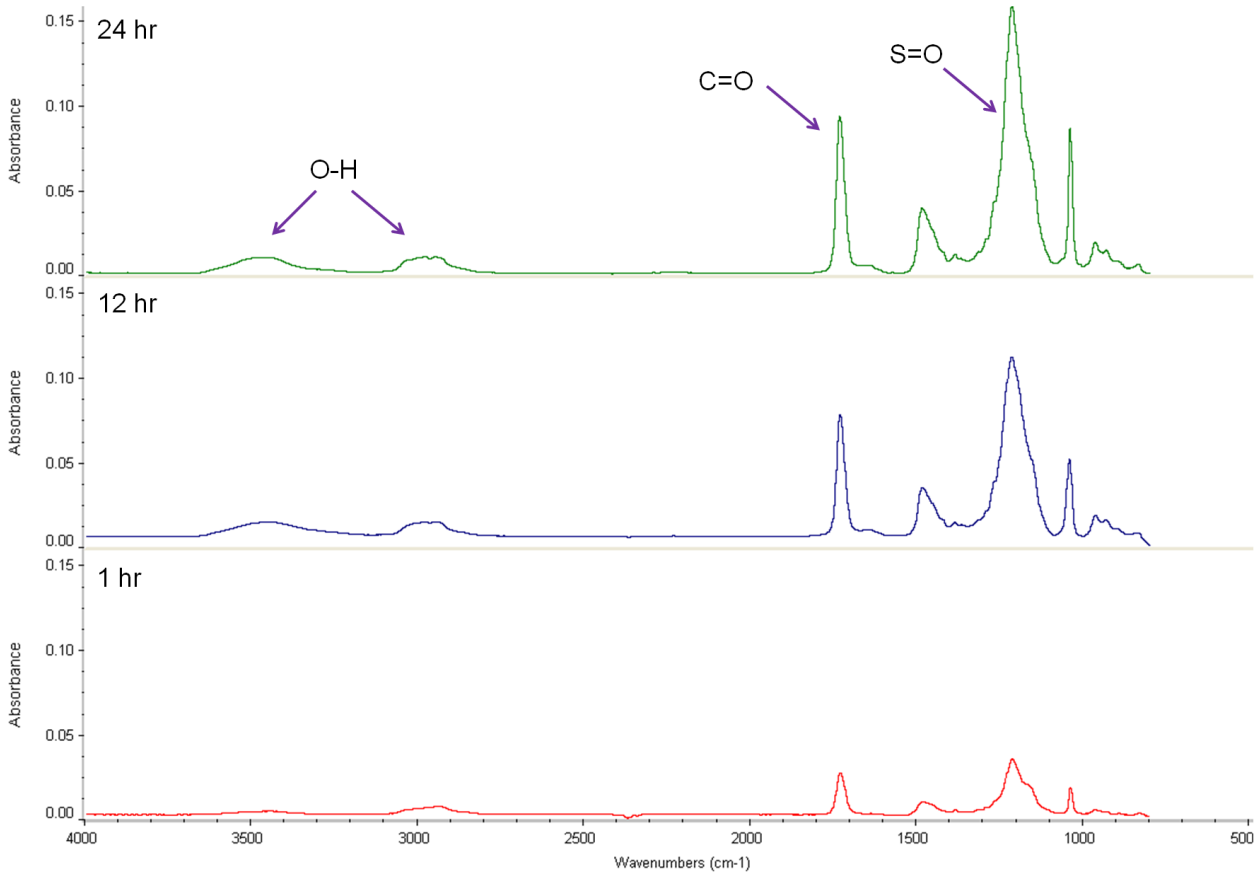

Figure 6.2. FT-IR of PMEDSAH hydrogels generated from 50% initiator coatings as a function of reaction time.

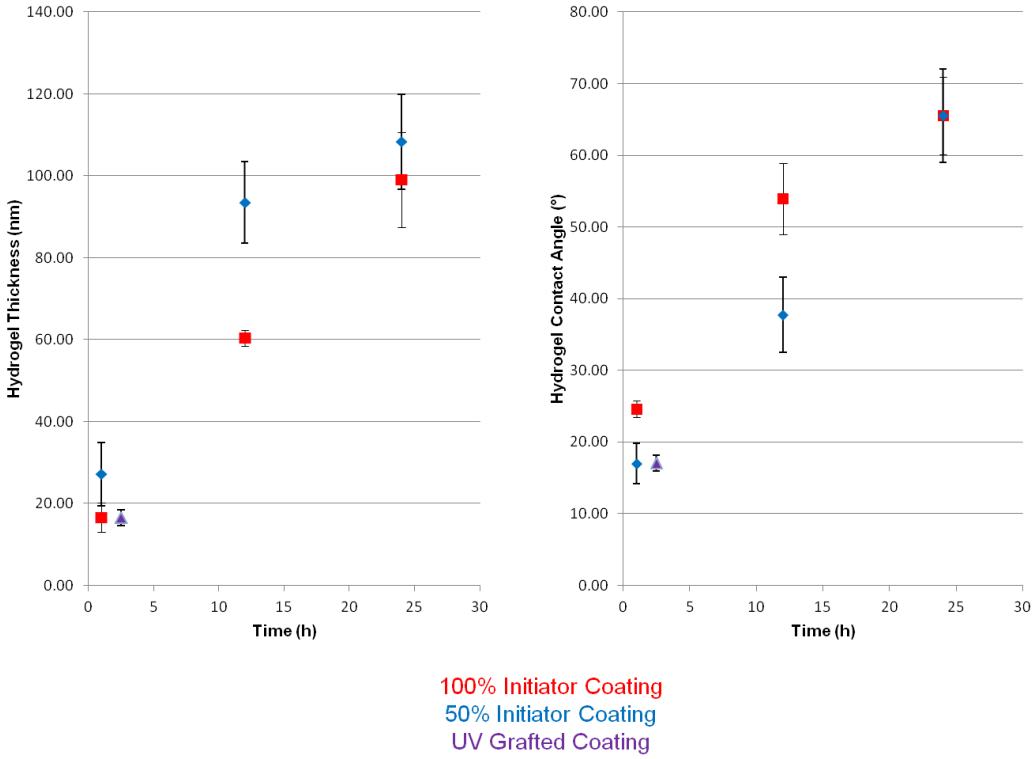

Figure 6.3.Hydrogel thickness and wettability as a function of reaction time for ATRP modified surfaces for 100% initiator coatings (red) and 50% initiator coatings (blue). The material properties of the UV grafted control are provided (purple) as a reference.

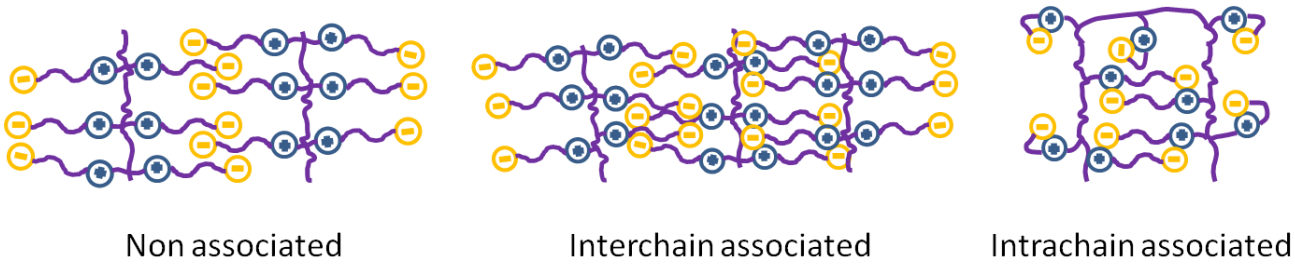

Figure 6.4. Schematic of zwitterionic chain associations during PMEDSAH ATRP.

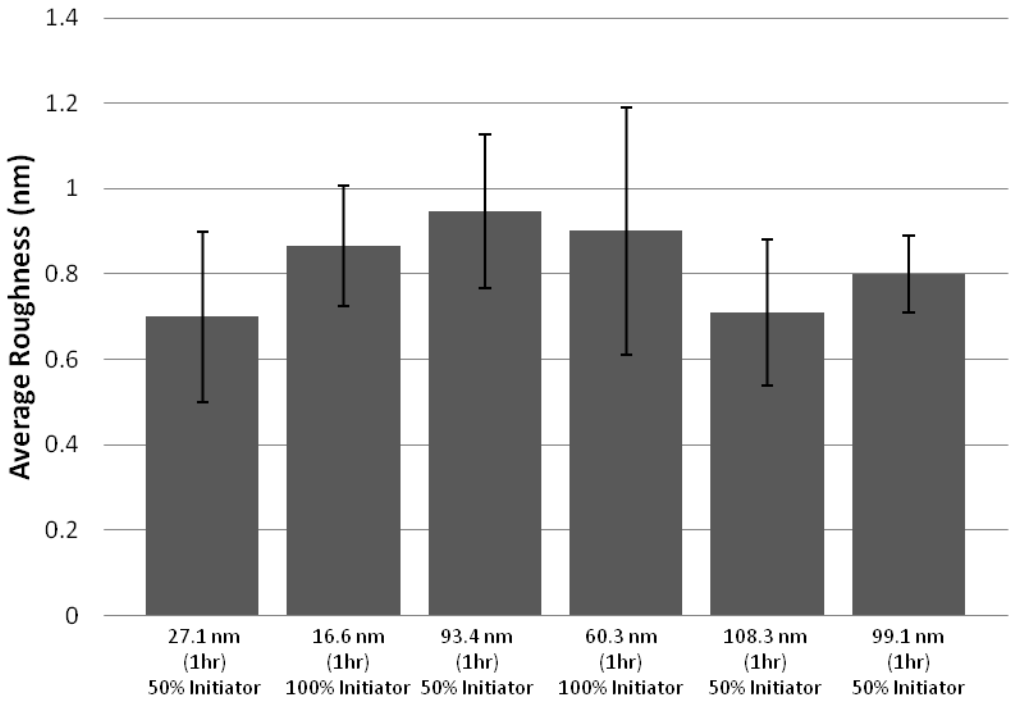

Figure 6.5. Hydrogel roughness as a function of hydrogel thickness and initiator type. Error bars specify standard deviation.

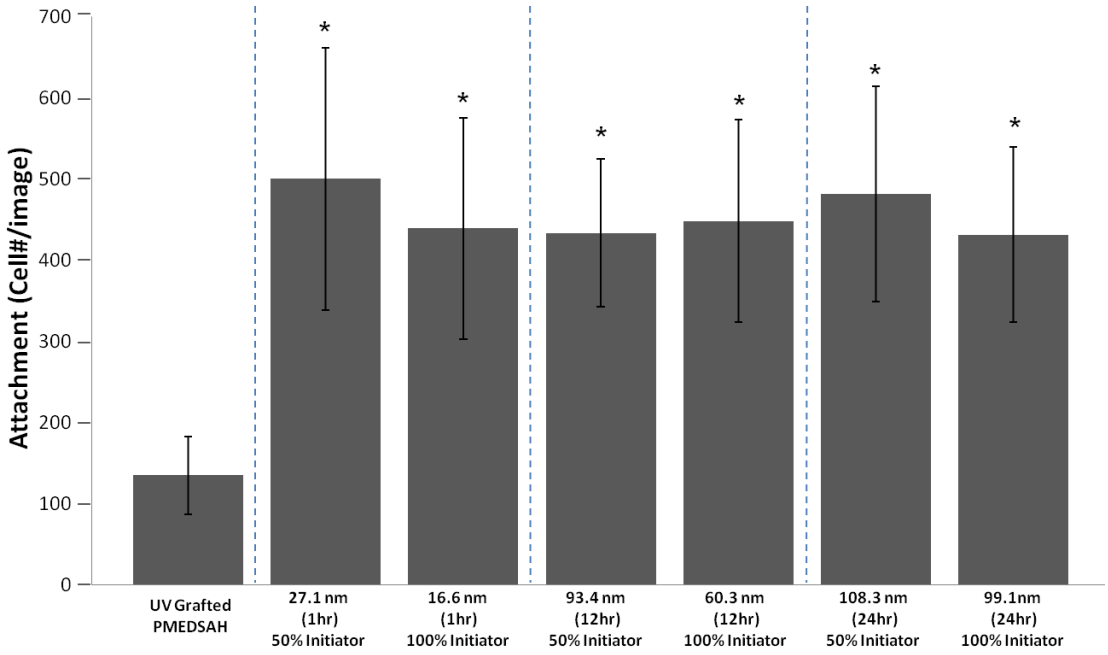

Figure 6.6. hMSC attachment to grafted and ATRP-modified PMEDSAH surfaces after 7 days of culture. Error bars specify standard deviation and * indicates a significant difference ($p<0.05$) between the ATRP-modified coatings and that of the UV grafted control.

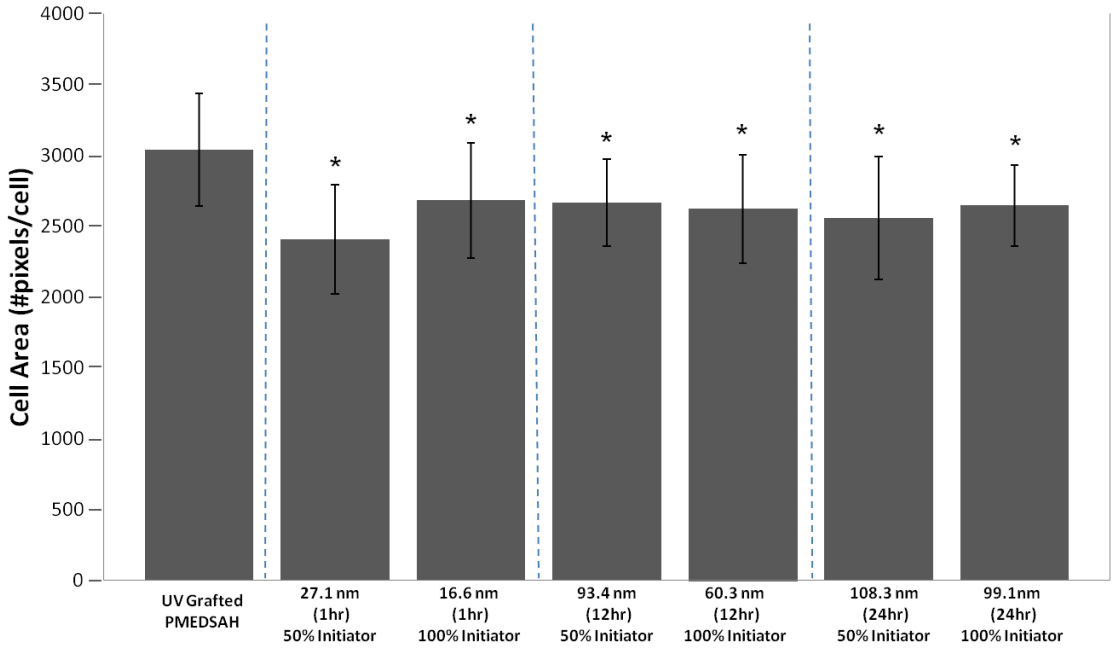

Figure 6.7. hMSC morphology on grafted and ATRP-modified PMEDSAH surfaces after 7 days of culture. Error bars specify standard deviation and * indicates a significant difference ($p<0.05$) between the ATRP-modified coatings and that of the UV grafted control.

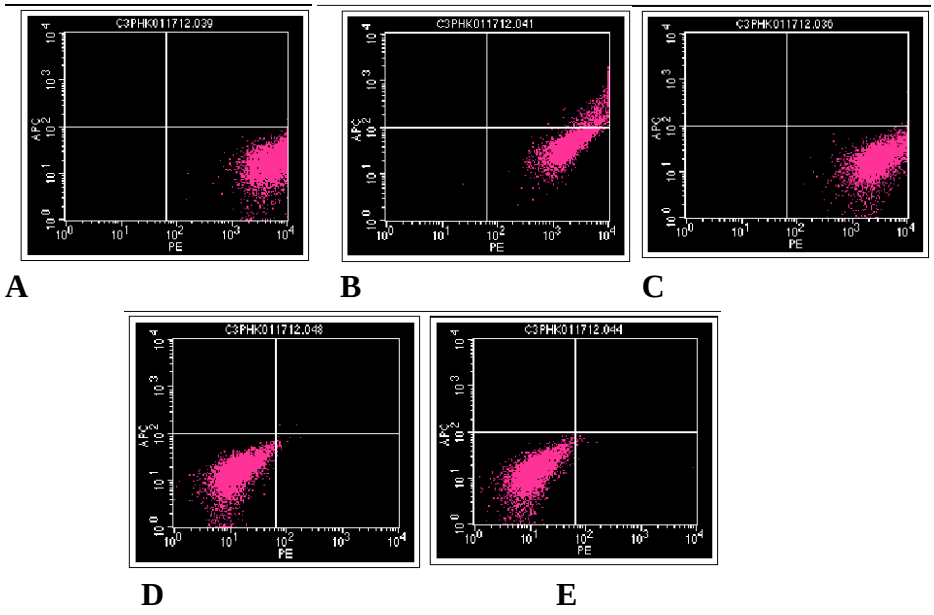

Figure 6.8. Flow cytometry analysis of hMSCs after 7 days of culture on an ATRP-modified PMEDSAH surface (27 nm). Cells were and positive for hMSC markers such as (A) CD 73 (B) CD 166 (C) CD 105 and negative for hematopoietic stem cell markers (D) CD 34 (E) CD 45.

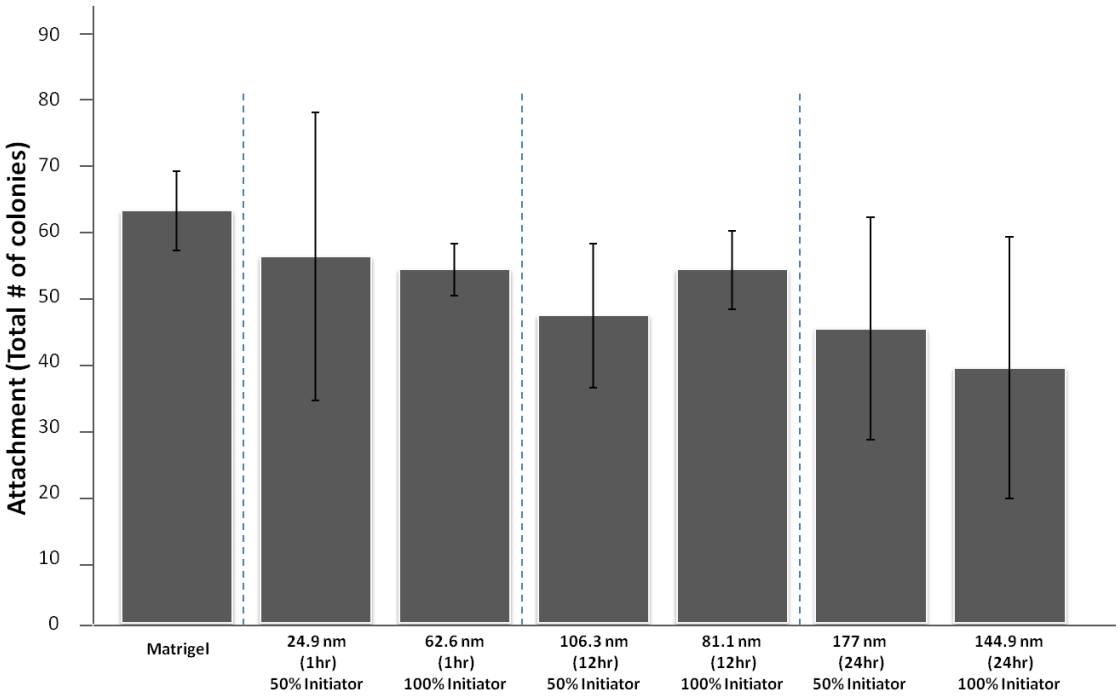

Figure 6.9. hESC attachment on Matrigel^{TM} and ATRP-modified PMEDSAH surfaces after 7 days of culture. Error bars specify standard deviation.

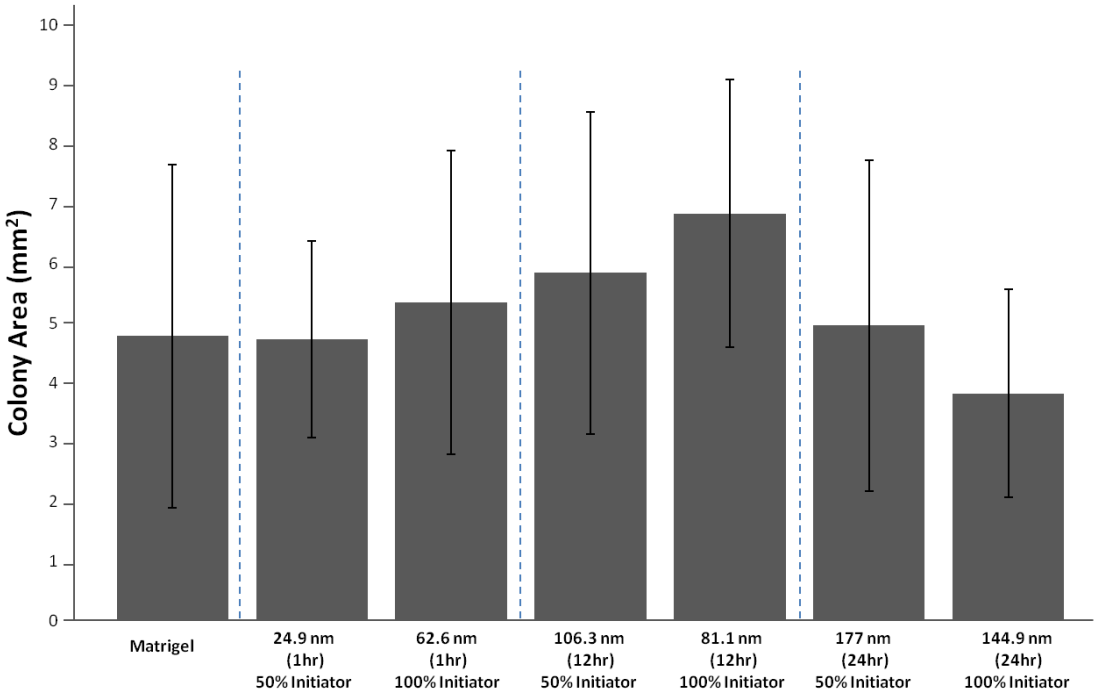

Figure 6.10. hESC morphology on Matrigel^{TM} and ATRP-modified PMEDSAH surfaces after 7 days of culture. Error bars specify standard deviation.

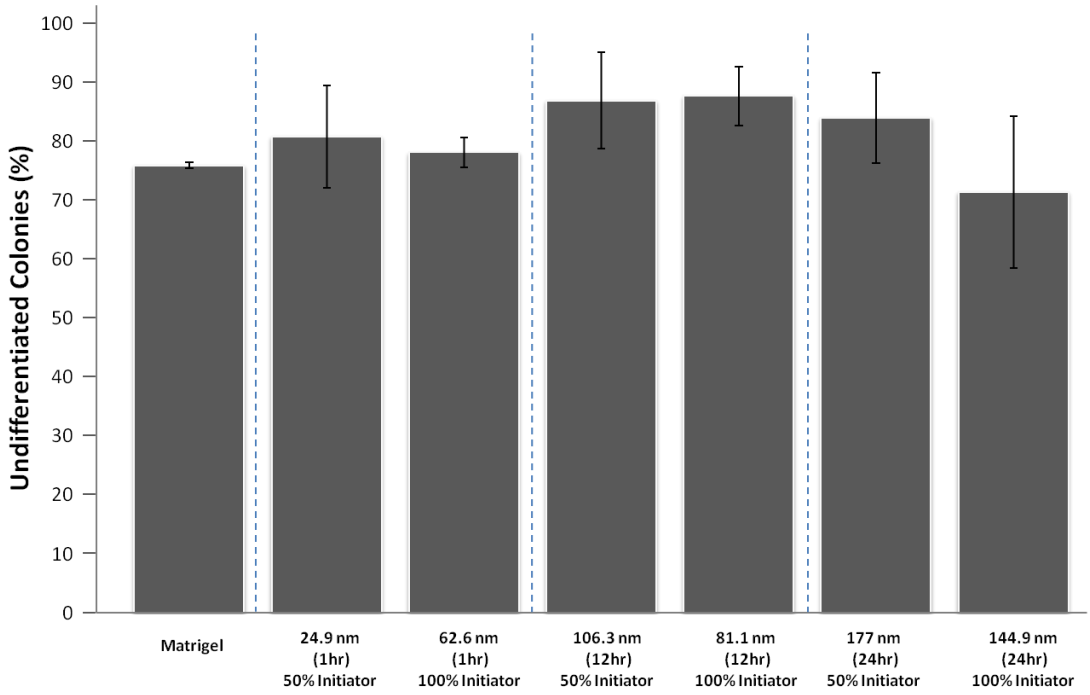

Figure 6.11. hESC differentiation via image analysis after 7 days of culture on ATRP-modified PMEDSAH surfaces and Matrigel™. Error bars specify standard deviation.

6.6 REFERENCES

1. Geiger, B.; Spatz, J. P.; Bershadsky, A. D., Environmental sensing through focal adhesions. *Nature Reviews Molecular Cell Biology* **2009,** 10, (1), 21-33.
2. Sniadecki, N. J.; Anguelouch, A.; Yang, M. T.; Lamb, C. M.; Liu, Z.; Kirschner, S. B.; Liu, Y.; Reich, D. H.; Chen, C. S., Magnetic microposts as an approach to apply forces to living cells. *Proceedings of the National Academy of Sciences of the United States of America* **2007,** 104, 14553-14558.
3. Dalby, M. J.; Riehle, M. O.; Sutherland, D. S.; Agheli, H.; Curtis, A. S. G., Use of nanotopography to study mechanotransduction in fibroblasts - methods and perspectives. *European Journal of Cell Biology* **2004,** 83, (4), 159-169.
4. Huang, J. H.; Grater, S. V.; Corbellinl, F.; Rinck, S.; Bock, E.; Kemkemer, R.; Kessler, H.; Ding, J. D.; Spatz, J. P., Impact of Order and Disorder in RGD Nanopatterns on Cell Adhesion. *Nano Letters* **2009,** 9, (3), 1111-1116.
5. Dalby, M. J.; Gadegaard, N.; Tare, R.; Andar, A.; Riehle, M. O.; Herzyk, P.; Wilkinson, C. D. W.; Oreffo, R. O. C., The control of human mesenchymal cell differentiation using nanoscale symmetry and disorder. *Nature Materials* **2007,** 6, (12), 997-1003.
6. Arnold, M.; Schwieder, M.; Blummel, J.; Cavalcanti-Adam, E. A.; Lopez-Garcia, M.; Kessler, H.; Geiger, B.; Spatz, J. P., Cell interactions with hierarchically structured nano-patterned adhesive surfaces. *Soft Matter* **2009,** 5, (1), 72-77.
7. Stevens, M. M.; George, J. H., Exploring and engineering the cell surface interface. *Science* **2005,** 310, (5751), 1135-1138.
8. Lehnert, D.; Wehrle-Haller, B.; David, C.; Weiland, U.; Ballestrem, C.; Imhof, B. A.; Bastmeyer, M., Cell behaviour on micropatterned substrata: limits of extracellular matrix geometry for spreading and adhesion. *Journal of Cell Science* **2004,** 117, (1), 41-52.
9. Alves, N. M.; Pashkuleva, I.; Reis, R. L.; Mano, J. F., Controlling Cell Behavior Through the Design of Polymer Surfaces. *Small* **2010,** 6, (20), 2208-2220.
10. Molnar, P.; Wang, W. S.; Natarajan, A.; Rumsey, J. W.; Hickman, J. J., Photolithographic patterning of C2C12 myotubes using vitronectin as growth substrate in serum-free medium. *Biotechnology Progress* **2007,** 23, (1), 265-268.
11. Hatakeyama, H.; Kikuchi, A.; Yamato, M.; Okano, T., Patterned biofunctional designs of thermoresponsive surfaces for spatiotemporally controlled cell adhesion, growth, and thermally induced detachment. *Biomaterials* **2007,** 28, (25), 3632-3643.
12. Whitesides, G. M.; Ostuni, E.; Takayama, S.; Jiang, X. Y.; Ingber, D. E., Soft lithography in biology and biochemistry. *Annual Review of Biomedical Engineering* **2001,** 3, 335-373.
13. Chou, S. Y.; Cheng, C. M.; Leduc, P. R., Composite polymer systems with control of local substrate elasticity and their effect on cytoskeletal and morphological characteristics of adherent cells. *Biomaterials* **2009,** 30, (18), 3136-3142.
14. Engler, A. J.; Sen, S.; Sweeney, H. L.; Discher, D. E., Matrix elasticity directs stem cell lineage specification. *Cell* **2006,** 126, (4), 677-689.
15. Galli, C.; Passeri, G.; Ravanetti, F.; Elezi, E.; Pedrazzoni, M.; Macaluso, G. M., Rough surface topography enhances the activation of Wnt/beta-catenin signaling in

mesenchymal cells. *Journal of Biomedical Materials Research Part A* **2010,** 95A, (3), 682-690.
16. Phillips, J. E.; Petrie, T. A.; Creighton, F. P.; Garcia, A. J., Human mesenchymal stem cell differentiation on self-assembled monolayers presenting different surface chemistries. *Acta Biomaterialia* **2010,** 6, (1), 12-20.
17. Marletta, G.; Ciapetti, G.; Satriano, C.; Perut, F.; Salerno, M.; Baldini, N., Improved osteogenic differentiation of human marrow stromal cells cultured on ion-induced chemically structured poly-epsilon-caprolactone. *Biomaterials* **2007,** 28, (6), 1132-1140.
18. Sawase, T.; Jimbo, R.; Baba, K.; Shibata, Y.; Ikeda, T.; Atsuta, M., Photo-induced hydrophilicity enhances initial cell behavior and early bone apposition. *Clinical Oral Implants Research* **2008,** 19, (5), 491-496.
19. Takahashi, K.; Tanabe, K.; Ohnuki, M.; Narita, M.; Ichisaka, T.; Tomoda, K.; Yamanaka, S., Induction of pluripotent stem cells from adult human fibroblasts by defined factors. *Cell* **2007,** 131, (5), 861-872.
20. Takahashi, K.; Yamanaka, S., Induction of pluripotent stem cells from mouse embryonic and adult fibroblast cultures by defined factors. *Cell* **2006,** 126, (4), 663-676.
21. Thomson, J. A.; Itskovitz-Eldor, J.; Shapiro, S. S.; Waknitz, M. A.; Swiergiel, J. J.; Marshall, V. S.; Jones, J. M., Embryonic stem cell lines derived from human blastocysts. *Science* **1998,** 282, (5391), 1145-1147.
22. Gong, J.; Sagiv, O.; Cai, H.; Tsang, S. H.; Del Priore, L. V., Effects of extracellular matrix and neighboring cells on induction of human embryonic stem cells into retinal or retinal pigment epithelial progenitors. *Experimental Eye Research* **2008,** 86, (6), 957-965.
23. Chen, F. H.; Tuan, R. S., Mesenchymal stem cells in arthritic diseases. *Arthritis Research & Therapy* **2008,** 10, (5), 12.
24. Jung, S.; Panchalingam, K. M.; Wuerth, R. D.; Rosenberg, L.; Behie, L. A., Large-scale production of human mesenchymal stem cells for clinical applications. *Biotechnology and Applied Biochemistry* **2012,** 59, (2), 106-120.
25. Serra, M.; Brito, C.; Correia, C.; Alves, P. M., Process engineering of human pluripotent stem cells for clinical application. *Trends in Biotechnology* **2012,** 30, (6), 350-359.
26. Villa-Diaz, L. G.; Nandivada, H.; Ding, J.; Nogueira-De-Souza, N. C.; Krebsbach, P. H.; O'Shea, K. S.; Lahann, J.; Smith, G. D., Synthetic polymer coatings for long-term growth of human embryonic stem cells. *Nature Biotechnology* **2010,** 28, (6), 581-583.
27. Villa-Diaz, L. G.; Brown, S. E.; Liu, Y.; Ross, A. M.; Lahann, J.; Parent, J. M.; Krebsbach, P. H., Derivation of Mesenchymal Stem Cells from Human Induced Pluripotent Stem Cells Cultured on Synthetic Substrates. *Stem Cells* **2012,** 30, (6), 1174-1181.
28. Ross, A. M.; Nandivada, H.; Ryan, A. L.; Lahann, J., Synthetic substrates for long-term stem cell culture. *Polymer* **2012,** 53, (13), 2533-2539.
29. Xu, F. J.; Neoh, K. G.; Kang, E. T., Bioactive surfaces and biomaterials via atom transfer radical polymerization. *Progress in Polymer Science* **2009,** 34, (8), 719-761.

30. Wang, J. S.; Matyjaszewski, K., Controlled Living Radical Polymerization - Halogen Atom-Transfer Radical Polymerization Promoted By A Cu(I)Cu(Ii) Redox Process. *Macromolecules* **1995,** 28, (23), 7901-7910.
31. Chen, R. X.; Feng, W.; Zhu, S. P.; Botton, G.; Ong, B.; Wu, Y. L., Surface-initiated atom transfer radical polymerization of polyhedral oligomeric silsesquioxane (POSS) methacrylate from flat silicon wafer. *Polymer* **2006,** 47, (4), 1119-1123.
32. Cheng, N.; Brown, A. A.; Azzaroni, O.; Huck, W. T. S., Thickness-dependent properties of polyzwitterionic brushes. *Macromolecules* **2008,** 41, (17), 6317-6321.

CHAPTER 7

CONCLUSIONS AND FUTURE DIRECTIONS

7.1 CONCLUSIONS

This dissertation research details the use of chemical vapor deposition (CVD) polymerization as a platform for surface modification for a host of biomedical applications. Holistically, it has added to the evolution of toolboxes available to material scientists, biologists, and engineers.

In **Chapter 3**, for the first time, CVD substrates are used as spatially-resolved, quantitative, biomolecular sensing arrays. Before use, CVD films of poly(4-pentafluoropropionyl-*p*-xylylene-*co*-*p*-xylylene) (PPX-COC_2F_5) are thoroughly characterized with surface analysis techniques including Fourier transform infrared spectroscopy (FT-IR), electrochemical impedance spectroscopy, atomic force microscopy (AFM), and ellipsometry. This model CVD coating was made sufficiently thin, from 3-60 nm, such that it could be utilized as a flexible binding substrate for surface plasmon resonance enhanced imaging ellipsometry (SPREE) binding studies. The sensing array was generated via microcontact printing (μCP) of a hydrazide moiety that is attached to the surface via a ketone-hydrazide coupling. Subsequent attachment of a cascade of biomolecules was evidenced quantitatively via SPREE sensograms and qualitatively by

fluorescence microscopy. The impact of coating thickness on SPREE sensing was assessed. As expected, the SPREE binding signal was attenuated as coating thickness increased as this surface sensitive technique was inhibited when interactions occurred further from the sensing surface.

In **Chapter 4,** reactive CVD coatings of [2.2]paracyclophane-4-methyl 2-bromoisobutyrate (PPX-EB), parylene N (PPX-N), [2.2]paracyclophane-4-furan (PPX-Furan), and 4-(3,4-dibromomaleimide)[2.2]paracyclophane (PPX-BrMal) were developed as platforms for thiol-based "click" chemistry reactions or Diels Alder "click" chemistries and were further utilized to generate multifunctional surfaces. This is the first instance in which CVD coatings are employed as reactive partners in thio-bromo "click" chemistry and a Diels Alder "click" reaction for maleimide immobilization. Specifically, CVD coatings were assessed by x-ray photoelectron spectroscopy (XPS), FT-IR, and imaging ellipsometry after the initial coating and during subsequent surface modification steps. Herein, a reactive thiol or maleimide was spatio-selectively immobilized onto the CVD coating. For PPX-EB specifically, the remaining surface area was exploited in a subsequent surface initiated polymerization by atom transfer radical polymerization (ATRP) of poly(ethylene glycol methacrylate) (PEGMA). PEGMA is known to be protein resistant and as such the functionality of the patterned and unpatterned areas is assessed via adsorption of a fluorescently labeled protein. Selective adsorption of the protein onto the thiol or maleimide patterned areas of PPX-EB, PPX-BrMal, and PPX-Furan indicated the generation of a multifunctional surface. This work has applications in molecular self-assembly.

In **Chapter 5**, a critical analysis of synthetic materials available for pluripotent stem cell culture was undertaken and new data indicating the feasibility of a zwitterionic hydrogel, poly[2-(methacryloyloxy)ethyl dimethyl-(3-sulfopropyl)ammonium hydroxide] (PMEDSAH), developed in our lab is presented. Clinical adoption of stem cells for therapeutic applications is hindered by the availability of culture systems that lack animal products, leading to a host of immunogenic concerns. Furthermore, ideal culture substrates would be generated from scalable processes, be compatible with common batch sterilization techniques, display long-term stability, have compatibility with multiple stem cell lines/types, be relatively inexpensive, and maintain stem cells in the undifferentiated state for long-term passage. The aforementioned criteria were used to evaluate and compare current synthetic culture systems. PMEDSAH properties were examined before and after exposure to two common sterilization techniques, e-beam and gamma radiation, and few changes in composition were noted indicating compatibility with these sterilization techniques. Furthermore, FT-IR revealed the stability of PMEDSAH coatings in air at room temperature for a prolonged storage period satisfying the requirement for long-term stability. Results from this work may be used in biomaterials design for pluripotent stem cell culture systems.

In **Chapter 6**, a more controlled polymerization process, ATRP is employed to create PMEDSAH coatings with defined thickness. Augmenting coating thickness results in changes in surface properties providing an opportunity to decouple the influence of material properties from the influence of the surface chemistry. PMEDSAH hydrogels ranging from 20 to over 100 nanometers were evaluated in this study. In particular, coatings are assessed in terms of thickness, roughness, and wettability (how water attracts

or repels on a surface). As the coating thickness increased, so did the hydrophobicity of the coatings, which had water contact angles that ranged from 15-65°. This was expected as more interchain and intrachain associations occur as the polymer chains propagate leading to more physical crosslinks. Once the material properties of the cells are assessed, the ability of the hydrogels to support human pluripotent stem cell culture was determined. In particular the adhesion, morphology, and differentiation state of human embryonic stem cells (hESCs) and human mesenchymal stem cell (hMSCs) were evaluated. Imaging and flow cytometry studies indicated the ability of the PMEDSAH coatings to support hPSC culture irrespective of coating thickness. However, the percentage of undifferentiated hESCs cultured on ~80 nm thick PMEDSAH hydrogels may be greater than that of the other ATRP-modified coatings and the Matrigel™ control. The work in this portion of the dissertation research lays the foundation for investigating structural-property relationships as mechanisms of action that enable this zwitterionic hydrogel to support hPSC culture.

7.2 FUTURE DIRECTIONS

7.2.1 Culture of Human Pluripotent Stem Cells on Zwitterionic Hydrogels

Creating defined microenvironments for stem cell culture facilitates basic research by reducing variability in and providing enhanced control of the cellular environment. As a result, a firm foundation for exploring factors that contributes to stem cell form and function is provided which may further impact stem cell therapeutics. PMEDSAH coatings generated by atom transfer radical polymerization (ATRP) enabled the control of coating thickness and consequently, corresponding material properties in

this dissertation research. This work provided initial insight into the influence of these properties on human pluripotent stem cell culture (hPSC). Coatings demonstrated efficacy as synthetic culture substrates as indicated by cell morphology, attachment, and differentiation after one week of culture. Studies assessing hPSC culture on PMEDSAH coatings after long-term culture should also be undertaken to ensure efficacy in the long term which affords additional clinical relevance. In addition to morphology, attachment, and differentiation, these long term studies should also evaluate the ability of hPSCs to undergo directed differentiation into specific lineages as expanded hPSCs will ultimately be used in this manner. Two hPSC types, human embryonic stem cells and human mesenchymal stem cells are examined in this dissertation research. However, a universal synthetic culture system is highly desirable and therefore, the efficacy of the PMEDSAH coatings as culture systems for other stem cell lines and types should also be assessed.

The structure of the PMEDSAH hydrogel should also be systematically augmented in order to elucidate structure-function relationships on hPSC culture. This zwitterionic hydrogel offers a host of possible structural modifications. These modifications include but are not limited to the type of anionic or cationic group utilized and the chain distance between these groups. Once synthesized, the ability of this library of PMEDSAH derivatives to undergo ATRP will need to be evaluated. After ATRP, PMEDSAH derivatives should be thoroughly characterized prior to cell studies. The chemical composition of the hydrogels is confirmed via XPS and the presence of the expected functional groups is indicated by FT-IR. Moreover, the thickness of the hydrogels is determined via ellipsometry and the corresponding wettability is ascertained by means of static water contact angle measurements. Then the same assessments of

attachment, proliferation, and morphology of hMSCs after one week of culture should be undertaken to demonstrate initial biocompatibility and viability.

A plethora of opportunities exist in the areas of surface modification for sensing, thiol-reactive coatings, and tissue engineering/regenerative medicine and a few of these were highlighted herein. Specifically, initial work has demonstrated the efficacy of CVD co-polymers as chemical warfare agent sensors. Furthermore, information gleaned from this chemical warfare sensing approach could be leveraged in the use of co-polymers as chemical diagnostic sensors of VOCs. The applicability of thiol chemistries for substrates other than noble medals was evident via the synthesis and characterization of new thiol-reactive CVD coatings. In addition, an approach for evaluating hPSC morphology and function for long-term cell culture is outlined. The preliminary work described in this chapter provides a firm foundation for future work in the aforementioned arenas.

7.2.2 Sensing: Volatile Organic Compounds for Disease Diagnostics

The ability of CVD coatings to serve as molecular binding sensors has been demonstrated in this dissertation research opening up a host of possibilities for sensing approaches using CVD coatings as the base platform. Specifically, CVD coatings could serve as a sensor in cancer diagnostics. Cancer is the second leading cause of death globally and early detection is still a critical factor in reducing patient mortality.[1, 2] Breath analysis is one of the least invasive methods for clinical diagnosis and disease state monitoring.[3] Though the breath is comprised of thousands of compounds, including volatile organic compounds (VOCs), it is less complex than blood and other bodily fluids

making it easier to assess.[4, 5] Furthermore, the breath is a rich source of VOCs indicative of diseases such as breast, prostate, and lung cancers.[6, 7]

Creating a sensor that could specifically interact with breath VOCs rapidly at low concentrations, could improve patient outcomes with early detection. Reactive CVD coatings could be used to develop a new generation of breath VOC sensors. Methods of VOC detection include electronic noses, which contain sensing arrays that undergo changes in electronic properties when in contact with analytes. Some of these arrays require high temperatures and power which leads to increased costs, while others are temperature and humidity sensitive making them less durable.[8, 9] The previous work with electronic noses could be extended by using the CVD polymerization of [2.2]paracyclophanes as sensing elements, thus addressing many of the aforementioned challenges. CVD coatings are robust, maintaining stability in numerous environments, are relatively inexpensive, and reusable.[10, 11] Additionally, coatings afford control of film composition and architecture, are highly adhesive (substrate-independent), and solvent free.[12] Moreover, multifunctional surfaces may be generated by making copolymers of paracyclophanes with different reactivities. The chemical composition and structure of the CVD films would be characterized by XPS and Fourier transformed infrared spectroscopy (FT-IR) while physical characterization of the films will consist of thickness measurements taken via ellipsometry after CVD deposition. As surface wettability may influence the adsorption of VOCs to the CVD films, contact angle measurements would also be assessed. Possible copolymer combinations include amine/flurorine, alcohol/fluorine, and aldehyde/fluorine functionalities. The fluorine functionality should be utilized because it is hydrophobic and should thus inhibit water

adsorption on the surface, further concentrating the analytes of interest on the substrate surface. The other part of the copolymer should be reactive with some of the target VOCs or can be easily surface modified to react with target VOCs. VOC adsorption would be evaluated via quartz crystal microbalance (QCM).

7.2.3 Sensing: Chemical Warfare Agents

Chemical warfare has been a part of war in the modern era and as a result, there is a need for rapid sensing of these agents in order to prevent casualties. In addition to disease state diagnostics/monitoring, reactive paracylophanes (PPX) can also be utilized as chemical warfare agent sensors and preliminary work for this application has begun in the Lahann Lab. Initially, a wide range of functionalized paracylophanes was selected for initial testing including poly(chloro-p-xylylene) (PPX-Cl), poly(4-heptadecafluorononanoyl-p-xylylene-co-p-xylylene) (PPX-COC_8F_{17}), poly(4-aminomethyl-p-xylylene-co-p-xylylene) (PPX-CH_2NH_2), and poly(4-formyl-*p*-xylylene)-*co*-(*p*-xylylene) (PPX-OH). These coatings were selected as they vary in wettability from moderately hydrophilic at 71° (PPX-OH) to moderately hydrophobic at 114° (PPX- PPX-COC_8F_{17}) and wettability may influence adsorption of a chemical warfare simulant. In this instance, dimethyl methylphosphonate (DMMP), a chemical warfare simulant for the nerve gas sarin is used. Initially, the DMMP vapor is adsorbed onto the functionalized CVD coatings in the dry state for five min and then adsorption is evaluated via FT-IR. **Figures 7.1-7.4** display the IR spectra of the various homopolymers before and after DMMP vapor exposure. Of the homopolymers tested, functionalized PPX-OH and PPX-CH_2NH_2 displayed FT-IR bands indicative of DMMP adsorption. Both of these surfaces

are hydrophilic (water contact angle less than 90°). For PPX-CH_2NH_2 specifically, an FT-IR stretch at 1240 cm^{-1} is indicative of P=O and stretches corresponding to methoxy and methyl groups bound to the phosphine are also evident at 912, 1036, 1078, and 1309 cm^{-1}. Furthermore, these same vibrational modes are clearly seen at 918, 1040, and 1312 cm^{-1} in the FT-IR spectra of the PPX-OH in addition to a vibrational shift of the O-H at 3384cm^{-1}, which denotes H-bonding after DMMP absorption. However, none of these vibrational stretches are obvious in the FT-IR of the paracyclophanes that were hydrophobic (water contact angle greater than 90°). As a result, PPX-Cl was eliminated from further testing.

Though promising, the preliminary work undertaken thus far was conducted in a dry state and we live in a wet/humid environment. Therefore, subsequent testing was undertaken using wet DMMP vapor to determine the impact of humidity on the sensing capabilities of the functionalized paracyclophanes. A wet environment is created by passing the DMMP vapor through a vial containing wet Ar prior to exposure to the CVD-coated substrate. Though PPX-COC_8F_{17} did not show efficacy as a DMMP sensor in the dry state, it was hypothesized that the hydrophobic properties of this CVD coating could be exploited in wet DMMP vapor testing in combination with PPX-OH or PPX-CH_2NH_2 which had shown efficacy as sensors for dry DMMP vapor. Thus, copolymers comprised of PPX-COC_8F_{17}/-OH (copolymer I) and PPX- COC_8F_{17}/-CH_2NH_2 (copolymer II) were generated. Copolymers were characterized via FT-IR and then adsorption of wet DMMP vapor to these copolymers is compared to that of their respective hydrophilic homopolymers. The FT-IR spectra in **Figures 7.5 and 7.6** display successful copolymerization, as the copolymer is a combination of the respective homopolymer FT-

IR spectras. Once copolymerization was confirmed, the adsorption of wet DMMP vapor is evaluated at selected time intervals. For the PPX-OH homopolymer, DMMP adsorption starts to occur at 5 mins and the surface continues to become more saturated as exposure time is increased (**Figure 7.7**). In comparison to PPX-OH, copolymer I shows signs of DMMP adsorption at shorter exposure times as indicated by the shoulder at 1040 cm-1 which appears after just 1 minute of DMMP exposure and saturates after 5 mins of DMMP exposure (**Figure 7.8**). Contrastingly, the PPX-CH_2NH_2 homopolymer did not display signs of DMMP adsorption even after 16 min of exposure as no vibrational stretches indicative of DMMP adsorption are apparent (**Figure 7.9**). Moreover, in comparison to PPX-CH_2NH_2, copolymer II denotes DMMP adsorption beginning after just 3 mins of DMMP exposure becoming saturated at approximately 10 mins of DMMP exposure (**Figure 7.10**). Taken together, the results indicate that copolymers I and II were effective adsorbents of wet DMMP vapor and therefore demonstrate feasibility as chemical warfare sensors.

7.3 FIGURES AND TABLES

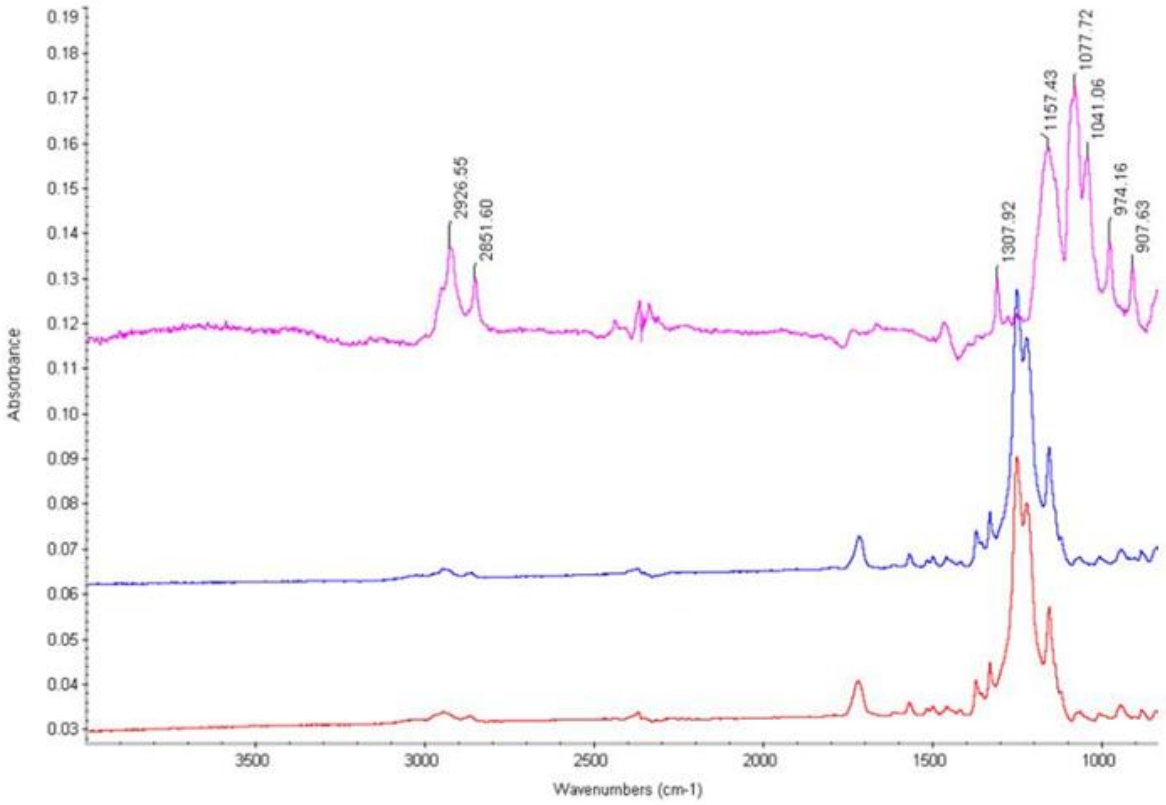

Figure 7.1. FT-IR spectra of PPX-COC8F17 coatings on gold substrates before (bottom) and after (middle) exposure to DMMP vapor. The top spectra represents DMMP adsorption onto bare gold.

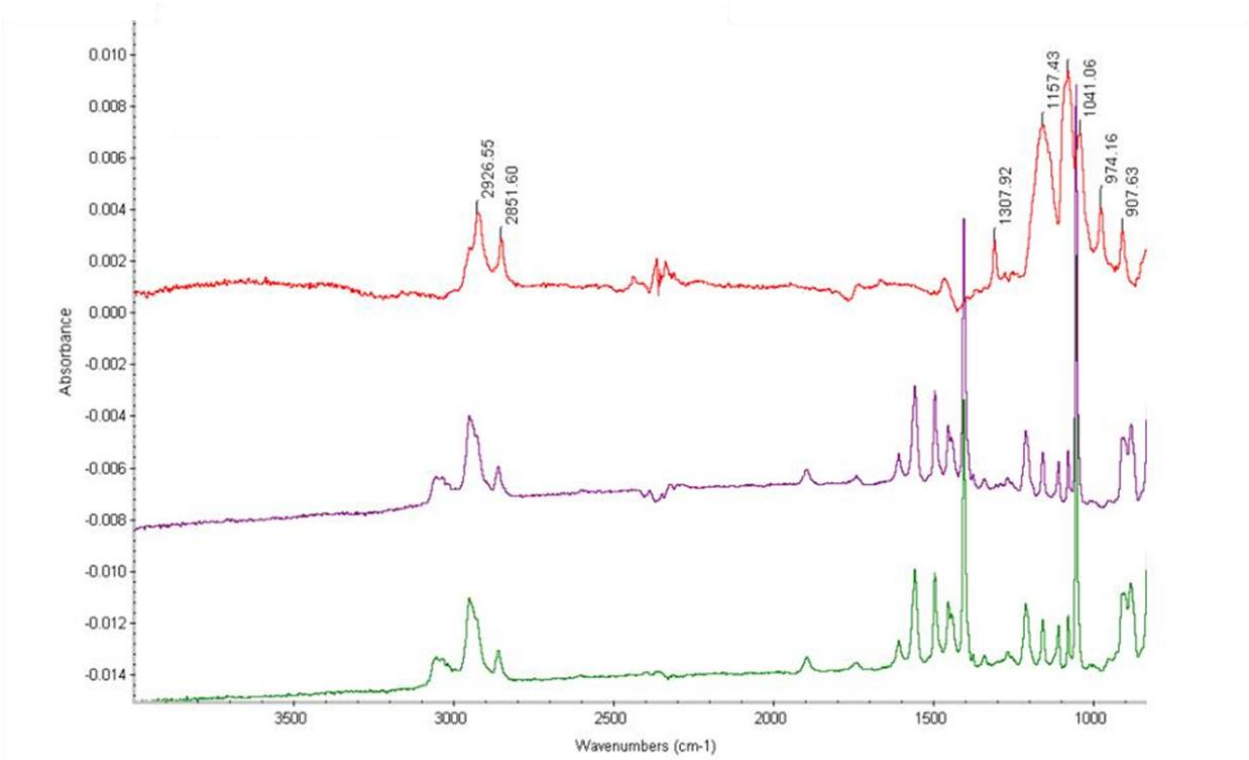

Figure 7.2. FT-IR spectra of PPX-Cl coatings on gold substrates before (bottom) and after (middle) exposure to DMMP vapor. The top spectra represents DMMP adsorption onto bare gold.

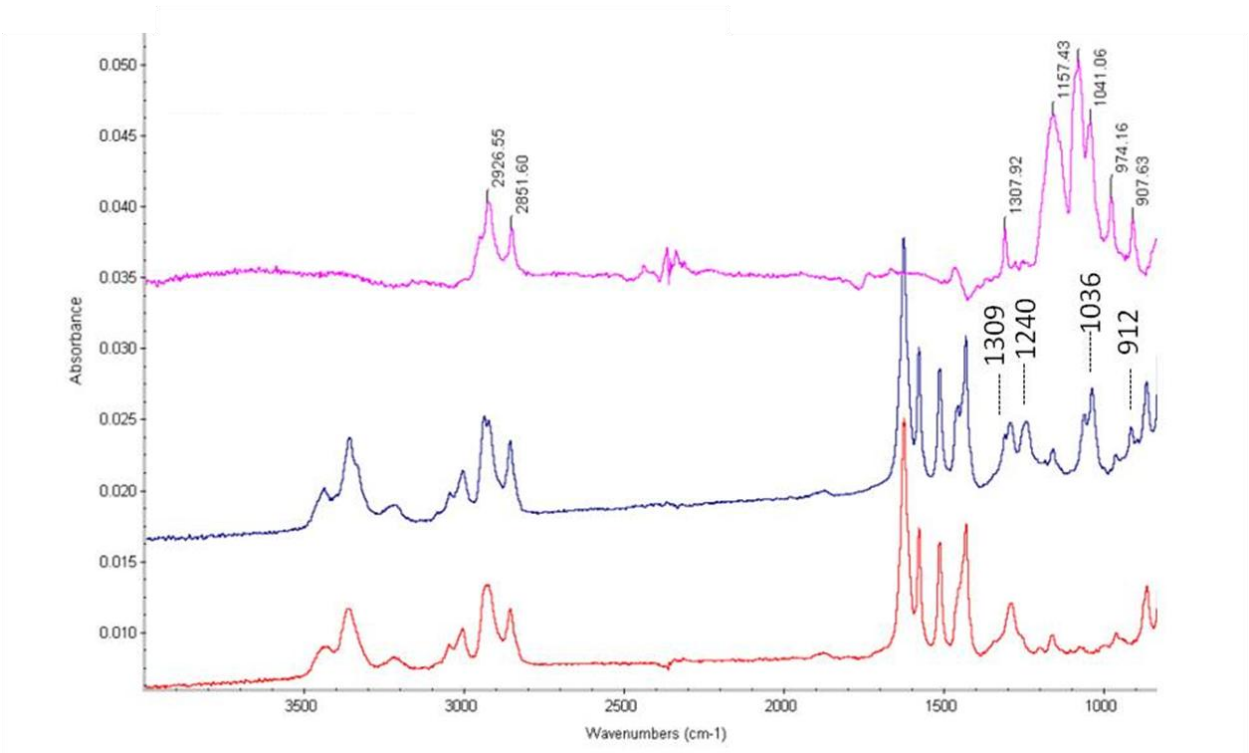

Figure 7.3. FT-IR spectra of PPX-CH2NH2 coatings on gold substrates before (bottom) and after (middle) exposure to DMMP vapor. The top spectra represents DMMP adsorption onto bare gold.

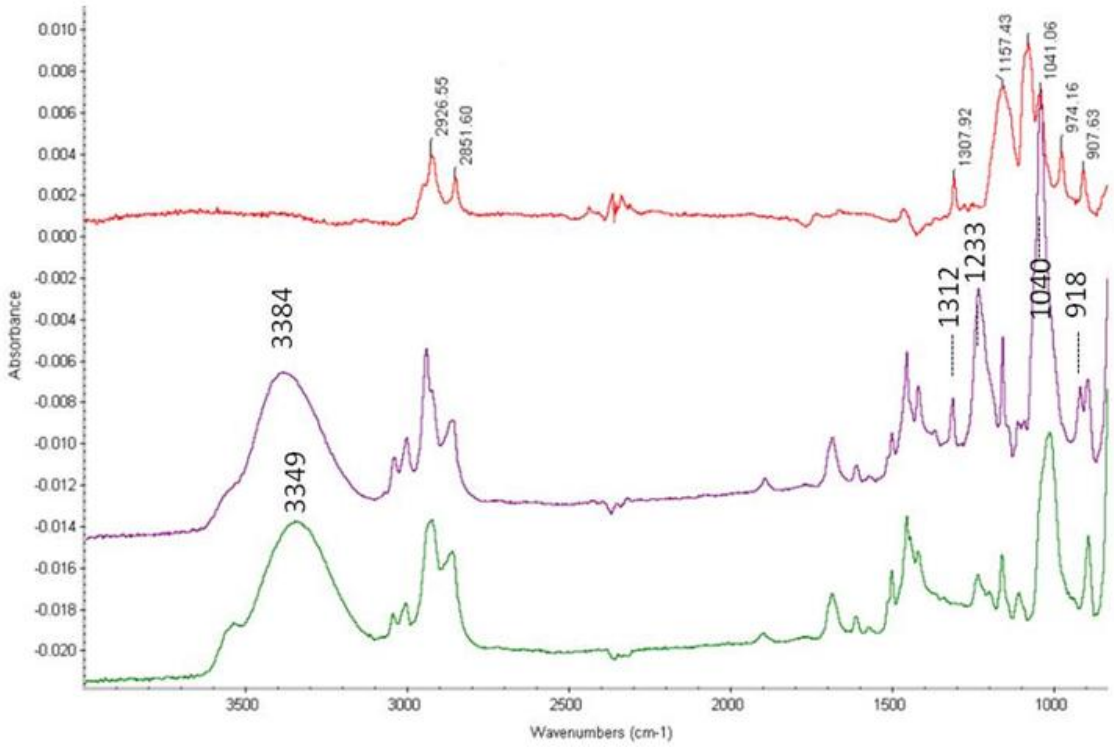

Figure 7.4. FT-IR spectra of PPX-OH coatings on gold substrates before (bottom) and after (middle) exposure to DMMP vapor. The top spectra represents DMMP adsorption onto bare gold.

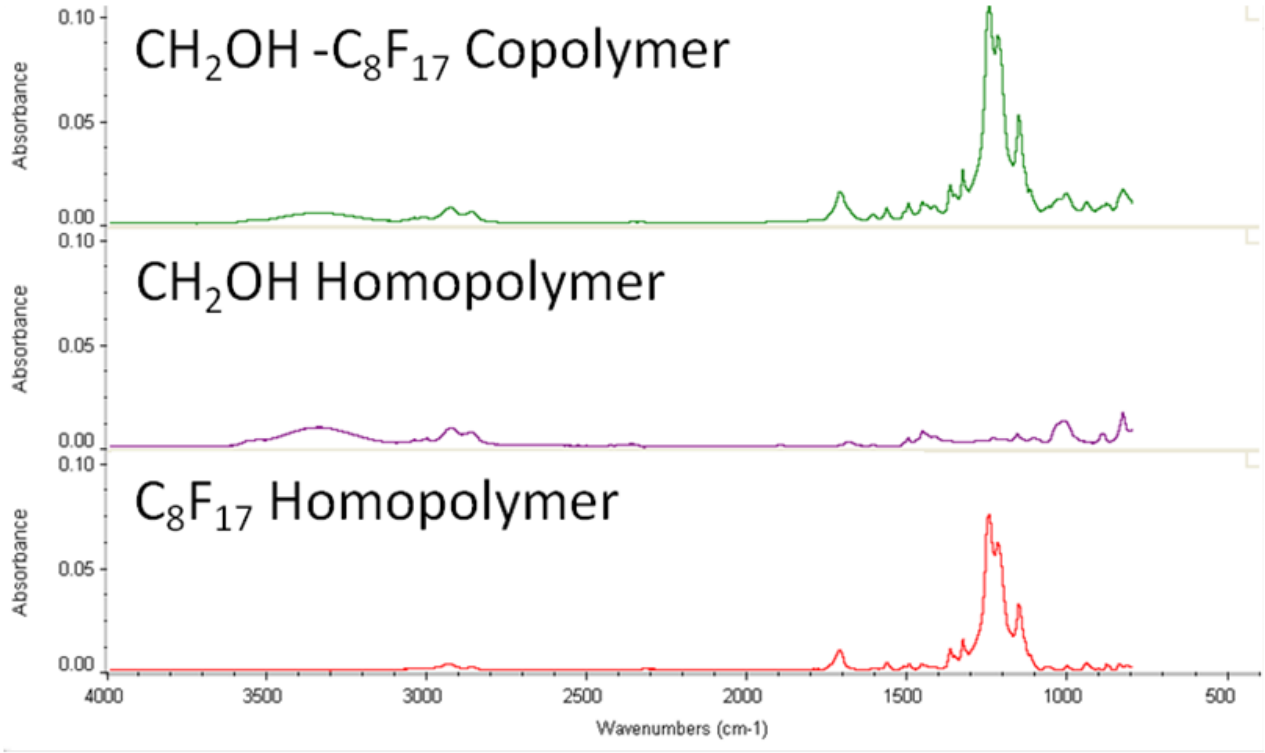

Figure 7.5. FT-IR spectra of PPX-C8F17 (bottom) PPX-CH2OH (middle) homopolymers and their resultant copolymer (top) after CVD polymerization.

.

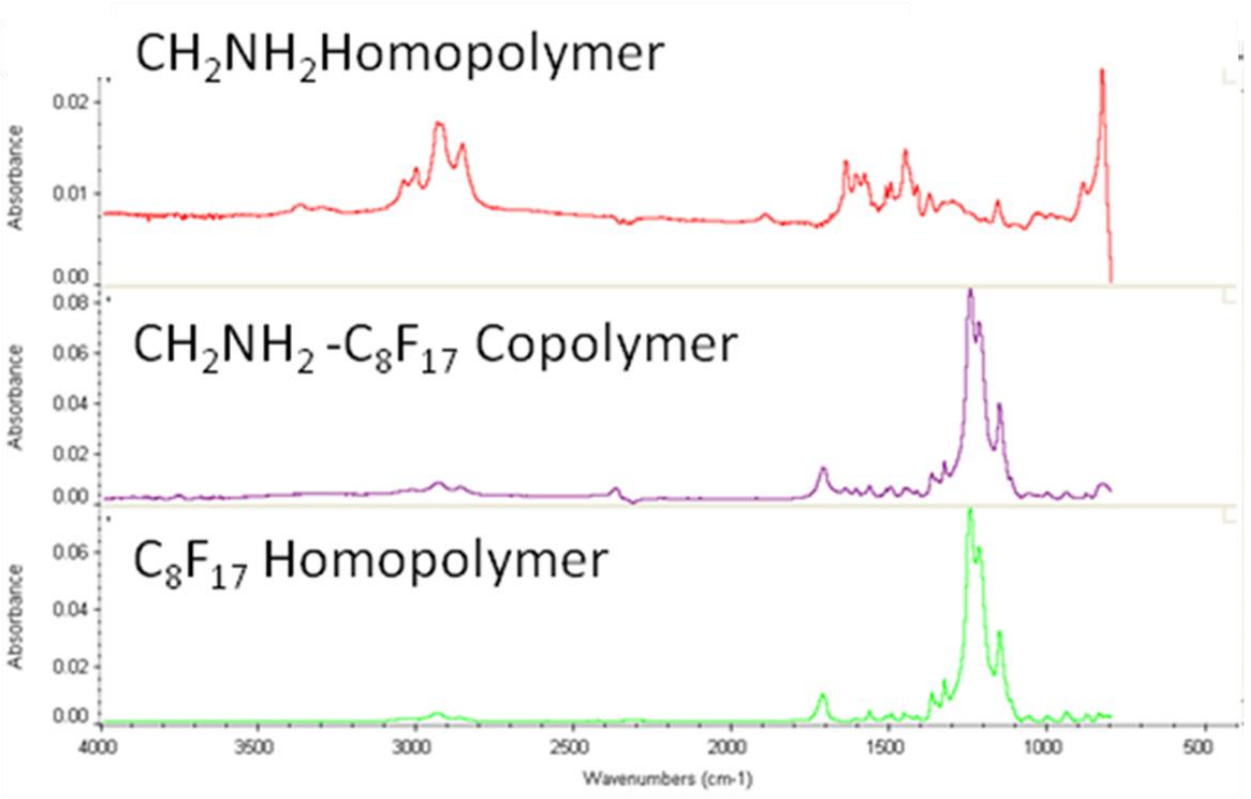

Figure 7.6. FT-IR spectra of PPX-C8F17 (bottom) PPX-CH2NH2 (top) homopolymers and their resultant copolymer (middle) after CVD polymerization.

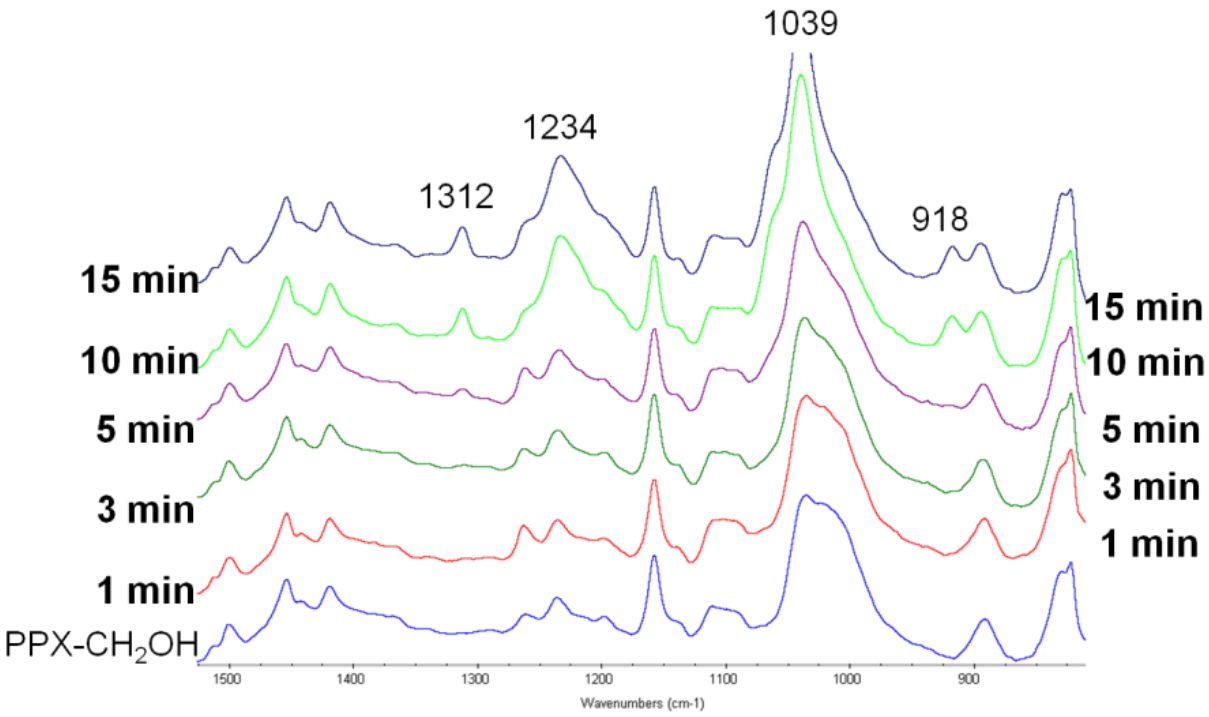

Figure 7.7. FT-IR spectra of PPX-CH2OH homopolymer exposed to wet DMMP vapor at various exposure times.

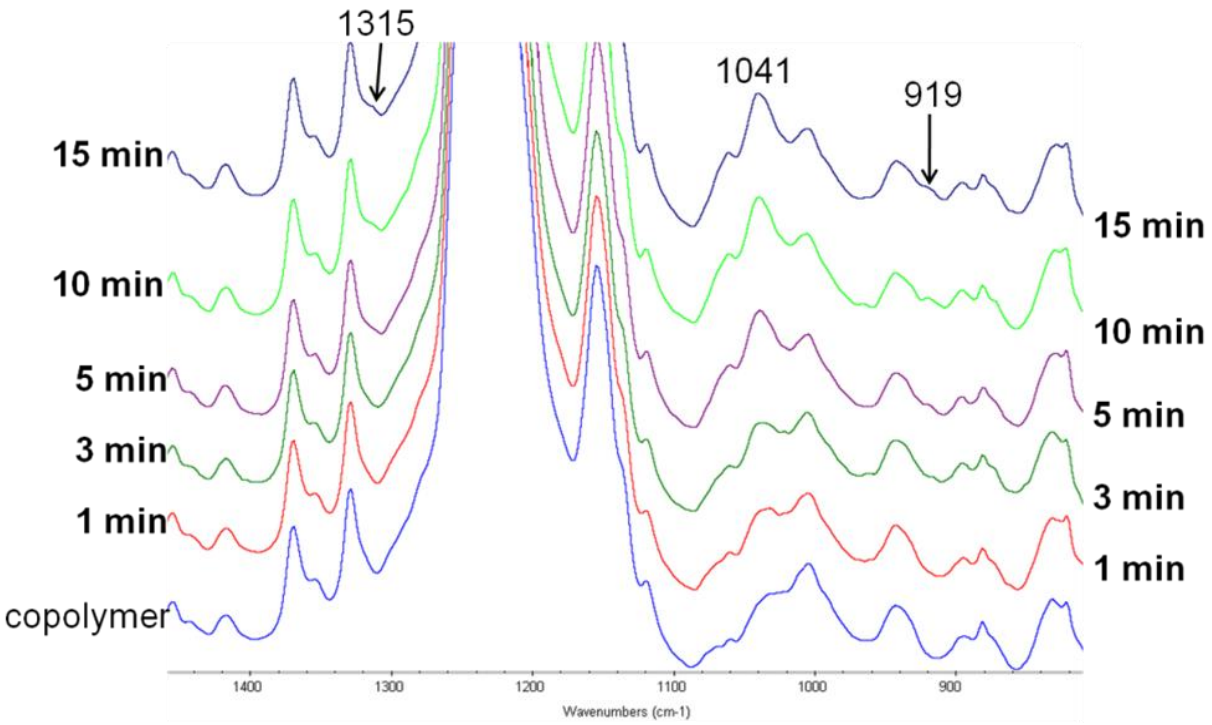

Figure 7.8. FT-IR spectra of copolymer I exposed to wet DMMP vapor at various exposure times.

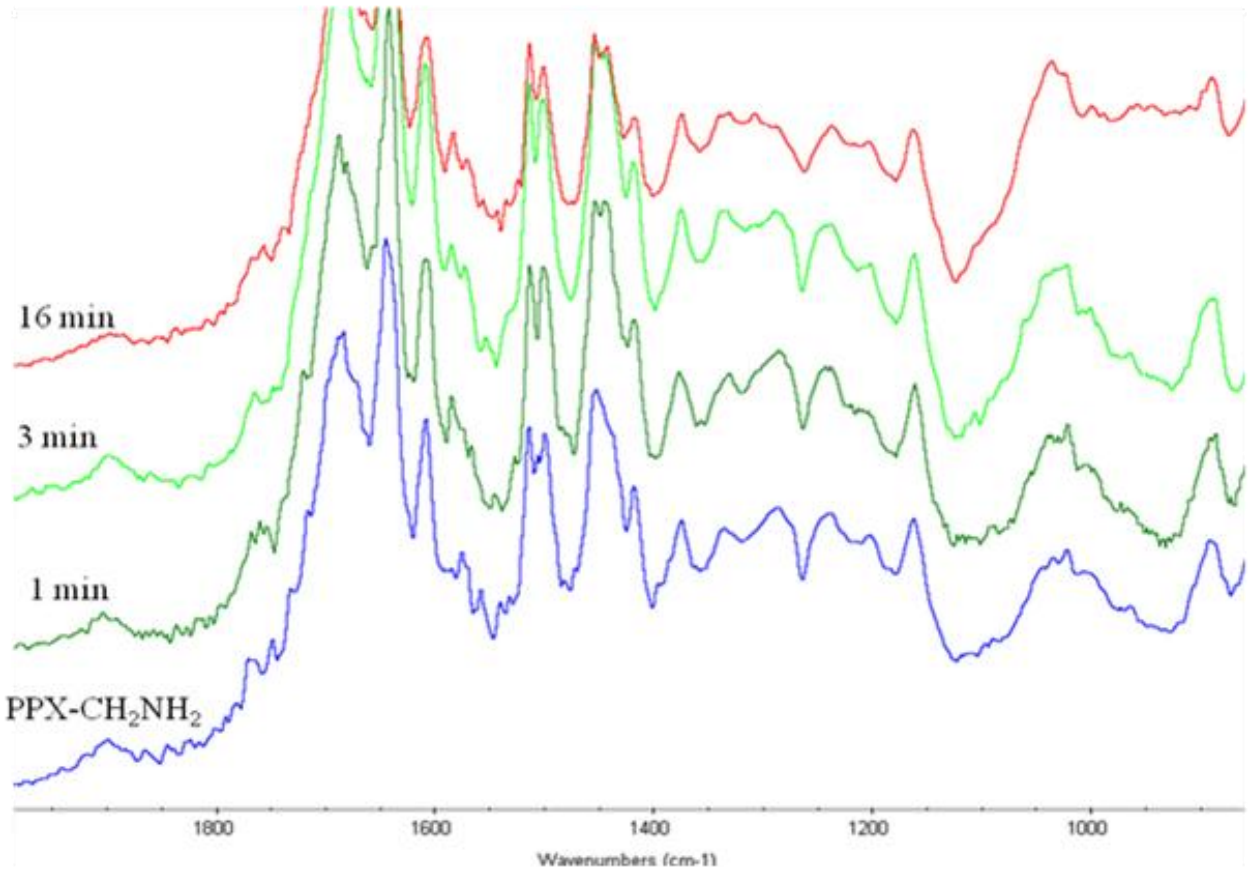

Figure 7.9. FT-IR spectra of PPX-CH2NH2 homopolymer exposed to wet DMMP vapor at various exposure times.

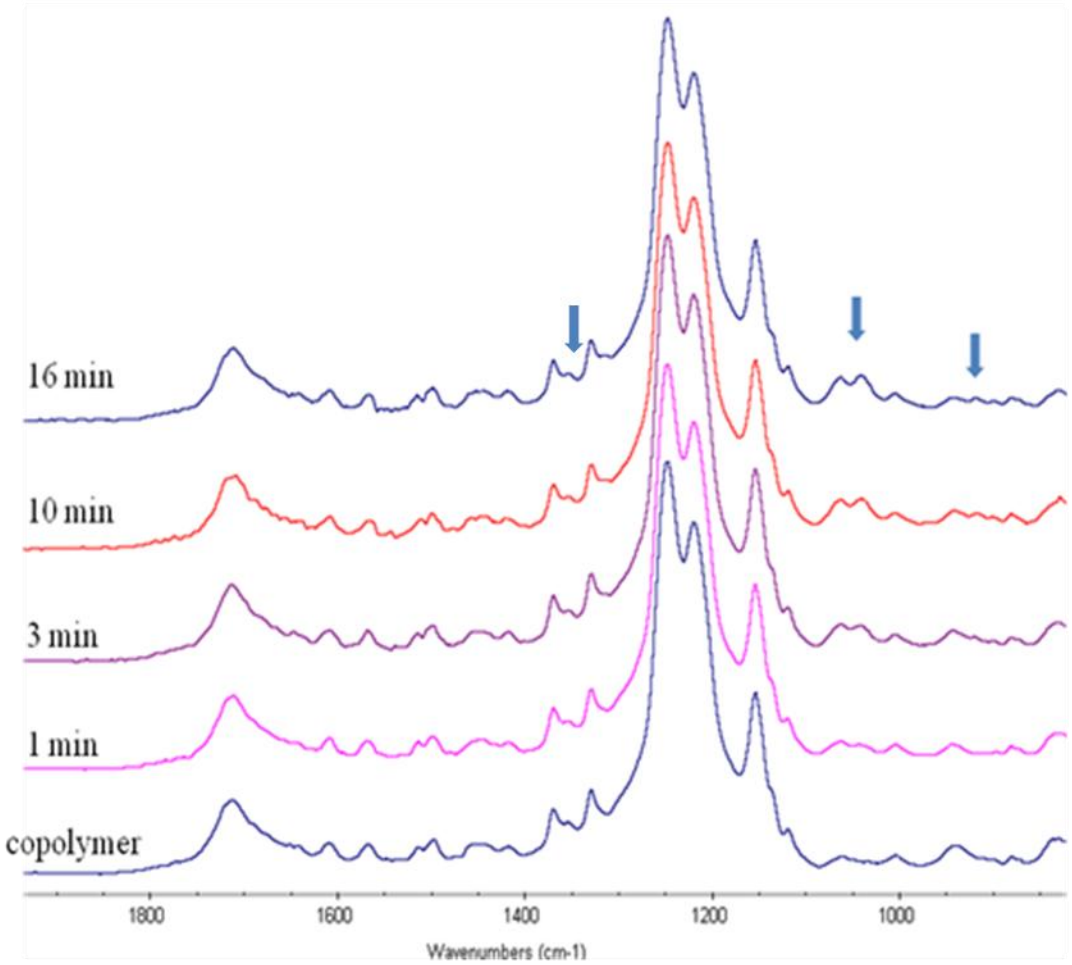

Figure 7.10. FT-IR spectra of copolymer II exposed to wet DMMP vapor at various exposure times.

7.4 REFERENCES

1. Ting, G.; Chang, C. H.; Wang, H. E., Cancer Nanotargeted Radiopharmaceuticals for Tumor Imaging and Therapy. *Anticancer Research* **2009,** 29, (10), 4107-4118.
2. Welch, H. G.; Schwartz, L. M.; Woloshin, S., Are increasing 5-year survival rates evidence of success against cancer? *Jama-Journal of the American Medical Association* **2000,** 283, (22), 2975-2978.
3. Cao, W. Q.; Duan, Y. X., Breath analysis: Potential for clinical diagnosis and exposure assessment. *Clinical Chemistry* **2006,** 52, (5), 800-811.
4. Phillips, M.; Herrera, J.; Krishnan, S.; Zain, M.; Greenberg, J.; Cataneo, R. N., Variation in volatile organic compounds in the breath of normal humans. *Journal of Chromatography B* **1999,** 729, (1-2), 75-88.
5. Libardoni, M.; Stevens, P. T.; Waite, J. H.; Sacks, R., Analysis of human breath samples with a multi-bed sorption trap and comprehensive two-dimensional gas chromatography (GC x GC). *Journal of Chromatography B-Analytical Technologies in the Biomedical and Life Sciences* **2006,** 842, (1), 13-21.
6. Peng, G.; Hakim, M.; Broza, Y. Y.; Billan, S.; Abdah-Bortnyak, R.; Kuten, A.; Tisch, U.; Haick, H., Detection of lung, breast, colorectal, and prostate cancers from exhaled breath using a single array of nanosensors. *British Journal of Cancer* **2010,** 103, (4), 542-551.
7. Phillips, M.; Gleeson, K.; Hughes, J. M. B.; Greenberg, J.; Cataneo, R. N.; Baker, L.; McVay, W. P., Volatile organic compounds in breath as markers of lung cancer: a cross-sectional study. *Lancet* **1999,** 353, (9168), 1930-1933.
8. Wilson, A. D.; Baietto, M., Applications and Advances in Electronic-Nose Technologies. *Sensors* **2009,** 9, (7), 5099-5148.
9. Thaler, E. R.; Kennedy, D. W.; Hanson, C. W., Medical applications of electronic nose technology: Review of current status. *American Journal of Rhinology* **2001,** 15, (5), 291-295.
10. Schurmann, K.; Lahann, J.; Niggemann, P.; Klosterhalfen, B.; Meyer, J.; Kulisch, A.; Klee, D.; Gunther, R. W.; Vorwerk, D., Biologic response to polymer-coated stents: In vitro analysis and results in an iliac artery sheep model. *Radiology* **2004,** 230, (1), 151-162.
11. Lahann, J., Vapor-based polymer coatings for potential biomedical applications. *Polymer International* **2006,** 55, (12), 1361-1370.
12. Chen, H. Y.; Lahann, J., Designable Biointerfaces Using Vapor-Based Reactive Polymers. *Langmuir* **2011,** 27, (1), 34-48.